

MONGE-KANTOROVICH FITTING WITH SOBOLEV BUDGETS

FOREST KOBAYASHI, JONATHAN HAYASE, AND YOUNG-HEON KIM

ABSTRACT. Given $m < n$, we consider the problem of “best” approximating an n -d probability measure ρ via an m -d measure ν such that $\text{supp } \nu$ has bounded total “complexity.” When ρ is concentrated near an m -d set we may interpret this as a *manifold learning problem with noisy data*. However, we do not restrict our analysis to this case, as the more general formulation has broader applications.

We quantify ν ’s performance in approximating ρ via the Monge-Kantorovich (also called *Wasserstein*) p -cost $\mathbb{W}_p^p(\rho, \nu)$, and constrain the complexity by requiring $\text{supp } \nu$ to be coverable by an $f : \mathbb{R}^m \rightarrow \mathbb{R}^n$ whose $W^{k,q}$ Sobolev norm is bounded by $\ell \geq 0$. This allows us to reformulate the problem as minimizing a functional $\mathcal{G}_p(f)$ under the Sobolev “budget” ℓ . This problem is closely related to (but distinct from) *principal curves with length constraints* when $m = 1, k = 1$ and an unsupervised analogue of *smoothing splines* when $k > 1$. New challenges arise from the higher-order differentiability condition.

We study the “gradient” of \mathcal{G}_p , which is given by a certain vector field that we call the *barycenter field*, and use it to prove a nontrivial (almost) strict monotonicity result. We also provide a natural discretization scheme and establish its consistency. We use this scheme as a toy model for a generative learning task, and by analogy, propose novel interpretations for the role regularization plays in improving training.

2020 *Mathematics Subject Classification.* 49Q10, 49Q20, 49Q22, 65D10.

Key words and phrases. Monge-Kantorovich fitting, principal curves, principal manifolds, manifold learning, Sobolev constraint.

FK is supported by the 4YF doctoral fellowship of the University of British Columbia. JH is supported by NSF award 2134012 and the NSF Graduate Research Fellowship Program. YHK is partially supported by the Natural Sciences and Engineering Research Council of Canada (NSERC), with Discovery Grant RGPIN-2019-03926, as well as Exploration Grant (NFRFE-2019-00944) from the New Frontiers in Research Fund (NFRF). YHK is also a member of the Kantorovich Initiative (KI) which is supported by the PIMS Research Network (PRN) program of the Pacific Institute for the Mathematical Sciences (PIMS). We thank PIMS for their generous support; report identifier PIMS-20240925-PRN01. Part of this work was completed during YHK and FK’s visit at the Korea Advanced Institute of Science and Technology (KAIST), and we thank them for their hospitality and the excellent environment. ©2024 by the author. All rights reserved.

CONTENTS

1. Introduction	3
1.1. Motivation	3
1.2. The General Problem	4
1.3. Optimal Transport Interpretation	5
1.4. Hypotheses	5
1.5. Discussion of Main Results	6
1.6. Example Applications	8
1.7. Relationships with Existing Work	10
1.8. Acknowledgements	14
2. Preliminaries	14
2.1. The Sobolev Constraint	14
2.2. The Objective	16
2.3. Continuity Properties of \mathcal{G}_p	18
3. Existence of Optimizers and Properties of J	19
3.1. Existence & Nonuniqueness of Optimizers	19
3.2. Properties of J	20
3.3. Asymptotics for J	22
4. The “Gradient” of \mathcal{G}_p : The Barycenter Field.	23
4.1. Motivation for The Barycenter Field and Comparison to Previous Techniques	24
4.2. The Barycenter Field	26
4.3. $F_{\hat{\pi}_X}$ as a (Negative) Gradient	30
4.4. Local Improvements and First-Order Conditions	35
5. The Discrete Problem & Simulations	37
5.1. Discretizing ρ	37
5.2. Representing f by Samples	38
5.3. Simulations Of (SP) In Two Dimensions With Uniform Target Measure	41
6. Toward Applications to Generative Learning	46
6.1. Brief Overview of Generative Learning Problems	47
6.2. WGAN and The Constrained Monge-Kantorovich Fitting Problem	49
6.3. Training Neural Networks with a $k = 1$ Penalty	53
6.4. Demonstrating the Interpolation Benefits of a $k = 1$ Penalty	57
7. Conclusion	59
References	59
Appendix A. Gallery of Numerical Experiments	63
A.1. Triangular Domain	63
A.2. Hexagonal Star Domain	65
A.3. Chevron Domain	67

1. INTRODUCTION

We begin with a motivating example.

1.1. Motivation. *Given a rope of length ℓ , what shape should one bend it into to best “fill” Ω ?* In simple cases it is easy to distinguish between “good” and “bad” solutions. The idea is that a “good” solution should minimize the average distance from a point in Ω to the closest point on the rope. With this in mind, one can clearly see the curve in Fig. 1a performs better than the one in Fig. 1b (note the sample points are identical).

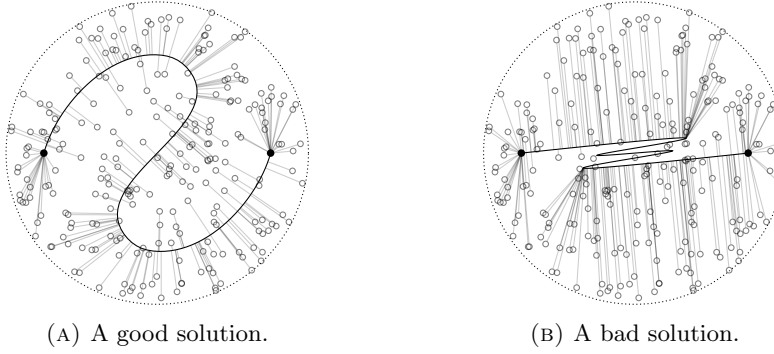


FIGURE 1. Closest points for $N = 250$ uniformly-sampled $\omega \in \Omega$.

Explicitly: Parametrizing the curves by $f_{\text{good}}, f_{\text{bad}} : [0, 1] \rightarrow \Omega$, we have

$$(1.1) \quad \mathbb{E} \left[\inf_{x \in [0,1]} |\omega - f_{\text{good}}(x)| \right] < \frac{1}{2} \mathbb{E} \left[\inf_{x \in [0,1]} |\omega - f_{\text{bad}}(x)| \right].$$

If we endow Ω with a measure ρ more concentrated along the horizontal we find the “bad” solution now performs better than the “good” one. Thus we may generalize (1.1) by replacing the expectations with ρ -expectations. As a real-world example, this could model a courier service wanting to find an efficient delivery route for clients distributed as ρ in a city Ω .

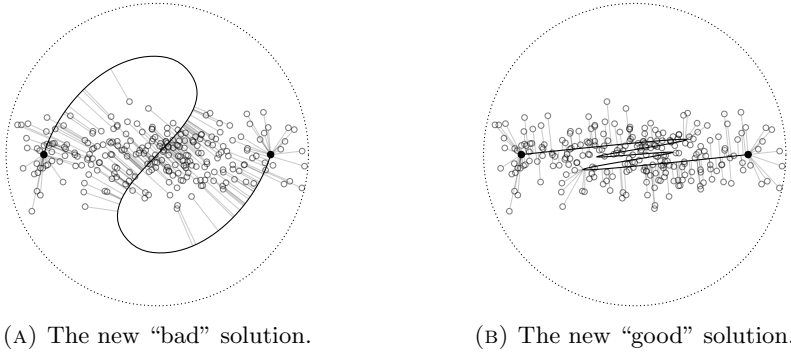


FIGURE 2. Closest point projections for $N = 250$ points sampled according to $\rho = \mathcal{N}(\mathbf{0}; [\sigma_X^2 \ 0; \ 0 \ \sigma_Y^2])$ (truncated to Ω), where $\sigma_X^2 = 1$, $\sigma_Y^2 = 9/121$.

This problem is closely related to the *average-distance problem* introduced in [8, 7]; those works considered optimizing the expectations in (1.1) over closed, connected sets $\Sigma \subseteq \Omega$ with Hausdorff 1-measure $\mathcal{H}^1(\Sigma) \leq \ell$. In a similar vein, we might try formalizing our problem as an optimization over $f \in C([0, 1]; \Omega)$ with $\mathcal{H}^1(f([0, 1])) \leq \ell$. However, as we now discuss, this has some disadvantages.

Note (1.1) is equally meaningful in the context of trying to fill a ρ on $\Omega \subseteq \mathbb{R}^n$ with some kind of m -surface. For example, this could represent the problem of trying to design an optimal catalytic surface for reagents in a vessel $\Omega \subseteq \mathbb{R}^3$, or a manifold learning problem where data noise causes ρ to “spread” off of the generating m -manifold. Regardless, when $m > 1$, the m -dimensional Hausdorff measure $\mathcal{H}^m(f(X))$ is no longer a meaningful constraint, since one may obtain arbitrarily-good approximations of ρ for which $\mathcal{H}^m(f) = 0$ by degenerating $f(X)$ to an $(m - 1)$ -surface. Thus in our problem we will replace \mathcal{H}^m with a constraint \mathcal{C} that at least includes the derivatives $\partial_i f^j$, where f^j denotes the j^{th} component function of f . Our particular choice will be the Sobolev norm we discuss later in Section 2.1; for now, a simpler example is

$$\mathcal{C}(f) = \left(\sum \|\partial_i f^j\|_{L^q(X)}^q \right)^{1/q}.$$

Thinking again of the courier-service example, we see it is also quite natural to add higher-order terms to \mathcal{C} : Delivery routes that contain frequent acceleration might perform poorly in terms of fuel economy, thus incurring extra costs. The particular constraint we use in this paper shall be the Sobolev norm $\|f\|_{W^{k,q}(X;\Omega)}$, with which we can choose to penalize (weak) derivatives up to order k .

Lastly, we should also notice that it is meaningful to consider exponents p other than $p = 1$ on the distance function in (1.1). In analogy with L^p norms, we may interpret this as weighting the relative importance of “outliers” in ρ . Hence we end up with the fairly-general problem of trying to minimize the objective function

$$f \mapsto \mathbb{E}_\rho \left[\inf_{x \in X} |\omega - f(x)|^p \right] \text{ subject to a Sobolev constraint of } f.$$

With this motivation in mind we now formally define the problem in a slightly more general context, so as to facilitate comparisons to existing works. Note, from now on we will write the expectation \mathbb{E}_ρ as an integral.

1.2. The General Problem. Consider the following class of problems:

$$\text{Fix } m < n \text{ and let } X \subseteq \mathbb{R}^m \text{ and } \Omega \subseteq \mathbb{R}^n.$$

Also fix a class of admissible functions $\mathcal{F} \subseteq \{f \mid f : X \rightarrow \Omega\}$. Let ρ be a probability measure on Ω and for some $p \in (0, \infty)$ define the objective function $\mathcal{G}_p : \mathcal{F} \rightarrow \mathbb{R}^{\geq 0}$ by

$$(1.2) \quad \mathcal{G}_p(f) = \int_\Omega \inf_{x \in X} |\omega - f(x)|^p d\rho(\omega).$$

Then, given a constraint function $\mathcal{C} : \mathcal{F} \rightarrow \mathbb{R}^{\geq 0}$ and a budget $\ell \geq 0$, the goal is

Problem 1 (Hard Constraint (HC)). Minimize $\mathcal{G}_p(f)$ over $\{f \in \mathcal{F} \mid \mathcal{C}(f) \leq \ell\}$.

We define the *optimal-value function* for a given budget ℓ by

$$(1.3) \quad J(\ell) = \inf_{\{\mathcal{C}(f) \leq \ell\}} \mathcal{G}_p(f).$$

The typical constraints considered are usually either integral constraints, e.g. $\mathcal{C}(f) = \text{length}(f) = \int |f'| dx$ [39], or geometric constraints, e.g. $\mathcal{C}(f) = \mathcal{H}^1(f(X))$ where \mathcal{H}^1 denotes the Hausdorff 1-measure [8, 7]. Much work has been done on these problems and the literature is quite diverse so we will postpone a detailed discussion until Section 1.7. For now, we simply note that frameworks like these provide a way to study manifold learning problems where data noise is *explicitly* assumed—see [56, §3.5.2], and the references therein—as well as certain generative learning problems (Section 1.6.1).

As succinctly stated in [42], one may think of \mathcal{G}_p as measuring how well f approximates ρ while $\mathcal{C}(f)$ restricts the complexity of the approximation. In Proposition 2.7 we show \mathcal{G}_p has an interpretation in terms of an optimal transport cost. It is also common [50, 51, 42] to replace the hard constraint $\mathcal{C}(f) \leq \ell$ with a soft penalty by defining for a fixed parameter $\lambda > 0$

$$(1.4) \quad \mathcal{G}_p^\lambda(f) = \mathcal{G}_p(f) + \lambda \mathcal{C}(f),$$

whence the problem becomes

Problem 2 (Soft Penalty (SP)). Minimize \mathcal{G}_p^λ over $\{\mathcal{C} < \infty\}$.

(HC) and (SP) are very closely related but not always equivalent for every choice of \mathcal{C} ; see Section 1.7.4. For now, we simply note that solutions to (SP) recover solutions to (HC) but not necessarily vice versa, and also that (SP) is often more direct to implement numerically. Thus we will typically use (SP) in lieu of (HC) in our simulations.

1.3. Optimal Transport Interpretation. We can interpret (HC) in terms of a “free-source” version of the unequal-dimensional optimal transport studied in [55, 64]. Recall that given compact domains $X \subseteq \mathbb{R}^m, Y \subseteq \mathbb{R}^n$ (for now making no assumptions about the relative sizes of m, n), probability measures $\mu \in \mathcal{P}(X)$, $\nu \in \mathcal{P}(Y)$, and a cost function $c : X \times Y \rightarrow \mathbb{R}$, the *optimal transport cost* between μ and ν is given by

$$\mathcal{T}_c(\mu, \nu) = \inf_{\gamma \in \Gamma(\mu, \nu)} \int_{X \times Y} c(x, y) d\gamma(x, y),$$

where $\Gamma(\mu, \nu)$ denotes the set of all probability measures on $X \times Y$ with marginals μ and ν . When $m = n$ and $c(x, y) = |x - y|^p$, we let

$$(1.5) \quad \mathbb{W}_p(\mu, \nu) = (\mathcal{T}_c(\mu, \nu))^{1/p}$$

and call it the *Monge-Kantorovich p -distance* (also called the *Wasserstein p -distance*); see e.g. the books [77, 73, 68]. It is straightforward to show (see Proposition 2.7) that

$$(1.6) \quad J(\ell) = \inf_{\{\mathcal{C}(f) \leq \ell\}} \inf_{\nu \in \mathcal{P}(f(X))} \mathbb{W}_p^p(\rho, \nu).$$

1.4. Hypotheses. Having discussed the general problem, we now specify the particular instance we consider. The core hypotheses we employ are

- (H.1) $X \subseteq \mathbb{R}^m$ is a simply connected, compact domain with nonempty interior and $\partial X \in C^1$,
- (H.2) $\Omega \subseteq \mathbb{R}^n$ ($m < n$) is a compact, convex domain,
- (H.3) $\mathcal{C}(f)$ is given by a $W^{k,q}$ Sobolev norm ($k \geq 1$) where
 - (H.3.a) $1 < q < \infty$, and

- (H.3.b) $kq > m$, and
 (H.4) $p \geq 1$.

Broadly speaking, (H.1)–(H.3) are used for getting things like compactness and convexity of the feasible set and suitable continuity of \mathcal{G}_p , while (H.4) is used to give \mathcal{G}_p enough regularity to get a “gradient” in Section 4. On that note, while it is not a core hypothesis, the following addition of (H*) often allows one to dramatically simplify statements in Section 4; we will note this explicitly when relevant:

- (H*) ρ is absolutely continuous with respect to the Lebesgue measure.

The primary contribution of our work is the generality of (H.1)–(H.4), especially the free choice of $m < n$. A particular challenge is posed by the fact that taking $k > 1$ includes higher-order terms in $\mathcal{C}(f)$; this makes \mathcal{C} severely parametrization-dependent. As a consequence, typical local-modification arguments (see [8, Lemma 3.12], [18, Lemma 3.1]) for improving \mathcal{G}_p become unusable; we discuss this more in Section 1.7.3. For now, we simply note that the higher-order terms fundamentally change the flavor of the problem. We are forced to take a more abstract approach than in the $\mathcal{C}(f) = \text{length}(f)$ case and go on some detours to set up machinery. On the other hand, our proof strategies tend to be more general, and so might arguably expose more fundamental geometric features of the problem.

1.5. Discussion of Main Results. Under (H.1), (H.2), and (H.3) we establish existence of optimizers (Theorem 3.1) and discuss some trivial counterexamples to uniqueness (Theorem 3.4). We exhibit fundamental properties of \mathcal{G}_p such as joint continuity in (f, ρ) (Theorem 2.12) and lack of convexity/concavity (Section 2.2.1). Similarly, for the optimal-value function $J(\ell)$ we establish some basic properties including continuity (Theorem 3.5; c.f. [18, Lem. 3.1.i]) and an asymptotic lower bound in terms of the budget ℓ (Proposition 3.9; c.f. [8, Thm 3.16]).

A natural question is whether J must be strictly monotone. In other words,

- (1.7) “Does increasing the budget allow us to create strictly-better solutions?”

This is surprisingly nontrivial. A closely related result we can show via elementary methods is that for all ℓ large enough to guarantee optimizers are nonconstant (Proposition 3.3), there exist optimizers saturating the constraint (Corollary 3.7). By contrast, the converse to (1.7) is immediate: Decreasing J always requires increasing the budget, since J is trivially nonincreasing.

The difficulty in getting a strict monotonicity result (1.7) is mainly due to the significant parametrization-dependence of \mathcal{C} when $k > 1$. Hence much of the remainder of the paper is dedicated to establishing local modification strategies that are compatible with \mathcal{C} and provably improve \mathcal{G}_p . Fundamental to this goal is the question:

“What is the gradient of $\mathcal{G}_p(f)$?”

To that end we consider a natural object, the first variation of \mathcal{G}_p . Versions of this have been considered in the literature (see e.g. [6, 42, 18]); the point is that we treat the case of general $p \geq 1$, and importantly remove common hypotheses on ρ (e.g. “vanishing on small sets”) for $p > 1$ while also establishing sharper hypotheses for the $p = 1$ case, thus unifying the results scattered in the literature. On the other hand, we also use this to provide a novel and nontrivial result on making a local modification to an optimizer while remaining in the Sobolev class.

The approach is as follows. First, in Section 4, under (H.4) we express the first variation of \mathcal{G}_p as a certain vector field attached to the map f ; we refer to this field as the *barycenter field*.

Definition 4.3 (Barycenter Field). Let $\hat{\pi}_X(\omega) \in \arg \min_{x \in X} |\omega - f(x)|$ and let $(\{\rho_x\}_{x \in X}, \mu_{\hat{\pi}_X})$ be the disintegration of ρ via $\hat{\pi}_X$. Then we define the *barycenter field* at x to be

$$F_{\hat{\pi}_X}(x) = p \int_{\hat{\pi}_X^{-1}(x)} |\omega - f(x)|^{p-2} (\omega - f(x)) \, d\rho_x(\omega).$$

Letting $Y = f(X)$ and $\hat{\pi}_Y(\omega) \in \arg \min_{y \in Y} |\omega - y|$ we may define $F_{\hat{\pi}_Y}$ analogously.

In the case $(m, p) = (1, 2)$ this trivially recovers the objects used in [42, 18]; see also similar ideas in [26, 6]. Note that in this definition there are some technical wrinkles arising from the fact that there might be multiple possible choices for the value $\hat{\pi}_X$ can take for ω in the so-called *ambiguity set* \mathcal{A}_f ; typically these are addressed by making assumptions on ρ [6, 42] or by exploiting structure particular to the case $p = 2$ [18]. We bypass such issues by applying a simple result on measurable selections; see Section 4.2.1.

Let $\hat{\Pi}_X$ denote the set of all measurable selections of $\omega \mapsto \arg \min_{x \in X} |\omega - f(x)|$ and for all $\hat{\pi}_X \in \hat{\Pi}_X$ let $\mu_{\hat{\pi}_X}$ denote the pushforward of ρ by the map $\hat{\pi}_X$. It turns out that the barycenter field is essentially the $L^2(\mu_{\hat{\pi}_X})$ -gradient of \mathcal{G}_p at f :

Theorem 4.8. Take (H.1), (H.2), and (H.4). Fix $f \in C(X; \Omega)$ and $\xi \in C(X; \mathbb{R}^n)$, and for all $\varepsilon > 0$ let $f_\varepsilon := f + \varepsilon \xi$ and $Y = f(X)$, $Y_\varepsilon = f_\varepsilon(X)$. If $p = 1$, let $Y_{\text{out}} = \{y \in Y \mid \liminf_{\varepsilon \rightarrow 0} 1_{Y_\varepsilon}(y) = 0\}$, and take the extra hypothesis $\rho(Y_{\text{out}}) = 0$. Then

$$\lim_{\varepsilon \rightarrow 0} \frac{\mathcal{G}_p(f_\varepsilon) - \mathcal{G}_p(f)}{\varepsilon} = \min_{\hat{\pi}_X \in \hat{\Pi}_X} \int_X \langle -F_{\hat{\pi}_X}(x), \xi(x) \rangle \, d\mu_{\hat{\pi}_X}(x).$$

Here the minimization of the set $\hat{\Pi}_X$ arises due to the ambiguity set \mathcal{A}_f .

Remark 1.1. An analogous result for the $(m, \mathcal{C}(\Sigma), p) = (1, \mathcal{H}^1(\Sigma), 1)$ case was established in [6] under the assumption that $\xi \in C^\infty$ and $\rho(E) = 0$ for all E such that $\mathcal{H}^{n-1}(E) = 0$. Similarly, if one takes (H*), $f, \xi \in C^2$, and $(m, \mathcal{C}(f), p) = (1, \text{length}(f), 2)$ then Theorem 4.8 is implied by the analysis in [42]. In [18] it was further shown that if f is an optimizer of (HC) and ξ is bounded and Borel, then exploiting an invariant particular to $p = 2$ allows removing the (H*) hypothesis of [42]. We reiterate that our hypotheses are more general, requiring only continuity of f, ξ , and a mild extra hypothesis on ρ for $p = 1$.

When $\rho(\mathcal{A}_f) = 0$ (e.g., via (H*)), adding an injectivity hypothesis to f and rewriting in terms of $F_{\hat{\pi}_Y}$ yields a much simpler form—see Corollary 4.10. However, even with this simplified form, it is nontrivial to construct local improvements to f while remaining in the Sobolev class. Indeed, in Section 4.2.2 we study some properties of $F_{\hat{\pi}_X}$, $F_{\hat{\pi}_Y}$, and demonstrate that they can be discontinuous even when $f \in C^\infty$ (Theorem 4.6) or Y is a C^1 -manifold (Theorem 4.7). This complicates attempts to employ $F_{\hat{\pi}_X}$, $F_{\hat{\pi}_Y}$ for gradient flow (c.f. [26, §5]), as such a scheme would require $f + \varepsilon F_{\hat{\pi}_X}$ to remain within the admissible set, that is, the Sobolev class for $k \geq 1$. Nevertheless, we show that if $F_{\hat{\pi}_X}$ is nontrivial we can construct a local improvement regardless of the choice of k :

Theorem 4.14. *Take the hypotheses of Theorem 4.8 and suppose that*

$$(1.8) \quad \text{for some } \hat{\pi}_X \in \hat{\Pi}_X \text{ we have } \mu_{\hat{\pi}_X}(\{F_{\hat{\pi}_X} \neq 0\}) > 0.$$

Then for all $\varepsilon > 0$ there exists $\xi_\varepsilon \in C^\infty(X; \mathbb{R}^n)$, depending on $F_{\hat{\pi}_X}$, such that

$$\mathcal{G}_p(f + \xi_\varepsilon) < \mathcal{G}_p(f) \quad \text{and} \quad \mathcal{C}(f + \xi_\varepsilon) < \mathcal{C}(f) + \varepsilon.$$

Furthermore, if $\mu_{\hat{\pi}_X}(f^{-1}(\partial\Omega)) = 0$, then ξ_ε can be chosen so that $f + \xi_\varepsilon$ takes values only in Ω , whence f is not a local minimum of \mathcal{G}_p in $W^{k,q}(X; \Omega)$.

This can of course be restated in terms of $Y, F_{\hat{\pi}_Y}$; see Corollary 4.10. In any case, this theorem almost establishes the desired “strict monotonicity” (1.7) of J , modulo the nontriviality condition $\mu_{\hat{\pi}_X}(\{F_{\hat{\pi}_X} \neq 0\}) > 0$; such nontriviality was called “default of self-consistency” in [18, Lemma 3.2] where it was established for the special case $(m, \mathcal{C}(f), p) = (1, \text{length}(f), 2)$. The assumption $\mu_{\hat{\pi}_X}(\{F_{\hat{\pi}_X} \neq 0\}) > 0$ is crucial for us, and we conjecture that it holds for each optimizer f of the hard constraint problem $J(\ell)$ (1.3), though unfortunately the proof of [18] does not generalize to our case, with challenges being provided by both $k > 1$ and $q > 1$.

In the later part of the paper we turn toward numerical simulations and applications to machine learning. In Section 5 we demonstrate consistency results for both (HC) and (SP) (Corollaries 5.1 and 5.2). We demonstrate an algorithm for computing discrete approximations to $F_{\hat{\pi}_X}$ and show an example output. In Section 6 we highlight a connection between (HC) and generative learning problems. We give an informal overview of why *a priori* we might expect such a connection (summarized in Section 1.6.1) and give numerical experiments demonstrating that the arc length constraint (c.f. [51], [18]) is a powerful regularization method in a simple image-generation problem, clearly outperforming an unregularized network as well as modestly outperforming weight-decay. Further experiments would be required to ensure this is not an artifact of lucky hyperparameter tuning, as well as to understand the impact of our constraint when $k > 1$. This is left for a future work.

1.6. Example Applications. We believe there are many practical directions that our results and perspectives can find new applications to. Here we list two examples.

1.6.1. Factorization of Wasserstein GANs. Given the relationship between \mathcal{G}_p and $\mathbb{W}_p^p(\rho, \nu)$ (see Section 1.3 and Proposition 2.7), our results can be connected to ideas in machine learning research, especially Wasserstein GANs [1]. First, one may trivially extend $\mathbb{W}_p(\mu, \nu)$ to the case $m < n$ by fixing a measurable $f : X \rightarrow Y$, letting $c(x, y) = |f(x) - y|^p$, and taking the infimum over $\gamma \in \Gamma(f_{\#}\mu, \nu)$. Then the essential idea of *Wasserstein GANs* (WGANs) is the problem of learning the best choice of f to minimize $\mathbb{W}_p(f_{\#}\mu, \nu)$.

Our problem is slightly different. From the double optimization structure (1.6) we may think of (HC) as trying to find the “best” $f \in \{\mathcal{C}(f) \leq \ell\}$ when we are free to choose *any* probability measure to put on $f(X)$, rather than just $f_{\#}\mu$ for the given μ . Here we may interpret the restriction to $\{\mathcal{C}(f) \leq \ell\}$ as penalizing overfitting of an empirical measure ρ_N in the presence of high-frequency noise, with increasing k yielding solutions f that have fewer “sharp bends.” Additionally, we may view the $k = 1$ term as penalizing “backtracking,” thus incentivizing choices of f for which locality in Ω corresponds more nicely to locality in X . This may be used to “factor” problems like WGAN (between μ and ρ) into two steps.

Factorization of WGAN (A Two-Step Approach):

- 1) A “hard” step (HC) consisting of finding a low-complexity m -to- n map f whose image best approximates a measure ρ on \mathbb{R}^n , and
- 2) An “easy” step (reparametrization) consisting of finding an m -to- m map φ such that $(f \circ \varphi)_{\#}\mu = \arg \min_{\nu \in \mathcal{P}(f(X))} \mathbb{W}_p^p(\rho, \nu)$.

We hypothesize that performing this sort of factorization could yield performance improvements over the existing methods, which generally try to solve the two problems simultaneously.

Essentially, the idea is that in the factored problem, the explicit regularization of f can help avoid situations where f gets stuck in a well whose local minimum has extremely low regularity (e.g. being not even continuous). Such low-regularity functions can be difficult to express in a given model class, leading to undesirable qualities such as slow convergence or training instabilities.

In fact, we propose that even in the “unfactored” context, adding regularization resembling \mathcal{C} could provide important benefits—see [76] for a similar idea. We discuss this and more connections to generative learning in Section 6; for now, we simply propose that theoretical analysis of (HC)/(SP) could be useful in developing qualitative intuition for problems like WGAN.

1.6.2. A Routing Problem with Sobolev constraint. The following application gives an idea of why it is relevant to consider for $\mathcal{C}(f)$ the Sobolev norm of f , i.e. including all the lower order terms.

In Section 1.1 we mentioned the example of a company trying to find an efficient route for delivering packages. We describe a similar drone-routing application involving $W^{2,q}$, inspired by [47, §7.2.1]. Note, however, that the authors of that work considered L^∞ constraints on the linear and angular velocities of the drone, and also required it to return to the start at predetermined times for charging. This is in contrast to our constraint, which is L^q and directly incorporates the acceleration ($k = 2$) term, thus allowing the optimization process itself to determine when the drone should return for charging.

Suppose an organization plans to fly drones over remote, wildfire-prone areas to attempt to locate new burns. Based on past data and weather modeling they have a rough idea of the distribution ρ where the risk of fire is the highest. What is the best path $f(t)$ for the drone to take, given its finite battery capacity?

There are three main factors. First, as the drone flies farther from the launch station, it requires more power to transmit a strong enough signal to stream data back; we encode this with $\|f\|_{L^1}$ (alternatively, one could interpret the 0th-order term as penalizing the expected cost of retrieval were the drone to malfunction and crash in the wilderness, as typically the transmission-power variation is small). Second, assuming low speeds, the drone must constantly expend energy proportional to its velocity in order to overcome drag; we encode this with $\|Df\|_{L^1}$. Lastly, the drone will need to expend energy any time it accelerates; we encode this by $\|D^2f\|_{L^1}$. Hence, up to a choice of coefficients $c_0, c_1, c_2 > 0$ our constraint becomes

$$\|f\|_{W^{2,1}([0,1];\Omega)} = c_0\|f\|_{L^1} + c_1\|Df\|_{L^1} + c_2\|D^2f\|_{L^1}.$$

Thus we see the Sobolev norm of f (the sum of lower and higher order terms), especially in this case with $k = 2$, is a meaningful constraint. We may interpret the replacement of $\|\cdot\|_{L^1}$ with $\|\cdot\|_{L^q}^q$ as a form of reweighting to penalize outliers.

For this particular application, we believe a discretized version of the barycenter field $F_{\hat{\pi}_X}$ (Theorem 5.3) could be particularly helpful if ρ is being approximated via data collected in real-time. For example, if satellite data shows that a region far from the current flight path is experiencing severe dry conditions, $F_{\hat{\pi}_X}$ could inform the operators how to most-efficiently modify the drone path to investigate the new area without having to recompute the entire trajectory from scratch.

1.7. Relationships with Existing Work.

1.7.1. Non-parametric vs. Parametric Formulation. When $m = 1$, (HC) is closely related to the “average distance problem” or “irrigation problem” first introduced in [8, 7] (a review is given in [48]). That work considered the particular case $p = 1$ and optimized over closed, connected sets $\Sigma \subseteq \mathbb{R}^n$ with finite Hausdorff \mathcal{H}^1 measure. We may view this as (HC) taking $\mathcal{F} = C(X; \Omega)$ and $\mathcal{C}(f) = \mathcal{H}^1(f(X))$.

A key distinguishing feature of the \mathcal{H}^1 formulation is that it makes it easy to make changes to the topology of $f(X)$: We may freely create “branches” in Σ , so long as it remains connected and we maintain $\mathcal{H}^1(\Sigma) \leq \ell$. By contrast, in the parametrization-dependent formulation of the cost \mathcal{C} these kinds of modifications are disincentivized: Creating a branch typically requires some form of “backtracking,” which is usually highly inefficient. In fact in [18] it was actually shown for the parametric formulation $(\mathcal{C}(f), n, p) = (\text{length}(f), 2, 2)$, that optimizers of (HC) *must* be injective, thus precluding backtracking of any kind.

We may interpret this as a reflection that the \mathcal{H}^1 formulation is best suited for problems with some form of parallel structure, e.g. designing an irrigation network: Once water flows in the pipes we can deliver it to all customers simultaneously. By contrast, the parametrization-dependent formulation is suited more to problems with a sequential structure, such as the courier problem: A delivery truck can only visit one address at a time.

1.7.2. Principal Curves and Surfaces. In [32] Hastie introduced the notion of *principal curves and surfaces*, defined (in our notation) to be injective maps f for which the $p = 2$ barycenter field $F_{\hat{\pi}_Y} \equiv 0$. A concise reference for this framework is found in [33]. In analogy with the standard technique of *principal component analysis*, we may understand principal curves as essentially performing nonlinear dimension reduction. However, this definition proved to be difficult to work with theoretically, hence the authors of [39] chose to redefine principal curves as (in our notation) solutions of (HC) when $m = 1$, $p = 2$, and $\mathcal{C}(f) = \text{length}(f)$. This is typically taken as the standard definition now [18]. Clearly, this problem is very similar to our case $\mathcal{C}(f) = \|f\|_{W^{k,q}(X;\Omega)}$, but there are some key differences as we now discuss.

1.7.3. The Arc Length Constraint. When $m = 1$, $k = 1$, our problem becomes similar to the case where $\mathcal{C}(f) = \text{length}(f)$. Indeed, since $|f|$ is bounded by $\text{diam}(\Omega)$ while $|Df|$ is unbounded, we see that as $\mathcal{C}(f) \rightarrow \infty$, $\|f\|_{W^{1,q}} \approx \|Df\|_{L^q}$, which is similar in spirit to $\text{length}(f)$. When $k > 1$ however the problem becomes very different.

To see this, suppose $X = [-1, 1]$, $\Omega = [-1, 1]^2$ with ρ_{unif} , and $f(x) = (x, 0)$. Suppose we wanted to prove that for all p , given ε extra budget, we can modify f in a way that improves \mathcal{G}_p . If $k = 1$ this is easy: We may add a “spike” of height $O(\varepsilon)$ by reparametrizing f to be constant on some $[x_0 - \delta, x_0 + \delta]$ ($\delta \ll 1$) and adding a perturbation (Fig. 3b). Importantly, the reparametrization step is trivial

since we can freely introduce jump discontinuities in Df at $x_0 \pm \delta$. By contrast, the cost of such a reparametrization is generally quantized when $k > 1$ and $Df(x_0) > 0$.

Thus if ε is sufficiently small, inserting a spike is no longer possible and the best we can do is typically something like Fig. 3c. This makes analyzing the effects on \mathcal{G}_p nontrivial since the image of the initial curve is no longer a subset of the image of the perturbed curve. This is the essential difference between the two problems.

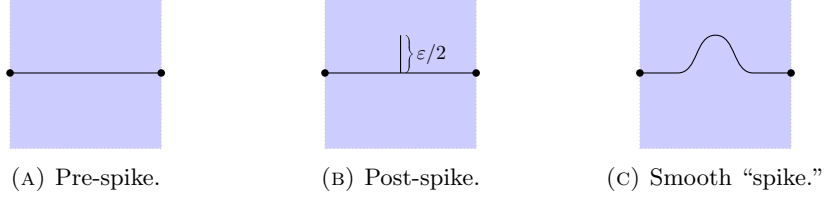


FIGURE 3. Adding two kinds of spikes.

1.7.4. The Soft Penalty Formulation. Earlier we mentioned the hard constraint and soft penalty (see [42, 49]) formulations are not entirely equivalent. Let us briefly discuss why. First note that the soft penalty problem (SP) recovers optimizers to the hard constraint problem (HC):

┌ If \hat{f} is a minimizer of the soft penalty problem $\mathcal{G}_p^\lambda(f)$, then
└ \hat{f} is a minimizer of the hard penalty problem $\mathcal{G}_p(f)$ over $\{C(f) \leq \hat{\ell} := C(\hat{f})\}$.

We also have an easy monotonicity result:

Lemma 1.2. *For each λ let f_λ be an optimizer of \mathcal{G}_p^λ of (SP). Then,*

$$C(f_{\lambda_2}) \leq C(f_{\lambda_1}) \text{ for all } \lambda_1 \leq \lambda_2.$$

Proof. Consider optimizers f_{λ_i} , for λ_i , $i = 1, 2$, respectively. By optimality,

$$\begin{aligned} \mathcal{G}_p(f_{\lambda_1}) + \lambda_1 C(f_{\lambda_1}) &\leq \mathcal{G}_p(f_{\lambda_2}) + \lambda_1 C(f_{\lambda_2}), \text{ and} \\ \mathcal{G}_p(f_{\lambda_2}) + \lambda_2 C(f_{\lambda_2}) &\leq \mathcal{G}_p(f_{\lambda_1}) + \lambda_2 C(f_{\lambda_1}). \end{aligned}$$

Adding these and rearranging yields

$$0 \leq (\lambda_2 - \lambda_1)(C(f_{\lambda_1}) - C(f_{\lambda_2})),$$

which completes the proof. ■

Regarding whether (HC) solutions are (SP) solutions, it should depend on the choice of C . First of all, solutions to the soft penalty problem are “maximally efficient” in the sense that if there exist multiple values of ℓ for which $J(\ell) = \mathcal{G}_p(\hat{f})$, then \mathcal{G}_p^λ will select the one with the smallest ℓ . A priori the hard constraint problem has less restriction. In particular, it is not true for general C that optimizers for \mathcal{G}_p over $\{C(f) \leq \ell\}$ saturate the constraint (i.e. occur only on $\{C(f) = \ell\}$), though this is expected for our choice of Sobolev cost C . Second, even with such a result, one would need to show that for every choice of budget ℓ (excluding two endpoint cases corresponding to $\lambda = 0$ and $\lambda = \infty$) there exists a corresponding λ_ℓ such that a maximally-efficient ℓ -optimizer of (HC) is a λ_ℓ -optimizer of (SP), so that (HC) and (SP) would become “equivalent” in the sense of having identical solution sets. This should be the case in our framework, though we were not able to prove it. To the best of our knowledge, the only result in this direction is a proof in [18] that

in the case $(\mathcal{C}(f), m, p) = (\text{length}(f), 1, 2)$ optimizers saturate the constraint, with more general cases remaining open.

Anyways, the maximal-efficiency property of (SP) is generally desirable in real-world implementations. After all, why pay more if you could get the same performance for less? On the other hand, (HC) is easier to analyze, as it makes the relationship between ℓ and the optimal value $J(\ell)$ more explicit. Indeed, in (SP) it is not always obvious a priori how the choice of λ will relate to the constraint value of an optimal solution. Still, we can derive any qualitative results for (SP) by analyzing (HC) as the solutions to the former belong to the latter. On the other hand, for the computation of optimizers we can use (SP).

To the last point, let us briefly discuss the advantages of employing (SP) in numerical contexts. By moving $\mathcal{C}(f)$ into the objective function, (SP) reduces the problem to an unconstrained optimization. Thus we eschew the need to explicitly parametrize $\{\mathcal{C}(f) \leq \ell\}$, whose structure might be complex. Compare this with the analogous encoding of (HC): Defining the indicator $\chi_\ell(f)$ to be 0 if $\mathcal{C}(f) \leq \ell$ and ∞ otherwise, one may consider the augmented objective $\mathcal{G}_p(f) + \chi_\ell(f)$. However, this functional is discontinuous with respect to the metric induced by $\mathcal{C}(f)$, thus preventing the use of any optimization methods that rely on calculus techniques.

1.7.5. Similar Sobolev Constraints. Our work is similar to some work in the field of image analysis; in particular, it is somewhat complementary to the frameworks of [13, 47]. Note that both of these papers treat only the case $m = 1$.

In [13] a convolution kernel is added to their analogue of \mathcal{G}_p , which has a nice interpretation in terms of the image problem they consider: Whether given a collection of discrete pixels comprising a computer screen or a set of discrete ink dots printed on a sheet of paper, at large enough distances the human eye perceives the image to be “continuous” rather than comprised of discrete pieces.

They show some results that are analogous to ours (particularly regarding existence and consistency), though their analysis is primarily concerned with discretized schemes. More similarly to our work, they also include some theoretical analysis of the case $\mathcal{F} = W^{1,\infty}(X; \Omega)$ and touch briefly on the case of $\mathcal{F} \subseteq W^{k,q}(X; \Omega)$ when exact L^q bounds are placed on the derivatives of each order (e.g. $\|D^\alpha f\|_{L^q} \leq C_\alpha$, where α is a multiindex and C_α is a given constant). By contrast, our work is concerned exclusively with the case $q \in (1, \infty)$, and only places bounds on the overall norm $\|f\|_{W^{k,q}(X; \Omega)}$.

The work of [47] uses a more direct analogue of our \mathcal{G}_2 and focuses particularly on developing numerical algorithms and highlighting some less-obvious example applications. Their algorithms are primarily concerned with the case where $k \in \{1, 2\}$, and $q = \infty$, and also the case where \mathcal{C} is taken to be a geometric constraint like the arc length or total curvature. Thus, to the best of our knowledge our treatment of $m > 1$ and $1 < q < \infty$ is novel.

1.7.6. Spline Smoothing & Surface Reconstruction. We now discuss some similar ideas to (SP) in the context of using splines to fit observed data. We begin with *smoothing splines*, or rather, one of their generalizations to $m \geq 1$, so-called *thin-plate splines*; see e.g. [29, §7.9].

In contravention of our standard notation, temporarily suppose $n = 1$, and suppose that we are given data $\{(x_i, \omega_i)\}_{i=1}^N \subseteq X \times \Omega$ where the ω_i are assumed to

be generated via some process

$$(1.9) \quad \omega_i = f(x_i) + \varepsilon_i.$$

Here, the model f is to-be-determined, and ε_i is a noise term representing error in the observation process; typically ε_i is assumed to have a particular form (e.g. i.i.d. Gaussians) based on domain-specific knowledge. Then, given a “roughness” parameter $\lambda > 0$, so-called *thin-plate splines* are minimizers of the variational problem

$$(1.10) \quad \inf_{f \in W^{k,2}(X;\mathbb{R})} \sum_{i=1}^N (\omega_i - f(x_i))^2 + \lambda \int_X \sum_{|\alpha|=k} (D^\alpha f(x))^2 dx.$$

Note, in some texts the term *thin-plate spline* refers particularly to the case $k = 2$, with $k > 2$ referred to as *higher-order thin-plate splines*.

The idea is that when the observation noise ε_i is nonnegligible, the penalty term in (1.10) helps the solution “smooth out” errors and recover the underlying generating process f in (1.9). In correspondence with our hypothesis of $kq > m$ (H.3.b), solutions of (1.10) exist iff $k \cdot 2 > m$ as well.¹ To summarize, the problem is that as soon as we leave the supercritical regime $k \cdot 2 > m$, the uniform convergence we will see in Corollary 2.5 can fail spectacularly. Since the data-fitting term in (1.10) is dependent only on the behavior of f at individual points, it becomes possible to perfectly interpolate $\{(x_i, \omega_i)\}$ while incurring arbitrarily-small roughness penalty, hence the inf in (1.10) is not achieved.

We highlight that (1.10) deals particularly with scalar-valued f . In [58], the general $n \geq 1$ case was treated under some restrictions on the covariance of the data noise; in [23] a solution is presented for the $m = 1, n \geq 1$ case allowing for general covariances. In any case, while (1.10) has some similarities with (SP) (particularly the case where $p = 2$ and ρ is taken to be an empirical measure on N samples), they remain distinct. First, while our Sobolev penalty $\mathcal{C}(f)$ disincentivizes complexity of all orders in f , the roughness penalty in (1.10) contains only the highest-order weak derivative. This has a nice interpretation as a squared projection distance from $W^{k,2}(X;\mathbb{R})$ onto the set of m -variable polynomials variables of degree at most $k - 1$; see e.g. [79, Ch. 2.8] or [82, Ch. 4.2.1.7].

The consequence is that *global* $(k - 1)$ -degree structure in thin-plate splines is “free;” for example, if $k = 2$ and the data (x_i, ω_i) are restricted to an m -hyperplane in \mathbb{R}^{m+1} , then the optimizer in (1.10) will perfectly interpolate the data regardless of the choice of λ . This is in contrast to the case of our full Sobolev penalty, which would yield solutions that are ≈ 0 when $\lambda \gg 1$ and slowly-expanding m -manifolds approximating $\text{ConvexHull}(\{(x_i, \omega_i)\}_{i=1}^N)$ (with a bias toward the mean of the data) as $\lambda \searrow 0$. Note in particular that solutions of (SP) are incentivized to stop growing soon after they have successfully fitted the data.

A second (and perhaps more important) distinction between the two problems is that the fitting performed by a thin-plate spline is *informed ahead of time* of the proper choice of x_i for each ω_i . No such information is available in (SP); as a consequence, we lose the convexity structure of (regularized) least squares and

¹A fantastic overview of this (and smoothing splines more generally) can be found in online lecture notes by Ryan Tibshirani. *Nonparametric Regression: Splines and RKHS Methods*, Advanced Topics in Statistical Learning, Spring 2024. https://www.stat.berkeley.edu/~ryantibs/statlearn-s24/lectures/splines_rkhs.pdf.

must use different analysis (indeed, \mathcal{G}_p lacks both convexity and concavity over $W^{k,q}(X;\Omega)$; see Section 2.2.1).

Still, there are some spline-based numerical methods (as well as many non-spline-based ones; see e.g. the reviews [40, 83, 86]) that aim to fit *unstructured* data sets. This problem is more similar to our case, though we note that we are not aware of a comprehensive abstract treatment comparable to our formulation. The literature is extensive and difficult to summarize succinctly; we simply mention, for example, [52, 81, 78, 85, 46, 45], particularly highlighting the similarity of the penalty term in [78, Eq. 12] to our Sobolev penalty.

Our context is distinct from these works in a key way: Fundamentally, we do not make any assumptions about the dimension of our target measure ρ —it could be uniform, supported on a fractal, or even a dirac—though we are particularly motivated by examples where ρ is of dimension strictly greater than m . By contrast, when the f in (1.9) is at least C^1 (essentially a necessary assumption given that the goal is to approximate f by objects with regularity), we see that the analogous target measure in the spline-fitting problem will always be at most m -dimensional (c.f. Proposition 3.8), modulo some diffusion introduced by the error term ε_i .

As a tangible example: In Fig. 9, we display simulations for our problem in which a curve grows to approximate the uniform measure on $[-1, 1]^2$. Note that because the target is fundamentally 2-dimensional, the curve becomes highly furrowed and fractal-esque, approaching a space-filling curve in the limit. By contrast, for a spline-fitting algorithm, the analogous problem would be to learn the 1-dimensional boundary set $\{|\omega|_\infty = 1\}$.

1.8. Acknowledgements. The authors owe a significant debt to Andrew Warren for bringing our attention to the existing literature on principal curves, as well as for pointing us toward the measurable selection tools in Section 4.2.1. We would also like to thank Pablo Shmerkin for providing the concise arguments in Lemma 4.12 and Corollary 4.13, and Rentian Yao for pointing out the similarities between our work and smoothing splines. In addition, we would like to thank Dejan Slepčev, Noé Ducharme, and Nitya Gadhiwala for many helpful discussions.

2. PRELIMINARIES

In this section we define the constraint and objective function and prove existence of optimizers. For the sake of brevity, we omit the proofs of the standard facts in Section 2.1.

2.1. The Sobolev Constraint. We use a vector-valued version of the Sobolev norm as our constraint \mathcal{C} . There are established ways to extend the scalar Sobolev norm to such contexts; see e.g. [21, 9, 43]. In order to simplify some arguments we have chosen a slightly different definition that nonetheless yields an equivalent norm in our context. Note, since Sobolev functions are defined on open sets we will temporarily replace X with X° until we can recover X via the Sobolev inequality.

Definition 2.1. As usual we let $W^{k,q}(X^\circ)$ denote the scalar-valued (k, q) Sobolev space on X° . Endow $W^{k,q}(X^\circ; \mathbb{R}^n) := \bigoplus_{j=1}^n W^{k,q}(X^\circ)$ with the norm

$$\|f\|_{W^{k,q}(X^\circ; \mathbb{R}^n)} := \left(\sum_{j=1}^n \|f^j\|_{W^{k,q}(X^\circ)}^q \right)^{1/q},$$

where f^j denotes the j^{th} component function of f . We let $W^{k,q}(X^\circ; \Omega)$ be the restriction of $W^{k,q}(X^\circ; \mathbb{R}^n)$ to those f taking values in Ω and endow it with the inherited norm $\|f\|_{W^{k,q}(X; \Omega)}$ (note that since Ω is compact and convex (H.2), $W^{k,q}(X^\circ; \Omega)$ is not itself a Banach space, but rather a convex subset). We define our constraint function \mathcal{C} to be

$$(2.1) \quad \mathcal{C}(f) = \|f\|_{W^{k,q}(X; \Omega)}.$$

Remark 2.2. Let $S : X^\circ \rightarrow X^\circ$ and $T : \Omega \rightarrow \Omega$ be smooth isometries. Note that in general $\mathcal{C}(f \circ S) = \mathcal{C}(f)$. By contrast we can only guarantee $\mathcal{C}(T \circ f) = \mathcal{C}(f)$ when $q = 2$, since for $q \neq 2$ the q -norms on \mathbb{R}^n are not rotationally-invariant.

2.1.1. *Basic technical facts for the Sobolev constraint \mathcal{C} .* Since $1 < q < \infty$ (H.3.a), $W^{k,q}(X^\circ)$ is a reflexive, separable Banach space whence $W^{k,q}(X^\circ; \mathbb{R}^n)$ is as well. Due to compactness and convexity of Ω (H.2), applying textbook results like [5, Cor. 3.22, Thm. 3.29], we get the following lemma.

Lemma 2.3. *Let Ω be compact and convex (H.2) and let $1 < q < \infty$ (H.3.a). Fix $f \in W^{k,q}(X^\circ; \Omega)$ and for concision let $\mathcal{B}_\ell(f) := \overline{\mathcal{B}}_\ell(f; W^{k,q}(X^\circ; \Omega))$, the closed ball of radius ℓ around f . Then $\mathcal{B}_\ell(f)$ is weakly compact and weakly metrizable.*

Weak metrizability makes weak sequential continuity equivalent to weak continuity. One sees our objective function \mathcal{J}_p (1.2) is continuous on $L^\infty(X; \Omega)$, hence if we can get a relationship between weak convergence in $W^{k,q}(X^\circ; \Omega)$ and uniform convergence this will make it easy to show weak continuity of \mathcal{J}_p . To that end we first recall the Sobolev inequality, which is readily extended to our context.

Proposition 2.4 (General Sobolev Inequality). *Suppose that X° is bounded and that ∂X° is C^1 (H.1). Let $k, q \in \mathbb{N}$ such that $kq > m$ (H.3.b) and let $f \in W^{k,q}(X^\circ; \mathbb{R}^n)$. Define*

$$a := k - 1 - \left\lfloor \frac{m}{q} \right\rfloor$$

$$\gamma := \begin{cases} 1 - \left(\frac{m}{q} - \left\lfloor \frac{m}{q} \right\rfloor \right) & \frac{m}{q} \in \mathbb{N} \\ \text{any positive number} < 1 & \frac{m}{q} \notin \mathbb{N}. \end{cases}$$

Then $f \in C^{a,\gamma}(\overline{X^\circ}; \mathbb{R}^n)$ and there exists a constant C depending only on k, q, m, γ , and X° such that

$$\|f\|_{C^{a,\gamma}(\overline{X^\circ}; \mathbb{R}^n)} \leq C \|f\|_{W^{k,q}(X^\circ; \mathbb{R}^n)}.$$

Conveniently, $C^{a,\gamma}(\overline{X^\circ}; \mathbb{R}^n)$ gives enough structure to show that weak convergence must be at least uniform.

Corollary 2.5. *Take (H.1), (H.2), and (H.3.b). Let $\{f_j\}_{j=1}^\infty$ be a sequence in $W^{k,q}(X; \Omega)$ with $f_j \rightharpoonup f$. Then in fact $f_j \rightarrow f$ uniformly.*

The proof of Corollary 2.5 is a straightforward Arzelà-Ascoli argument. Compactness of Ω (H.2) gives a uniform bound to the $\{f_j\}$ while (H.1), (H.3.b) mean Proposition 2.4 can be used to obtain equicontinuity via a uniform bound to the Hölder coefficients. Then, translating from a uniformly-convergent subsequence to uniform convergence overall can be done via uniqueness of weak limits.

2.1.2. Discussion of Assumptions. Unless stated otherwise, from now on we assume (H.1), (H.2), and (H.3.b), whence we may make free use of Lemma 2.3, Proposition 2.4, and Corollary 2.5. In particular, we may apply Proposition 2.4 to represent any $f \in W^{k,q}(X^\circ; \Omega)$ with an a.e.-equivalent $C^{a,\gamma}(X; \Omega)$ representative. Hence we will interpret “ $W^{k,q}(X; \Omega)$ ” to mean the embedded copy of $W^{k,q}(X^\circ; \Omega) \hookrightarrow C^{a,\gamma}(X; \Omega)$, and we will use the notation $\mathcal{C}(f)$ to denote $\|f\|_{W^{k,q}(X; \Omega)}$.

2.2. The Objective. We now formally define the objective.

Definition 2.6 (Objective Function). For $0 < p < \infty$ let

$$\mathcal{G}_p(f) := \int_{\Omega} \inf_{x \in X} |\omega - f(x)|^p d\rho(\omega).$$

When necessary we will use the notation $\mathcal{G}_p(f; \rho)$ to specify the target measure ρ explicitly.

We are not aware of a reference treating the $0 < p < 1$ regime in detail; in similar fashion we will largely restrict our attention to $1 \leq p < \infty$ (H.4) unless the general case presents no additional complexity. In any case, note \mathcal{G}_p depends only on the image $f(X)$ and not on the parametrization f . We also note that \mathcal{G}_p has a very close relationship to Monge-Kantorovich transport costs (1.5):

Proposition 2.7. *Given fixed $f : X \rightarrow \Omega$, as usual let $Y = f(X)$ and let ν_ρ denote the pushforward of ρ under the closest-point projection $\pi_f : \Omega \rightarrow Y$, tiebreaking measurably (e.g. Proposition 4.1) when π_f is not uniquely-determined. Then*

$$\mathcal{G}_p(f) = \mathbb{W}_p^p(\rho, \nu_\rho) = \inf_{\nu \in \mathcal{P}(Y)} \mathbb{W}_p^p(\rho, \nu).$$

Proof. We begin with the first equality. Define $\gamma^* = (\text{id}, \pi_f)_\# \rho$ and note $\gamma^* \in \Gamma(\rho, \nu_\rho)$. By definition $\mathcal{G}_p(f) = \int_{\Omega} |\omega - \pi_f(\omega)|^p d\rho = \int_{\Omega \times Y} |\omega - y|^p d\gamma^*(\omega, y)$, so we see $\mathcal{G}_p(f) \geq \mathbb{W}_p^p(\nu_\rho, \rho)$. Suppose, to obtain a contradiction, that the inequality were strict. Then there exists a more efficient transport plan $\tilde{\gamma}^* \in \Gamma(\rho, \nu_\rho)$ and a set $A \subseteq \Omega$ such that

$$\int_{A \times Y} |\omega - y|^p d\tilde{\gamma}^*(\omega, y) < \int_{A \times Y} |\omega - y|^p d\gamma^*(\omega, y) = \int_{A \times Y} |\omega - \pi_f(\omega)|^p d\rho(\omega).$$

By the marginal condition, $\tilde{\gamma}^*(A \times Y) = \rho(A) = \gamma^*(A \times Y)$. So there exists at least one (ω_0, y_0) pair such that $|\omega_0 - y_0|^p < |\omega_0 - \pi_f(\omega_0)|^p$, a contradiction to the definition of π_f . So $\mathcal{G}_p = \mathbb{W}_p^p(\nu_\rho, \rho)$ as desired.

For the second equality, note we already have $\mathbb{W}_p^p(\rho, \nu_\rho) \geq \inf_{\nu} \mathbb{W}_p^p(\rho, \nu)$. Hence suppose, to obtain a contradiction, that there exists ν_0 such that $\mathbb{W}_p^p(\rho, \nu_\rho) > \mathbb{W}_p^p(\rho, \nu_0)$. Let $\gamma^* \in \Gamma(\rho, \nu_\rho)$ and $\tilde{\gamma}^* \in \Gamma(\rho, \nu_0)$. Since both measures share the same first marginal one may proceed exactly as before to derive a contradiction. ■

This justifies the intuitive statements we made previously about $\mathcal{G}_p(f)$ measuring how well f “approximates” ρ .

Remark 2.8. Note that in light of Proposition 2.7, when $0 < p < 1$ one could develop economic interpretations for \mathcal{G}_p analogous to those given for $\mathbb{W}_p^p(\cdot, \cdot)$ in [25]. In particular, it would be interesting to study how qualitative properties of optimizers change at the critical value $p = 1$.

2.2.1. *Nonconcavity and Nonconvexity of \mathcal{G}_p .* Given Proposition 2.7 it is natural to ask whether \mathcal{G}_p possesses any sort of concavity or convexity. This turns out to be too much to hope for: in general, \mathcal{G}_p is both nonconcave and nonconvex.

For nonconcavity, note that when $p \geq 1$ (H.4), the p^{th} -power function $x \mapsto |x|^p$ is a nonlinear, convex function, and thus nonconcave. When $p > 1$, \mathcal{G}_p inherits this nonconcavity trivially, as can be seen by interpolating between any pair of constant functions $f_0 \neq f_1$. When $p = 1$ the nonconcavity behavior is slightly different, but can still be obtained as long as $n > 1$ (as can be seen by considering $\Omega = [0, 1]$ and $\rho = \frac{1}{2}(\delta_0 + \delta_1)$, this $n > 1$ hypothesis is essential).

On the other hand, even with convexity of $|x|^p$, it is easy to demonstrate that \mathcal{G}_p is not convex either. To make the argument simpler we first note a trivial property of \mathcal{G}_p .

Proposition 2.9. *Let $f_0, f_1 : X \rightarrow \Omega$; denote their images by Y_0, Y_1 . Suppose $Y_0 \subseteq Y_1$. Then $\mathcal{G}_p(f_1) \leq \mathcal{G}_p(f_0)$. If, further, there exists $y \in Y_1 \setminus Y_0$ such that (1) $y \in \text{supp}(\rho)$ and (2) $d(y, Y_0) > 0$, then $\mathcal{G}_p(f_1) < \mathcal{G}_p(f_0)$.*

Then we have:

Counterexample 2.10 (Nonconvexity). Suppose $\text{supp}(\rho)$ contains at least two distinct points, call them ω_0 and ω_1 . Fix an arbitrary smooth surjection $\varphi : X \rightarrow [0, 1]$. (e.g. projection on an axis plus normalization). By (H.2) Ω is convex, so

$$f_0(x) := (1 - \varphi(x))\omega_0 + \varphi(x)\omega_1 \quad \text{and} \quad f_1(x) := \varphi(x)\omega_0 + (1 - \varphi(x))\omega_1$$

are both admissible in $W^{k,q}(X; \Omega)$. Define $f_{.5} = \frac{1}{2}(f_0 + f_1) \equiv \frac{\omega_0 + \omega_1}{2}$. Since $\mathcal{G}_p(f_0) = \mathcal{G}_p(f_1)$, applying Proposition 2.9 gives $\frac{1}{2}(\mathcal{G}_p(f_0) + \mathcal{G}_p(f_1)) = \mathcal{G}_p(f_0) < \mathcal{G}_p(f_{.5})$.

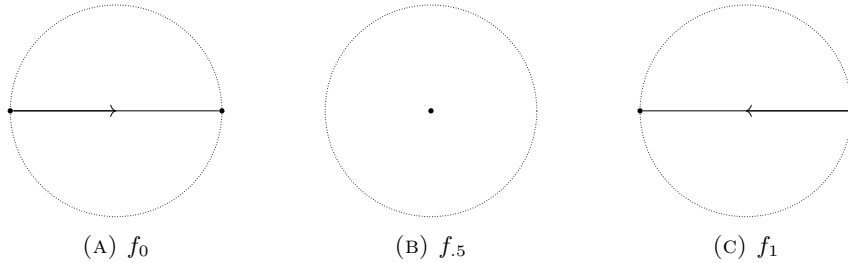


FIGURE 4. Example for $\Omega = B_1(0; \mathbb{R}^2)$ and $(\pm 1, 0) \in \text{supp}(\rho)$.

Theorem 2.10 is “trivial” in the sense that we have $Y_0 = Y_1$. Many other counterexamples can be constructed in which Y_0, Y_1 are equivalent under symmetry action on Ω (for example, $Y_0 = [0, 1] \times \{0\}$, $Y_1 = [-1, 0] \times \{0\}$). Thus one might wonder if it is possible to salvage convexity of \mathcal{G}_p by modding out by the “right”

choice of symmetry group of Ω . Unfortunately, Theorem 2.11 seems to imply the answer is no.

Counterexample 2.11 (Nonconvexity, Asymmetric Example). One may apply Proposition 2.9 to $f_0, f_{.5}, f_1$ having the following images:

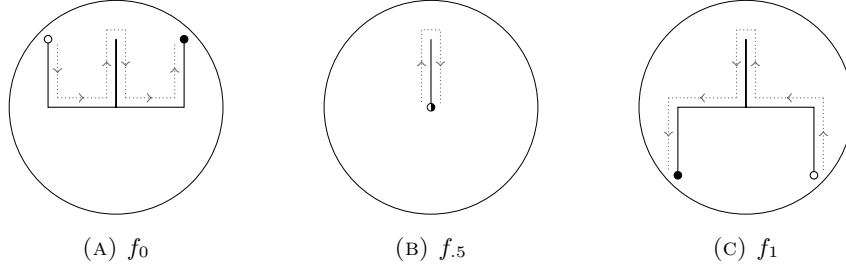


FIGURE 5. Example $f_0, f_{.5}$ and f_1 for which $Y_0 \neq Y_1$.

Note in Fig. 5 the unfilled/filled circles represent the starting/ending points in a 1-d parametrization à la $\varphi(x)$ in Theorem 2.10. Using an argument similar to Lemma 3.6 one may show that φ can be made smooth whence $f_0, f_{.5}$, and f_1 are all admissible.

In any case, the intuition is that nonconvexity tends to arise from cancellation, while nonconcavity (when $p > 1$) tends to arise from the convexity of $x \mapsto |x|^p$. Both appear to be fundamental features of the problem.

2.3. Continuity Properties of \mathcal{G}_p . $\mathcal{G}_p(f; \rho)$ has a very helpful continuity property that will be used in proving existence of optimizers and also in establishing the consistency results later on. Note this result does not rely on (H.4).

Theorem 2.12 (Joint Sequential Continuity). *Take (H.2) and let $\{f_M\}, \{\rho_N\}$ be convergent in $C(X; \Omega)$ and $\mathcal{P}(\Omega)$, respectively, with the former given the topology of uniform convergence and the latter given the usual weak-* topology. Then*

$$\lim_{M, N \rightarrow \infty} \mathcal{G}_p(f_M; \rho_N) = \mathcal{G}_p(f_\infty; \rho_\infty).$$

In particular, if one also takes (H.1) and (H.3.b), then by Corollary 2.5 if $\{f_M\}$ is any sequence converging weakly in $W^{k,q}(X; \Omega)$, the same result holds.

Proof. We employ the Moore-Osgood theorem for double limits. It suffices to show

- (i) $\mathcal{G}_p(f_M; \rho_N) \rightarrow \mathcal{G}_p(f_\infty; \rho_N)$ uniformly in N , and
- (ii) for each M , $\mathcal{G}_p(f_M; \rho_N) \rightarrow \mathcal{G}_p(f_M; \rho_\infty)$.

For (i): For all x, ω , we have $||f_M(x) - \omega| - |f_\infty(x) - \omega|| \leq |f_M(x) - f_\infty(x)|$, and so $f_M \xrightarrow{u} f_\infty$ gives $d(f_M, \omega) \xrightarrow{u} d(f_\infty, \omega)$ in ω . Then since Ω is compact (H.2),

$$\inf_{x \in X} |f_M(x) - \omega|^p \xrightarrow{u} \inf_{x \in X} |f_\infty(x) - \omega|^p$$

as functions of ω . Finally since the ρ_N are probability measures we have $\mathcal{G}_p(f_M; \rho_N) \rightarrow \mathcal{G}_p(f_\infty; \rho_N)$ uniformly in N , as desired.

For (ii): Note that $\inf_{x \in X} |f_M(x) - \omega|^p$ is a bounded, continuous function of ω , so by weak convergence of the ρ_N we immediately get

$$\int_{\Omega} \inf_{x \in X} |f(x) - \omega|^p d\rho_N \rightarrow \int_{\Omega} \inf_{x \in X} |f(x) - \omega|^p d\rho,$$

as desired. Thus the double limit exists, namely,

$$\lim_{M, N \rightarrow \infty} \mathcal{G}_p(f_M; \rho_N) = \lim_{M \rightarrow \infty} \lim_{N \rightarrow \infty} \mathcal{G}_p(f_M; \rho_N) = \lim_{M \rightarrow \infty} \mathcal{G}_p(f_M; \rho_\infty) = \mathcal{G}_p(f_\infty; \rho_\infty)$$

as desired. \blacksquare

3. EXISTENCE OF OPTIMIZERS AND PROPERTIES OF J

We now have everything we need to show existence of solutions to (HC). But first we address a small technical detail when $0 \notin \Omega$. We remind the reader that when writing $\{C(f) \leq \ell\}$ it should be understood that we are considering only $f \in W^{k,q}(X; \Omega)$. Define

$$(3.1) \quad \ell_{\min} = \inf \{\ell \mid \{C(f) \leq \ell\} \neq \emptyset\}.$$

Recall our global assumptions (H.2) and (H.3.a), which stipulate that Ω is compact and convex and that $q > 1$. So in general ℓ_{\min} is achieved by a unique constant function

$$(3.2) \quad \omega_C = \arg \min_{\omega \in \Omega} C(\omega) = \arg \min_{\omega \in \Omega} |\omega|^q.$$

Clearly $0 \in \Omega$ iff $\omega_C = 0$ iff $\ell_{\min} = 0$. Not much would be lost by assuming $0 \in \Omega$; nonetheless, we treat the general case since doing so adds little complexity and the case $\ell_{\min} \neq 0$ might be of interest in applications (for example, if a package delivery service has its central warehouse located outside a city modeled by Ω).

3.1. Existence & Nonuniqueness of Optimizers.

Theorem 3.1 (Existence of Optima). *Take (H.1), (H.2), (H.3.a), and (H.3.b). Fix $\ell \geq \ell_{\min}$. Then \mathcal{G}_p attains its optima on $\{C(f) \leq \ell\}$. In particular (HC) has solutions.*

Proof. Using (H.2), (H.3.a), the definition of ℓ_{\min} implies $\{C(f) \leq \ell\}$ is nonempty, and by Lemma 2.3, $\{C(f) \leq \ell\}$ is weakly compact and weakly metrizable. From weak metrizability we get that weak continuity and weak sequential continuity are equivalent. By (H.1), (H.2), and (H.3.b), Theorem 2.12 implies \mathcal{G}_p is weakly sequentially continuous, hence it is weakly continuous on $\{C(f) \leq \ell\}$. So continuity-compactness gives that \mathcal{G}_p achieves its optima on $\{C(f) \leq \ell\}$. \blacksquare

Note that Theorem 3.1 relies on the fact that ρ is a probability measure. However, it does not require (H.4), (H*). In any case, we will refer to solutions of (HC) as ℓ -optimizers. We now discuss some trivial cases of nonuniqueness arising when the optimizer is nonconstant. We first show that for all ℓ sufficiently large, the optimizers *must* be nonconstant. To that end we define another special constant function:

$$(3.3) \quad \omega_g \in \arg \min_{\omega \in \Omega} \mathcal{G}_p(\omega).$$

Here ω_g (known as the p -mean; see [17, 16]) corresponds to the geometric median of ρ when $p = 1$ and the ρ -mean when $p = 2$. It is unique for $p > 1$ as well as when $p = 1$ as long as ρ is not essentially 1-dimensional [16].

Remark 3.2. The theory becomes cleaner if one assumes $\omega_C = \omega_g$. In general $\omega_C = 0$ or $\omega_C \in \partial\Omega$; on the other hand, (H*) gives $\omega_g \in \Omega^\circ$. So the only way to force $\omega_C = \omega_g$ is to make the translation $\Omega \mapsto \Omega - \omega_g$. Doing so is a nontrivial

simplification that will qualitatively change ℓ -optimizers for small ℓ ; nevertheless as $\ell \rightarrow \infty$ the differences between Ω and $\Omega - \omega_g$ are no longer so important as the 0th-order term in \mathcal{C} becomes negligible. So the assumption is not severe if one is only treating asymptotics.

Let us define

$$(3.4) \quad \ell_{\text{nc}} := \mathcal{C}(\omega_g).$$

The subscript “nc” was chosen for “non-constant” in light of the following:

Proposition 3.3. *Suppose Ω is convex (e.g. via (H.2)) and $\mathcal{C}(f)$ is a seminorm that is finite on smooth functions (e.g. via (H.3)). Then if $\rho \neq \delta_{\omega_g}$, then for all $\ell > \ell_{\text{nc}}$, ℓ -optimizers are nonconstant.*

Notice that ℓ -optimizers can be non-unique, and one may obtain trivial counterexamples for $q = 2$ when $\text{supp}(\rho)$ has symmetries. To that end first recall that if $\varphi : A \subseteq \mathbb{R}^N \rightarrow A$ is an isometry then $\varphi(a) = Ta + b$ where T is an orthogonal linear transformation; thus $|D\varphi| = 1$ and $|D^\alpha \varphi| = 0$ for higher α .

Counterexample 3.4 (Nonuniqueness). Suppose $\rho \neq \delta_{\omega_g}$ and for some $\ell > \ell_{\text{nc}}$ let f_ℓ be an ℓ -optimizer. Suppose $\psi : \Omega \rightarrow \Omega$ is a nontrivial isometry with $\psi_\#(\rho) = \rho$, and let $\tilde{f}_\ell = \psi \circ f_\ell$. Then $\mathcal{G}_p(\tilde{f}_\ell) = \mathcal{G}_p(f_\ell)$ and (provided $q = 2$) $\mathcal{C}(\tilde{f}_\ell) = \mathcal{C}(f_\ell)$, but $\tilde{f}_\ell \neq f_\ell$. Note that f_ℓ being nonconstant is important for getting $\tilde{f}_\ell \neq f_\ell$; otherwise f_ℓ could be the fixed point of ψ .

3.2. Properties of J . Recall $J : [\ell_{\min}, \infty) \rightarrow \mathbb{R}^{\geq 0}$ given in (1.3). In view of Theorem 2.12, the following result is straightforward:

Theorem 3.5. *Take (H.1), (H.2), (H.3.a), and (H.3.b). Then J is nonincreasing, bounded, and continuous.*

Proof. The fact that J being nonincreasing is immediate: For all $\ell_{\min} \leq \ell_0 \leq \ell_1$, $\{\mathcal{C}(f) \leq \ell_0\} \subseteq \{\mathcal{C}(f) \leq \ell_1\}$ so $J(\ell_1) \leq J(\ell_0)$. For boundedness: The value $J(\ell)$ is trivially bounded below by 0 and above by $J(\ell_{\min}) = \mathcal{G}_p(\omega_{\mathcal{C}})$.

Now we show J is right continuous. Fix $\ell_0 \geq \ell_{\min}$ and let $\{\ell_j^+\}_{j=1}^\infty$ with $\ell_j^+ \searrow \ell_0$. Since $J(\ell)$ is nonincreasing in ℓ , $J(\ell_j^+)$ is nondecreasing in j and also bounded above by $J(\ell_0)$. Thus $J(\ell_j^+)$ converges to some $J_\infty^+ \leq J(\ell_0)$. We claim $J_\infty^+ \geq J(\ell_0)$ too. For each j let f_j^+ be an ℓ_j^+ -optimizer. Note $\{f_j^+\}_{j=1}^\infty \subseteq \{\mathcal{C}(f) \leq \ell_1^+\}$, which by Lemma 2.3 (H.2), (H.3.a) is weakly compact. Thus there exists a subsequence $\{f_{j_i}^+\}_{i=1}^\infty$ converging weakly to some $f_\infty^+ \in \{\mathcal{C}(f) \leq \ell_1^+\}$; by Theorem 2.12 (H.1), (H.2), (H.3.a), (H.3.b) we see $\mathcal{G}_p(f_\infty^+) = J_\infty^+$. Finally since \mathcal{C} is defined via a norm it is weakly-l.s.c. whence $\mathcal{C}(f_\infty^+) \leq \ell_0$. In particular since $J(\ell_0)$ is the minimum value over $\{\mathcal{C}(f) \leq \ell_0\}$ we get $J(\ell_0) \leq \mathcal{G}_p(f_\infty^+) = J_\infty^+$. So J is right-continuous as desired.

Now we show J is left continuous. Fix $\ell_0 > \ell_{\min}$ and let $\{\ell_j^-\}_{j=1}^\infty$ with $\ell_j^- \nearrow \ell_0$. Let f_0 be a ℓ_0 -optimizer and for all j define $t_j = (\ell_j^- - \ell_{\min})/(\ell_0 - \ell_{\min})$ and $f_j^- = t_j f_0 + (1 - t_j)\omega_{\mathcal{C}}$. Note that since Ω is convex (H.2) and f_j^- is constructed via a convex combination, $f_j^-(X) \subseteq \Omega$. Also note that

$$\mathcal{C}(f_j^-) \leq t_j \ell_0 + (1 - t_j)\ell_{\min} = \ell_j^-,$$

whence $\mathcal{G}_p(f_j^-) \geq J(\ell_j^-) \geq J(\ell_0) = \mathcal{G}_p(f_0)$. Since $f_j^- \rightarrow f_0$ strongly, as in the previous case weak continuity implies $\mathcal{G}_p(f_j^-) \rightarrow \mathcal{G}_p(f_0)$, whence $J(\ell_j^-) \rightarrow J(\ell_0)$ as well. So $J(\ell)$ is both left-continuous and right-continuous; thus it is continuous. ■

Supposing the constraint is *effective* (i.e. “ $\mathcal{C}(f) < \infty$ implies $\mathcal{G}_p(f) \neq 0$ ”; see Proposition 3.8) we expect J to be *strictly decreasing* rather than just nonincreasing. This was shown for $\mathcal{C}(f) = \text{length}(f)$ in [18], but as usual the local modification argument does not carry over when $k > 1$. It would suffice to prove optimizers can occur only on $\{\mathcal{C}(f) = \ell\}$; we were unable to find a proof of this, but show in Corollary 3.7 that at least $\{\mathcal{C}(f) = \ell\}$ is always guaranteed to contain an optimizer. In fact, this is a simple consequence of reparametrization and does not depend on (H.1)–(H.3.b).

Lemma 3.6 (Arbitrarily Bad Reparametrizations). *Let f be nonconstant with $\ell = \mathcal{C}(f)$. Then for all $\tilde{\ell} > \ell$ there exists $\varphi : X \rightarrow X$ such that*

- i) $\tilde{f} := f \circ \varphi \in W^{k,q}(X; \Omega)$,
- ii) $\tilde{f}(X) = f(X)$, and
- iii) $\mathcal{C}(\tilde{f}) = \tilde{\ell}$.

Proof. We have two cases: $k > 1$ and $k = 1$. For $k > 1$: First, we exhibit a family of smooth surjections $\varphi_\varepsilon : B_1(0; \mathbb{R}^m) \rightarrow B_1(0; \mathbb{R}^m)$ where $\varepsilon \in (0, 1]$ such that $\varphi_1 = \text{id}(x)$ and for all multiindices $|\alpha| > 1$, $\lim_{\varepsilon \rightarrow 0^+} \|D^\alpha \varphi_\varepsilon\|_{L^q} = \infty$. Let

$$\sigma(t) = \begin{cases} 0 & t \in (-\infty, 0] \\ \frac{e^{-1/t}}{e^{-1/t} + e^{-1/(1-t)}} & t \in (0, 1) \\ 1 & t \in [1, \infty). \end{cases}$$

For all $\varepsilon \in (0, 1]$ let $\psi_\varepsilon(x) = \hat{x}\sigma(|x|/\varepsilon)$. $\psi_\varepsilon(x)$ is a smooth surjection and for $|\alpha| > 1$, $\lim_{\varepsilon \rightarrow 0^+} \|D^\alpha \psi_\varepsilon\|_{L^q} = \infty$. Now let $\varphi_\varepsilon(x) = (1 - \varepsilon)\psi_\varepsilon(x) + \varepsilon \text{id}(x)$. By construction φ_ε is smooth. To see φ_ε is surjective write $\varphi_\varepsilon(x) = \hat{x}\left((1 - \varepsilon)|\psi_\varepsilon(x)| + \varepsilon|x|\right)$ and note that for all $\varepsilon \in (0, 1]$, the scalar term is 0 when $|x| = 0$, 1 when $|x| = 1$, and strictly increasing in $|x|$. Now we use the φ_ε to define \tilde{f} . Let $x \in X$ such that f is nonconstant at x_0 . Fix $r > 0$ and define

$$\tilde{f}_\varepsilon(x) = \begin{cases} f(x) & x \notin B_r(x_0) \\ f(x_0 + r\varphi_\varepsilon(\frac{x-x_0}{r})) & x \in B_r(x_0). \end{cases}$$

By smoothness and surjectivity of φ_ε we have $\tilde{f}_\varepsilon \in W^{k,q}(X; \Omega)$ and $\tilde{f}_\varepsilon(X) = f(X)$. Note $\mathcal{C}(\tilde{f}_\varepsilon)$ is continuous in ε and $\lim_{\varepsilon \rightarrow 0^+} \mathcal{C}(\tilde{f}_\varepsilon) = \infty$. Hence there exists a particular ε yielding $\mathcal{C}(\tilde{f}_\varepsilon) = \tilde{\ell}$ as desired.

For the case $k = 1$, the same flavor of construction works if one modifies ψ_ε such that its values oscillate between 0 and ∂B_1 arbitrarily many times as $\varepsilon \rightarrow 0^+$. ■

Corollary 3.7 (Existence of Saturating Optimizers). *For all $\ell > \ell_{\text{nc}}$, there exists $f \in \{\mathcal{C}(f) = \ell\}$ with $\mathcal{G}_p(f) = J(\ell)$.*

Proof. Let f_ℓ be an ℓ -optimizer. If $\mathcal{C}(f_\ell) < \ell$ then we can use Lemma 3.6 to reparametrize to get \tilde{f}_ℓ such that $\mathcal{C}(\tilde{f}_\ell) = \ell$ and $\tilde{f}_\ell(X) = f_\ell(X)$, whence $\mathcal{G}_p(\tilde{f}_\ell) = \mathcal{G}_p(f_\ell) = J(\ell)$. ■

3.3. Asymptotics for J . We discuss how $J(\ell)$ behaves as $\ell \rightarrow \infty$.

A first question is whether it is possible to achieve $J(\ell) = 0$ with finite ℓ . Proposition 3.8 gives sufficient conditions for guaranteeing this does not occur. Note (H.3.b) is used only in getting Proposition 2.4, while (H.1) appears in the proof on its own.

Proposition 3.8 (Effectiveness of $\mathcal{C}(f)$). *Recall (see e.g. [54]) that we may extend the notion of Hausdorff dimension from subsets of \mathbb{R}^n to Borel measures by letting*

$$\dim_{\mathcal{H}}(\rho) = \inf \{ \dim_{\mathcal{H}}(A) \mid A \text{ is Borel and } \rho(A) > 0 \}.$$

Take (H.1), (H.3.b) and let $C^{a,\gamma}(X; \Omega)$ be the Hölder space guaranteed by Proposition 2.4. Then if

- (1) $a \geq 1$ and $\dim_{\mathcal{H}}(\rho) > m$, or
- (2) $a = 0$ and $\dim_{\mathcal{H}}(\rho) > m/\gamma$,

then the constraint is effective (i.e. for all $f \in W^{k,q}(X; \Omega)$, $\mathcal{G}_p(f) > 0$) and as a consequence, for all $\ell \in [\ell_{\min}, \infty)$ we have $J(\ell) > 0$.

Proof. Fix an arbitrary $f \in W^{k,q}(X; \Omega)$. In the first case, since $f \in C^1$ we see $\dim_{\mathcal{H}}(f(X)) \leq m$, hence $\rho(\text{supp}(\rho) \setminus f(X)) > 0$ (otherwise, $\dim_{\mathcal{H}}(\rho) \leq m$ a contradiction) and thus $\mathcal{G}_p(f) > 0$. For the second case, denote the d -dimensional Hausdorff measure by \mathcal{H}^d . Then a standard argument shows that there exists a constant C depending only on d, γ such that

$$\mathcal{H}^{d/\gamma}(f(X)) \leq C\mathcal{H}^d(X).$$

In particular, (H.1) gives $\dim_{\mathcal{H}}(X) = m$, whence for all $d > m$ we have $\mathcal{H}^{d/\gamma}(f(X)) \leq C\mathcal{H}^d(X) = 0$. Thus $\dim_{\mathcal{H}}(f(X)) \leq m/\gamma$ and so $\rho(\text{supp}(\rho) \setminus f(X)) > 0$, whence $\mathcal{G}_p(f) > 0$. Lastly, fixing $\ell \in [\ell_{\min}, \infty)$ and an ℓ -optimizer $f_\ell \in \{\mathcal{C}(f) \leq \ell\}$, the above gives $J(\ell) = \mathcal{G}_p(f_\ell) > 0$. \blacksquare

When the constraint is effective, it's meaningful to ask about the rate at which $J(\ell) \searrow 0$ as $\ell \rightarrow \infty$. Proposition 3.9 below provides a very coarse bound in this direction. Our argument centers around constructing a degenerate f with $\dim_{\mathcal{H}}(f(X)) = 1$ independent of m , hence we imagine there should exist a tighter bound highlighting the relationship between $\dim_{\mathcal{H}}(f(X))$ and $\dim_{\mathcal{H}}(\text{supp}(\rho))$ similarly to Proposition 3.8. In any case, note that when $k = p = 1$ and $q \rightarrow \infty$ Proposition 3.9 recovers the bound [8, Theorem 3.16], which inspired the proof below.

Proposition 3.9. *Take (H.1), (H.2), and (H.3.b). Then there exists a constant C depending only on X, Ω such that for all $\varepsilon > 0$, taking $\ell > C\varepsilon^{(1-n(k+q^{-1}))/p}$ yields $J(\ell) \leq \varepsilon$.*

Proof. Fix some $\varepsilon > 0$. We provide a sketch for the construction of an f with $\mathcal{C}(f) < \infty$ such that $\mathcal{G}_p(f) \leq \varepsilon^p$. To that end let M_ε be the ε -covering number of Ω and let $\{\omega_j^\varepsilon\}$ be an ε -covering of Ω by M_ε points. We may abstract $\{\omega_j^\varepsilon\}$ as a graph G_ε with M_ε vertices and edges between those $\omega_j, \omega_{j'}$ with $d(\omega_j, \omega_{j'}) < 2\varepsilon$. Call a walk on G_ε *spanning* if it visits every vertex at least once. Since Ω is connected (H.2), G_ε is connected, so there exists a minimal spanning tree T_ε . A simple inductive argument then shows that for $M_\varepsilon \geq 2$, T_ε has a spanning walk of length at most $N_\varepsilon \leq 2M_\varepsilon - 3$; denote this walk $\{v_1, v_2, \dots, v_{N_\varepsilon}\}$.

As in the proof of Lemma 3.6 let σ denote a smooth step function; note that $\sigma \in W^{k,q}([0, 1]; \mathbb{R})$. Now subdivide $[0, 1]$ into N_ε equal subintervals I_j and define a piecewise-smooth curve γ by

$$\gamma(t) = v_j + (v_{j+1} - v_j)\sigma(N_\varepsilon(t - t_j)) \quad \text{for } t \in I_j, \quad j = 1, \dots, N_\varepsilon.$$

Then since Ω is convex (H.2), $\gamma \in W^{k,q}([0, 1]; \Omega)$ with

$$\mathcal{C}(\gamma) \leq (\text{diam}(\Omega)^q + N_\varepsilon \varepsilon^q \|\sigma(N_\varepsilon t)\|_{W^{k,q}([0,1])}^q)^{1/q}.$$

Note that $\|\sigma(at)\|_{W^{k,q}([0,1]; \mathbb{R})}$ is $O(a^k)$ as $a \rightarrow \infty$; denote the constant by C_0 and note it is independent of X, Ω . As $\varepsilon \rightarrow 0$ we get $N_\varepsilon \rightarrow \infty$, whence

$$\begin{aligned} &\leq (\text{diam}(\Omega)^q + C_0 \varepsilon^q N_\varepsilon^{kq+1})^{1/q} \\ &\leq C_1 \varepsilon N_\varepsilon^{k+1/q}, \end{aligned}$$

where in the last line we have used the fact that the second term dominates as $\varepsilon \rightarrow 0$. Note C_1 depends only on Ω . Since $N_\varepsilon \leq 2M_\varepsilon - 3$, a standard covering number bound gives $\mathcal{C}(f) \leq C_2 \varepsilon^{1-n(k+(1/q))}$, with C_2 depending only on Ω . Define a smooth function $\varphi : X \rightarrow [0, 1]$ such that $\|\varphi\|_{W^{k,q}(X; [0,1])}$ depends only on X . Then $f := \gamma \circ \varphi \in W^{k,q}(X; \Omega)$ with $\mathcal{G}_p(f) \leq \varepsilon^p$ and for some C depending only on X, Ω we have $\mathcal{C}(f) \leq C \varepsilon^{1-n(k+q^{-1})}$, from which the claim follows. ■

As an alternative approach to the sort of argument in Proposition 3.9, one might consider starting with an $f \notin W^{k,q}(X; \Omega)$ but with $\mathcal{G}_p(f) = 0$ and finding ways to approximate it with elements of $W^{k,q}(X; \Omega)$.

Proposition 3.10 (Smoothing ρ -Fillings). *Take (H.1), (H.2), and (H.3.b). Let $f_\infty : X \rightarrow \Omega$ such that $\text{supp}(\rho) \subseteq f(X)$. Let $\varphi : X \rightarrow \mathbb{R}$ be a mollifier and define $\varphi_\theta(x) := \theta^{-m} \varphi(x/\theta)$. Suppose $f_N \xrightarrow{u} f_\infty$ (note that one could take $f_N = f_\infty$ for all N) and for all $\theta > 0$, define $f_N^\theta = f_N * \varphi_\theta$. Then $f_N^\theta \in W^{k,q}(X; \Omega)$ and*

$$\lim_{\substack{\theta \rightarrow 0 \\ N \rightarrow \infty}} \mathcal{G}_p(f_N^\theta) = \mathcal{G}_p(f_\infty) = 0.$$

The proof is a direct application of the Moore-Osgood theorem similar to the argument for Theorem 2.12.

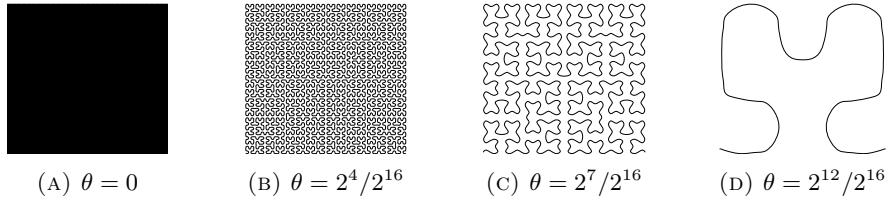


FIGURE 6. Mollifying an 8th-order Hilbert curve by bump functions of varying width θ .

4. THE “GRADIENT” OF \mathcal{G}_p : THE BARYCENTER FIELD.

We now turn to the “gradient” of the functional \mathcal{G}_p , which is relevant, in particular, to local improvement of $\mathcal{G}_p(f)$. For this purpose, we define a vector field we call the *barycenter field*, which is essentially a succinct way of encoding the first

variation of \mathcal{G}_p . Note that for now we will denote the barycenter field simply by F ; later notation will include subscripts to reflect dependencies on how one chooses to tiebreak ambiguities in the closest-point projection. In any case, we discuss relationships between F and existing work in Section 4.1 below; for now we summarize the main takeaways about F .

In general, F is defined on X and depends on the choice of variational perturbation ξ . The first main result of the section, Theorem 4.8, verifies under mild hypotheses that this F indeed encodes the first variation of $\mathcal{G}_p(f)$. Importantly, Theorem 4.8 does not require any regularity of f , ξ beyond continuity, and when $p > 1$, we need no hypotheses on ρ beyond $\rho \in \mathcal{P}(\Omega)$. When $p = 1$ we must add a hypothesis that a set of “problem points” in the image set $Y = f(X)$ is ρ -null. This is necessary due to the way we have defined F , reflecting the lower regularity of the $p = 1$ case.

The X -parametrized form of F used in Theorem 4.8 is an important theoretical tool. However, the generality of the hypotheses necessitates defining F through multiple implicit minimizations, some of which can make simulations computationally intractable. Thus we also consider a simplified case: When the set of self-intersections of f are null with respect to a certain measure we may instead parametrize F by the image $Y = f(X)$, and a further hypothesis that the closest-point projection is ρ -a.e. well-defined allows us to reduce F to the Frechét derivative of \mathcal{G}_p (Corollary 4.10).

However, from a theoretical standpoint, even in the Y -parametrized case it is nontrivial to use F to derive local improvements to a given f . This is because F often lacks regularity—it can be discontinuous even when Y is a C^1 -submanifold of Ω (Theorem 4.7)—and so $f + \varepsilon F$ might not remain in the Sobolev class. Nonetheless, in the second main result of the section (Theorem 4.14) we show that as long as F is “nontrivial” in some sense then there exists a smooth, local perturbation improving $\mathcal{G}_p(f)$. We conjecture that every ℓ -optimizer has this nontriviality property, whence the monotonicity in Theorem 3.5 would become strict. However, we were not able to find a proof.

The layout of the remainder of the section is as follows. In Section 4.1 we discuss similar ideas in the literature, with a particular eye toward motivating the relaxed hypotheses of Theorem 4.8. In Section 4.2 we introduce some measurable selection tools that are necessary for defining F in this relaxed case and also list some basic properties of F , including its lack of regularity. Section 4.3 establishes the relationship between F and the first variation of \mathcal{G}_p , and Section 4.4 shows that although F might lack regularity, when F is “nontrivial” we may still use it to obtain smooth, local improvements to $\mathcal{G}_p(f)$.

4.1. Motivation for The Barycenter Field and Comparison to Previous Techniques.

First, one might wonder why it is even necessary to appeal to the first variation of $\mathcal{G}_p(f)$ in order to obtain local improvements. For example, suppose f is a curve (i.e. $m = 1$): Is it not possible to simply “make the curve longer?”

If the special constant function ω_c defined in (3.2) is in $(\text{supp}(\rho))^\circ$ and if $\ell \ll \text{diam}(\Omega)$ then this will work. However, the general case is more difficult. For ℓ sufficiently large it becomes possible that $Y \cap \partial \text{supp}(\rho) \neq \emptyset$ in such a way that extending f past its endpoints might yield no improvement to \mathcal{G}_p (for example, take $\Omega = B_1(0)$, $\rho = \text{Unif}_\Omega$, and f a parametrization of a diameter). Importantly, in such cases, the inclusion of higher-order terms in our Sobolev constraint might

prevent us from adding a “sharp turn” to send the extended f back inside $\text{supp}(\rho)$. Thus, to analyze the Sobolev case we turn to the barycenter field F .

As stated earlier, F is essentially just a succinct way of encoding the first variation of \mathcal{G}_p at f with respect to a perturbation ξ ; denote this by $\delta\mathcal{G}_p[f; \xi]$. Note that $\delta\mathcal{G}_p[f; \xi]$ has been considered before in the literature, see e.g. [6, 26, 42, 18] and the references therein. However, we believe the importance of studying $\delta\mathcal{G}_p[f; \xi]$ in detail (and in particular, examining how it may be used to construct local modifications) has gone largely overlooked, as such analysis was unnecessary when using simpler constraints like $\mathcal{C}(f) = \text{length}(f)$.

A common challenge in analyzing $\delta\mathcal{G}_p[f; \xi]$ comes from the implicit dependence of \mathcal{G}_p ’s integrand $\inf_x |\omega - f(x)|^p$ on the “domain-projected” closest-point map $\hat{\pi}_X : \Omega \rightarrow X$ given by

$$(4.1) \quad \hat{\pi}_X(\omega) \in \arg \min_{x \in X} |\omega - f(x)|.$$

This is problematic because $\hat{\pi}_X$ is not always well-defined due to possible multiple minima. Denoting, as usual, $Y = f(X)$, the two failure modes are made apparent by writing $\hat{\pi}_X = f^{-1} \circ \hat{\pi}_Y$, where

$$(4.2) \quad \hat{\pi}_Y(\omega) \in \arg \min_{y \in Y} |\omega - f(y)|.$$

Namely,

- (FM1) $\hat{\pi}_Y$ fails to be uniquely-determined, and/or
- (FM2) f^{-1} fails to be uniquely-determined.

While these cases cause no problems when computing $\mathcal{G}_p(f)$ itself, $\delta\mathcal{G}_p[f; \xi]$ turns out to be sensitive to both.

To avoid (FM1) it is common to make some simplifying assumptions: For example (H*) [42]; ρ being null on $\{A \subseteq \Omega \mid \dim_{\text{H}}(A) \leq n - 1\}$ [6]; or (via a clever invariant) taking $p = 2$ and considering $\delta\mathcal{G}_p[f; \xi]$ only for optimal f [18]. The first two simplifications have the disadvantage of precluding analyzing $\delta\mathcal{G}_p[f; \xi]$ when ρ is discrete (as is often the case in applications) and the third precludes analyzing local modifications to suboptimal solutions (which is useful in computational methods if one starts with a random “seed” function f and wants to “evolve” it in the direction of the barycenter field to produce a better solution).

Similarly, to avoid (FM2) one can try to first establish that optimizers must be injective and then restrict one’s subsequent analysis to just optimizers. However, in addition to yielding the same difficulties as the third case above, the arguments in this vein are nontrivial. Indeed, in the case $(\mathcal{C}(f), m) = (\text{length}(f), 1)$, the best result we are aware of establishes injectivity only when $p = 2$ [18], so a similar argument with the more-complicated Sobolev constraint does not seem promising.

To address these concerns, in this section we show that (except perhaps for certain configurations in the $p = 1$ case) one may use the tools of measurable selections to encode $\delta\mathcal{G}_p[f; \xi]$ succinctly even when (FM1) and (FM2) occur simultaneously. Compared with previous results, this allows us to (again except perhaps when $p = 1$) extend the tools of calculus to the whole constraint set $\{\mathcal{C}(f) < \infty\}$, and importantly, to explicitly construct improvements to \mathcal{G}_p at nonstationary points. We reiterate that while our motivation came from the peculiarities of the Sobolev constraint, our analysis of $\delta\mathcal{G}_p[f; \xi]$ in Theorem 4.8 requires only continuity of

f , ξ , and hence applies to common costs like $C(f) = \text{length}(f)$ as well; similarly, the local improvement result Theorem 4.14 holds for any cost that satisfies $C(f + \xi) \lesssim C(f) + \|\xi\|_{C^\infty}$ for $\xi \in C^\infty$.

4.2. The Barycenter Field. First we introduce some preliminary concepts that will be essential to our analysis.

4.2.1. Measurable Selection and Disintegration. As usual, we use the shorthand $Y = f(X)$. Recall closest-point projection maps to X and Y , respectively, given in (4.1) and (4.2). As detailed in (FM1), (FM2), $\hat{\pi}_X$ and $\hat{\pi}_Y$ generally fail to be well-defined in some parts of Ω ; thus we begin by constructing measurable extensions. Define the set-valued functions $\pi_X : \Omega \rightarrow 2^X$ and $\pi_Y : \Omega \rightarrow 2^Y$ by

$$\pi_X(\omega) = \arg \min_{x \in X} |\omega - f(x)| \quad \text{and} \quad \pi_Y(\omega) = \arg \min_{y \in Y} |\omega - y|$$

Following the terminology of [33] we define the *ambiguity set* of f to be

$$(4.3) \quad \mathcal{A}_f = \{\omega \in \Omega \mid \pi_Y(\omega) \text{ is not a singleton}\}.$$

Note, \mathcal{A}_f is exactly the set of points ω where (FM1) occurs.

The set \mathcal{A}_f is closely related to the notion of the *medial axis*, which is commonly defined as follows: Given an open $E \subseteq \mathbb{R}^n$ with $\partial E \neq \emptyset$, the *medial axis* of E is

$$M(E) = \{v \in E \mid \arg \min_{v' \in \partial E} |v - v'| \text{ is not unique}\}.$$

Thus we see $\mathcal{A}_f = \Omega \cap M(\mathbb{R}^n \setminus Y)$. $M(E)$ is also called the *ambiguous locus* or *skeleton* [14, 31, 61]. In some applications $M(E)$ is treated interchangeably with its closure $\overline{M(E)}$ (called the *ridge set* or *cut locus*), though this is technically improper in the abstract setting as $\overline{M(E)}$ can behave much more pathologically than $M(E)$ in cases where ∂E lacks regularity [61]. In any case, $M(\mathbb{R}^n \setminus Y)$ is guaranteed to be Lebesgue-null [31], which is important in the second part of Corollary 4.2 below.

We now recall a result that will serve as the basic tool for our measurable selection statements. A proof may be found in [3, Prop. 7.33].

Proposition 4.1 (Measurable selection). *Suppose Ω is a metrizable space, Z a compact metrizable space, D a closed subset of $\Omega \times Z$, and $h : D \rightarrow \mathbb{R} \cup \{-\infty, \infty\}$ a lower semicontinuous function. For all ω let $D_\omega = \{z \mid (\omega, z) \in D\}$ and let $h^* : \text{proj}_\Omega(D) \rightarrow \mathbb{R} \cup \{-\infty, \infty\}$ be given by*

$$h^*(\omega) = \min_{z \in D_\omega} h(\omega, z).$$

Then $\text{proj}_\Omega(D)$ is closed in Ω , h^ is lower semicontinuous, and there exists a Borel-measurable function $\varphi : \text{proj}_\Omega(D) \rightarrow Z$ such that $\text{graph}(\varphi) \subseteq D$ and for all $\omega \in \text{proj}_\Omega(D)$*

$$h(\omega, \varphi(\omega)) = h^*(\omega).$$

In this case we call φ a measurable selection of the set-valued function $\omega \mapsto D_\omega$.

Applying this we can find measurable selections for the projections π_X, π_Y .

Corollary 4.2. *Suppose X is compact (H.1) and $f \in C(X; \Omega)$ (e.g. via Proposition 2.4). Then there exist Borel-measurable selections $\hat{\pi}_X$ of π_X and $\hat{\pi}_Y$ of π_Y that are well-defined on all of Ω . Furthermore, under (H*), $\hat{\pi}_Y$ is ρ -essentially unique.*

Proof. Existence of $\hat{\pi}_X$ follows immediately from Proposition 4.1 with $D = \Omega \times X$ and $h(\omega, x) = |\omega - f(x)|$; we then obtain $\hat{\pi}_Y$ by taking $\hat{\pi}_Y(\omega) := f(\hat{\pi}_X(\omega))$. For the second part, noting $\mathcal{A}_f \subseteq M(\mathbb{R}^n \setminus Y)$ we see \mathcal{A}_f is Lebesgue null [31], whence under (H*) we get $\rho(\mathcal{A}_f) = 0$. So $\hat{\pi}_Y$ is ρ -essentially unique. ■

In light of Corollary 4.2 we define

$$(4.4) \quad \hat{\Pi}_X = \{\hat{\pi}_X \mid \hat{\pi}_X \text{ is a measurable selection of } \pi_X\}$$

and

$$(4.5) \quad \hat{\Pi}_Y = \{\hat{\pi}_Y \mid \hat{\pi}_Y \text{ is a measurable selection of } \pi_Y\}.$$

With this we now apply disintegration of measures to decompose ρ by $\hat{\pi}_X \in \hat{\Pi}_X$ into $(\{\rho_{x, \hat{\pi}_X^*}\}_{x \in X}, \mu_{\hat{\pi}_X})$, and by $\hat{\pi}_Y \in \hat{\Pi}_Y$ into $(\{\rho_{y, \hat{\pi}_Y^*}\}_{y \in Y}, \nu_{\hat{\pi}_Y})$, where $\mu_{\hat{\pi}_X}$ -a.s. $\text{supp}(\rho_{x, \hat{\pi}_X^*}) = \hat{\pi}_X^{-1}(x)$ and $\nu_{\hat{\pi}_Y}$ -a.s. $\text{supp}(\rho_{y, \hat{\pi}_Y^*}) = \hat{\pi}_Y^{-1}(y)$. Thus we may express \mathcal{G}_p as

$$(4.6) \quad \mathcal{G}_p(f) = \int_X \left[\int_{\hat{\pi}_X^{-1}(x)} |\omega - f(x)|^p d\rho_{x, \hat{\pi}_X^*}(\omega) \right] d\mu_{\hat{\pi}_X}(x)$$

$$(4.7) \quad = \int_{f(X)} \left[\int_{\hat{\pi}_Y^{-1}(y)} |\omega - y|^p d\rho_{y, \hat{\pi}_Y^*}(\omega) \right] d\nu_{\hat{\pi}_Y}(y),$$

with the representation in (4.7) being unique if one takes (H*).

4.2.2. The Barycenter Field and Its Properties.

Definition 4.3 (Barycenter Field). Take (H.4). For fixed $\hat{\pi}_X \in \hat{\Pi}_X$ we define

$$F_{\hat{\pi}_X}(x) = \int_{\hat{\pi}_X^{-1}(x)} p|\omega - f(x)|^{p-2}(\omega - f(x)) d\rho_x(\omega),$$

taking the convention that $|v|^{p-2}v = 0$ when $v = 0$. Similarly, for fixed $\hat{\pi}_Y \in \hat{\Pi}_Y$ we let $F_{\hat{\pi}_Y}(y) = \int_{\hat{\pi}_Y^{-1}(y)} p|\omega - y|^{p-2}(\omega - y) d\rho_y(\omega)$.

Remark 4.4. 1) $F_{\hat{\pi}_X}, F_{\hat{\pi}_Y}$ are Borel-measurable. 2) Note that the integrands of $F_{\hat{\pi}_X}$ and $F_{\hat{\pi}_Y}$ are just the derivatives of the integrands in (4.6), (4.7); this is the standard outcome we expect in the context of gradient flows. 3) Whenever $F_{\hat{\pi}_X}, F_{\hat{\pi}_Y}$ are the same independent of the choice of $\hat{\pi}_X, \hat{\pi}_Y$ (see Corollary 4.10), we will simply write F_X, F_Y , respectively to denote the parametrizations in terms of X, Y .

We now examine some basic geometric properties of the barycenter field. In general, these are most easily visualized for F_Y . One should also note that some statements like Proposition 4.5 hold only for F_Y and lack analogues for F_X on account of the fact that f^{-1} can be discontinuous when it is not well-determined.

We recall two definitions that will be helpful. Let $A \subseteq \mathbb{R}^n$ and let $a \in A$. Then the *tangent cone* at a (denoted via the abuse of notation $T_a A$) is given by

$$T_a A = \left\{ v \in \mathbb{R}^n \mid v = 0 \text{ or } \exists \text{ a seq. } \{a_j\} \subseteq A \setminus \{a\} \text{ s.t. } a_j \rightarrow a \text{ and } \frac{a_j - a}{|a_j - a|} \rightarrow \hat{v} \right\}$$

where \hat{v} denotes the unit vector $\frac{v}{|v|}$. Now let $B \subseteq \mathbb{R}^n$. Then the *polar cone* of B is given by

$$\text{PCone}(B) = \{v \in \mathbb{R}^n \mid \forall b \in B, \langle v, b \rangle \leq 0\}.$$

With these in hand, we can characterize the fibers of $\hat{\pi}_Y$ more fully. Note we denote Minkowski addition by $+$.

Proposition 4.5. *Let $y \in Y$ be arbitrary. Then $\hat{\pi}_Y^{-1}(y)$ is convex, and $\hat{\pi}_Y^{-1}(y) \subseteq y + \text{PCone}(T_y Y)$.*

Proof. For all $y_0, y_1 \in Y$ with $y_0 \neq y_1$, define the half-space $H_{y_0, y_1} = \{u \in \mathbb{R}^n \mid |u - y_0| < |u - y_1|\}$, changing the $<$ to an \leq as needed to facilitate tiebreaking when $u \in \mathcal{A}_f$ and $y_0, y_1 \in \pi_Y(u)$. Then we have $\hat{\pi}_Y^{-1}(y_0) = \bigcap_{y_1 \neq y_0} H_{y_0, y_1} \cap \Omega$, which is an intersection of convex sets and hence convex.

For the second part, let $\omega \in \hat{\pi}_Y^{-1}(y_0)$ and $v_0 \in T_{y_0} Y$ be arbitrarily chosen. We want to show $\langle \omega - y_0, v_0 \rangle \leq 0$. If $v_0 = 0$ then the claim is trivial. Hence suppose $v_0 \neq 0$. Then there exists a sequence $y_j \rightarrow y_0$ such that $\frac{y_j - y_0}{|y_j - y_0|} \rightarrow \hat{v}_0$. Let $y_j^{\text{avg}} = (y_j + y_0)/2$ and $\hat{v}_j = (y_j - y_0)/|y_j - y_0|$. One may rewrite $H_{y_0, y_j} = \{u \in \mathbb{R}^n \mid \langle u - y_j^{\text{avg}}, \hat{v}_j \rangle < 0\}$, again replacing the $<$ with \leq as needed to facilitate tiebreaking. For each j , since $\omega \in H_{y_0, y_j}$ we get $\langle \omega - y_j^{\text{avg}}, \hat{v}_j \rangle < 0$. As $j \rightarrow \infty$ we see $y_j^{\text{avg}} \rightarrow y_0$ and $\hat{v}_j \rightarrow \hat{v}_0$, thus $\langle \omega - y_0, \hat{v}_0 \rangle \leq 0$. Since v_0 was arbitrary it follows that $\omega - y_0 \in \text{PCone}(T_{y_0} Y)$ from which the claim follows. \blacksquare

In particular, Proposition 4.5 implies that for all x , $F_X(x) \in f(x) + \text{PCone}(T_{f(x)} Y)$; similarly, for all y , $F_Y(y) \in y + \text{PCone}(T_y Y)$. However, note that if f fails to be injective, then unlike $\hat{\pi}_Y^{-1}(y)$, the fiber $\hat{\pi}_X^{-1}(x)$ could fail to be convex. This is because a priori we can only say $\hat{\pi}_Y^{-1}(y) = \bigsqcup_{x \in f^{-1}(y)} \hat{\pi}_X^{-1}(x)$; there is no structure enforced on exactly how the $\omega \in \hat{\pi}_Y^{-1}(y)$ are partitioned between the $\hat{\pi}_X^{-1}(x)$.

Next, one might ask whether we can expect any regularity from F_X, F_Y . Generally, the answer is no. Trivial examples arise when ρ is singular, for example $\rho = \delta_\omega$ for some $\omega \notin Y$. When ρ is absolutely continuous, easy examples can be obtained when the fibers $\hat{\pi}_X^{-1}(x)$ (respectively, $\hat{\pi}_Y^{-1}(y)$) have nonconstant Hausdorff dimension, such as when $f(\partial X) \subseteq \text{supp}(\rho)^\circ$ and f^{-1} is well-defined on $f(\partial X)$. For instance, consider ρ uniform on $\overline{B_1(0; \mathbb{R}^n)}$ with $f : \overline{B_1(0; \mathbb{R}^m)} \rightarrow \overline{B_1(0; \mathbb{R}^n)}$ given by $f(x) = \frac{9}{10}\iota(x)$ where ι is the inclusion map. Then $F_X \equiv 0$ on $B_1(0; \mathbb{R}^m)$ but points radially outward on $\partial \overline{B_1(0; \mathbb{R}^m)}$; analogously for F_Y on $B_{.9}(0; \mathbb{R}^n)$ and $\partial \overline{B_{.9}(0; \mathbb{R}^n)}$.

However, there are actually trivial counterexamples with $f \in C^\infty$ even when $\partial f(X) \subseteq \partial \text{supp}(\rho)$. This might sound surprising at first but becomes less so once one remembers that smoothness of f as a map is not the same thing as smoothness of $f(X)$ as a manifold. An elementary counterexample can be constructed by taking a smooth parametrization of the graph of $x \mapsto |x|$ as we now show.

Counterexample 4.6 ($f \in C^\infty$; Barycenter Field discontinuous). Let Ω be a diamond in \mathbb{R}^2 with vertices $(0, -2), (-2, 0), (0, 2)$, and $(2, 0)$ endowed with ρ_{unif} . Recall that in the proof of Lemma 3.6 we used $\sigma(x)$ to denote a smooth step function. We similarly define a smooth “dip” function $\tilde{\sigma} : \mathbb{R} \rightarrow [0, 1]$ by

$$\tilde{\sigma}(x) = \begin{cases} -\sigma(x+1) + 1 & x \in (-\infty, 0] \\ \sigma(x) & x \in [0, \infty). \end{cases}$$

Observe $\tilde{\sigma} \equiv 1$ on $\mathbb{R} \setminus [-1, 1]$, and that its derivatives of all orders vanish at 0. Finally, let $f : [-1, 1] \rightarrow \Omega$ be given by $f(x) = (\tilde{\sigma}(x) \text{sgn}(x), \tilde{\sigma}(x))$. Then $f \in C^\infty$ but F_X (respectively, F_Y) is discontinuous at 0 (respectively, $(0, 0)$).

Much more surprising is that even C^1 -ness of $f(X)$ as a manifold is insufficient to guarantee continuity of F_X, F_Y .

Counterexample 4.7 ($f(X)$ a C^1 -manifold; Barycenter Field discontinuous). Let $X = [-1, 1]$, $\Omega = [-1, 1]^2$, and $k = 1$. Define

$$f_2(t) = \begin{cases} t^3 \sin(1/t) & t < 0 \\ 0 & t \geq 0 \end{cases}$$

and let $f : X \rightarrow \Omega$ be given by $f(t) = (t, f_2(t))$. Observe that f is injective and C^1 with $f'(t) \neq 0$, so $f([-1, 1])$ is a C^1 -manifold.

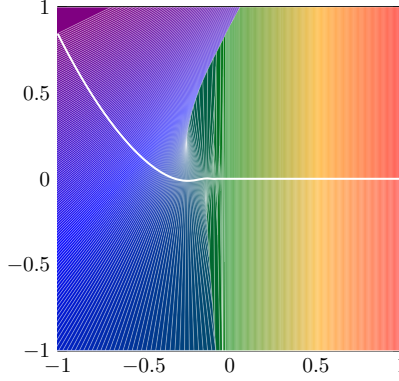


FIGURE 7. f and the $\hat{\pi}_Y^{-1}(y)$ visualized.

We claim F_Y is discontinuous at $(0, 0)$; in particular $\lim_{t \rightarrow 0} |F_Y(t)|$ does not exist. To that end note $\Omega \setminus Y$ has two connected components; call the upper Ω_1 and the lower Ω_2 . For each $y \in f(X)$ let $L_1(t) = \text{Length}(\hat{\pi}_Y^{-1}(y) \cap \Omega_1)$ and $L_2(t) = \text{Length}(\hat{\pi}_Y^{-1}(y) \cap \Omega_2)$. For concision, we use the notation $y_t = f(t)$.

From now on $t_0 \in (-1, 0)$ will always denote a local maximum of f_2 . Note that because $f_2''(t_0) < 0$, $\rho_{y_{t_0}}$ is nonuniform on $\hat{\pi}_Y^{-1}(y_{t_0})$, and in particular $|F_Y(y_{t_0})| > L_1(t_0) - L_2(t_0)$. So, to show F_Y is discontinuous at 0 it suffices to show that as $t_0 \rightarrow 0$, $L_2(t_0) \rightarrow 0$ while $L_1(t_0)$ is bounded below by some $c_0 > 0$. To treat $L_2(t_0)$: Let $R(t)$ denote the radius of curvature, where defined. We have

$$R(t) = \left| \frac{(1 + \dot{f}_2(t)^2)^{3/2}}{\ddot{f}_2(t)} \right| = \left| \frac{(1 + (t(3t \sin(1/t) - \cos(1/t)))^2)^{3/2}}{\frac{6t^2-1}{t} \sin(1/t) - 4 \cos(1/t)} \right|.$$

Y is locally a C^2 -manifold at $f(t_0)$, so by [61, Thm. 1.2], $L_2(t_0) \leq R(t_0)$. Since $\dot{f}_2(t_0) = 0$, for small t_0 one may verify $R(t_0) \approx \left| \frac{t_0}{\sin(1/t_0)} \right| \approx |t_0|$, so $\lim_{t_0 \rightarrow 0} L_2(t_0) = 0$.

Now we claim $\lim_{t_0 \rightarrow 0} L_1(t_0) > 0$; numerically it appears the value is ≈ 0.6671 . Hence for simplicity let $c_0 = 1/2$ and consider $\omega = (t_0, c_0)$. We claim $\hat{\pi}_Y(\omega) = f(t_0)$.

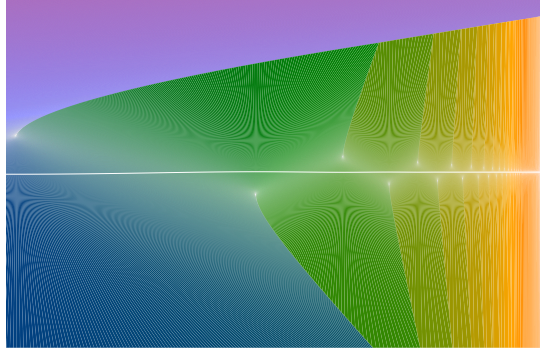


FIGURE 8. Closeup of $\hat{\pi}_Y^{-1}(y)$ for $-1 \ll t < 0$ (axes not scaled equally).

To see this note $\hat{\pi}_Y(\omega)$ minimizes $d^2(\omega, f(t)) = (t - t_0)^2 + (f_2(t) - c_0)^2$. Thus either $t = \pm 1$ or $0 = 2(t - t_0) + t \cos(1/t) + O(t^2)$. By direct comparison, one may verify that we can rule out $t = \pm 1$ as well as $t > 0$. Next one may show that for small t_0 the $2(t - t_0)$ term dominates, whence critical points will occur in some neighborhood N_{t_0} of t_0 with $\text{diam}(N_{t_0}) = O(|t_0|)$. For some ε sufficiently small, t_0 is the only critical point in $B_\varepsilon(t_0)$. Now suppose t' is a critical point not in $B_\varepsilon(t_0)$. We must have $t' < t_0$ or else $d^2(\omega, f(t')) > d^2(\omega, f(t_0))$. Define $\delta = |t' - t_0|$; observe $\delta \in O(|t_0|)$ since $\text{diam}(N_{t_0})$ is. Now

$$\begin{aligned} |f(t') - f(t_0)| &= |t'^3 \sin(1/t') - t_0^3 \sin(1/t_0)| \\ &\leq |(t_0 - \delta)^3 \sin(1/t') - t_0^3 \sin(1/t_0)| \\ &= O(t_0^3). \end{aligned}$$

Thus

$$\begin{aligned} d^2(\omega, f(t')) &= (t' - t_0)^2 + (f(t') - c_0)^2 \\ &= \delta^2 + (f(t') - f(t_0) + f(t_0) - c_0)^2 \\ &= \delta^2 + (f(t_0) - c_0)^2 + 2(f(t_0) - c_0)(f(t') - f(t_0)) + (f(t') - f(t_0))^2 \\ &= \delta^2 + d^2(\omega, f(t_0)) + O(t_0^3). \end{aligned}$$

So as $t_0 \rightarrow 0$ we see $d^2(\omega, f(t')) > d^2(\omega, f(t_0))$. Finally, comparing to $d^2(\omega, f(-1))$ and $d^2(\omega, f(1))$ we see $f(t_0)$ achieves the global minimum.

Thus we see for points of local maxima t_0 , $F_Y(y_{t_0}) \not\rightarrow 0$ as $t_0 \rightarrow 0^-$. By contrast, $\lim_{t \rightarrow 0^+} F_Y(y_t) = 0$. So F_Y is discontinuous at $(0, 0)$, despite the fact that Y is a local C^1 -manifold there. Since f is injective and $\rho \ll \mathcal{L}$, F_Y and F_X are equivalent and so F_X is similarly discontinuous.

4.3. $F_{\hat{\pi}_X}$ as a (Negative) Gradient. We now move to proving the first main result of this section. As mentioned previously the $p = 1$ case is special, which reflects the fact that the integrand $|\cdot|$ of \mathcal{G}_1 is only Lipschitz, as compared to the C^1 integrand $|\cdot|^p$ of \mathcal{G}_p for $p > 1$.

Theorem 4.8. *Take (H.1), (H.2), and (H.4). Fix $f \in C(X; \Omega)$ and $\xi \in C(X; \mathbb{R}^n)$, and for all $\varepsilon > 0$ let $f_\varepsilon := f + \varepsilon \xi$ and $Y = f(X)$, $Y_\varepsilon = f_\varepsilon(X)$. If $p = 1$, let*

$Y_{\text{out}} = \{y \in Y \mid \liminf_{\varepsilon \rightarrow 0} 1_{Y_\varepsilon}(y) = 0\}$, and take the extra hypothesis $\rho(Y_{\text{out}}) = 0$. Recall the definition of $\hat{\Pi}_X$ from (4.4). Then

$$(4.8) \quad \lim_{\varepsilon \rightarrow 0} \frac{\mathcal{G}_p(f_\varepsilon) - \mathcal{G}_p(f)}{\varepsilon} = \min_{\hat{\pi}_X \in \hat{\Pi}_X} \int_X \langle -F_{\hat{\pi}_X}(x), \xi(x) \rangle d\mu_{\hat{\pi}_X}(x).$$

Proof of Theorem 4.8. For concision write

$$\begin{aligned} \frac{\mathcal{G}_p(f_\varepsilon) - \mathcal{G}_p(f)}{\varepsilon} &= \int_\Omega \delta_\varepsilon(\omega) d\rho(\omega), \text{ where} \\ \delta_\varepsilon(\omega) &:= \frac{1}{\varepsilon} \left[\inf_{x_\varepsilon \in X} |\omega - f_\varepsilon(x_\varepsilon)|^p - \inf_{x \in X} |\omega - f(x)|^p \right]. \end{aligned}$$

Also, let

$$h(\omega, x) = \begin{cases} \langle -p|\omega - f(x)|^{p-2}(\omega - f(x)), \xi(x) \rangle & \text{if } \omega \neq f(x), \text{ and} \\ 0 & \text{if } \omega = f(x). \end{cases}$$

As we will show, the formula for h is related to $\langle -F_{\hat{\pi}_X}(x), \xi(x) \rangle$ in (4.8). Notice that h depends on ξ .

Case 1: Suppose $p > 1$. We will apply Proposition 4.1 to obtain a measurable selection of π_X . To that end, define $D = \{(\omega, x) \mid x \in \pi_X(\omega)\}$, $D_\omega = \{x \mid (\omega, x) \in D\}$, and let

$$h^*(\omega) = \min_{D_\omega} h(\omega, x).$$

Note that since $p > 1$, h is continuous, and so l.s.c. Moreover, it is easy to verify that D is closed. Thus Proposition 4.1 gives a measurable selection $\hat{\pi}_X^*$ of π_X with

$$h(\omega, \hat{\pi}_X^*(\omega)) = h^*(\omega).$$

Notice that by the definition of $\hat{\pi}_X^*(\omega)$, disintegrating $\int_\Omega h(\omega, \hat{\pi}_X^*(\omega)) d\rho$ gives the right-hand side of (4.8):

$$(4.9) \quad \int_\Omega h^*(\omega) d\rho = \int_\Omega h(\omega, \hat{\pi}_X^*(\omega)) d\rho = \min_{\hat{\pi}_X \in \hat{\Pi}_X} \int_X \langle -F_{\hat{\pi}_X}(x), \xi(x) \rangle d\mu_{\hat{\pi}_X}(x).$$

For the rest it suffices to show that

$$\text{for } \rho\text{-a.e. } \omega, \lim_{\varepsilon \rightarrow 0} \delta_\varepsilon(\omega) = h^*(\omega).$$

(Then, we can apply the dominated convergence theorem to get (4.8).)

Analogously to the construction of $\hat{\pi}_X^*$, define the set-valued map $\pi_{\varepsilon, X}(\omega) = \arg \min_{x \in X} |\omega - f_\varepsilon(x)|$ and let $D^\varepsilon = \{(\omega, x) \mid x \in \pi_{\varepsilon, X}(\omega)\}$. Then Proposition 4.1 yields a selection $\hat{\pi}_{\varepsilon, X}^*$ of $\pi_{\varepsilon, X}$ with $h(\omega, \hat{\pi}_{\varepsilon, X}^*(\omega)) = h_\varepsilon^*(\omega)$.

For concision define

$$g(\omega) = \omega - f(\hat{\pi}_X^*(\omega)) \quad \text{and} \quad g^\varepsilon(\omega) = \omega - f(\hat{\pi}_{\varepsilon, X}^*(\omega)).$$

Since $\pi_X, \pi_{\varepsilon, X}$ were defined via closest-point projection onto Y, Y_ε , and since $\hat{\pi}_X^*, \hat{\pi}_{\varepsilon, X}^*$ are selections of $\pi_X, \pi_{\varepsilon, X}$, respectively, it follows that

$$|g| \leq |g^\varepsilon| \quad \text{and} \quad |g^\varepsilon - \varepsilon \xi(\hat{\pi}_{\varepsilon, X}^*)| \leq |g - \varepsilon \xi(\hat{\pi}_X^*)|.$$

Therefore,

$$(4.10) \quad \underbrace{\frac{|g^\varepsilon - \varepsilon \xi(\hat{\pi}_{\varepsilon, X}^*)|^p - |g^\varepsilon|^p}{\varepsilon}}_{(I)} \leq \delta_\varepsilon \leq \underbrace{\frac{|g - \varepsilon \xi(\hat{\pi}_X^*)|^p - |g|^p}{\varepsilon}}_{(II)}.$$

We now rewrite the (I) and (II) in terms of (respectively) $h_\varepsilon^*(\omega)$ and $h^*(\omega)$, up to an error term that vanishes as $\varepsilon \rightarrow 0$. Note that for all $a, b \in \mathbb{R}^n$ with $a \neq 0$, Taylor expanding $\varepsilon \mapsto |a - \varepsilon b|^p = (\sum_i (a_i - \varepsilon b_i)^2)^{p/2}$ about $\varepsilon = 0$ yields

$$|a - \varepsilon b|^p = |a|^p + \varepsilon \cdot \langle -p|a|^{p-2}a, b \rangle + o(\varepsilon).$$

Thus if $g^\varepsilon(\omega) \neq 0$ then by the definition of h , (I) $= h(\omega, \hat{\pi}_{\varepsilon, X}^*) + o(1)$, and similarly if $g(\omega) \neq 0$ then (II) $= h(\omega, \hat{\pi}_X^*) + o(1)$.

On the other hand when $a = 0$ we get $|a - \varepsilon b|^p = \varepsilon^p |b|^p$; thus if $g^\varepsilon(\omega) = 0$ then (I) $= \varepsilon^{p-1} |\xi(\hat{\pi}_{\varepsilon, X}^*)|^p$ and if $g(\omega) = 0$ then (II) $= \varepsilon^{p-1} |\xi(\hat{\pi}_X^*)|^p$. Observe that since ξ is bounded (H.1) and $p > 1$, both of these expressions are $o(1)$.

So, in either case, (I) $= h(\omega, \hat{\pi}_{\varepsilon, X}^*) + o(1)$ and (II) $= h(\omega, \hat{\pi}_X^*) + o(1)$. Thus from (4.10) we get

$$(4.11) \quad h_\varepsilon^*(\omega) + o(1) \leq \delta_\varepsilon(\omega) \leq h^*(\omega) + o(1).$$

To conclude it suffices to show that for each ω , $h^*(\omega) \leq \liminf_{\varepsilon \rightarrow 0} h_\varepsilon^*(\omega)$. But this follows from the continuity of $(\omega, x) \mapsto h(\omega, x)$ and $\varepsilon \mapsto f_\varepsilon$. This concludes the $p > 1$ case.

Case 2: Suppose $p = 1$. In this case, h is no longer globally l.s.c.

Consider $\Omega_{\text{out}} = \Omega \setminus Y$. Define D , D^ε , h , and so on as in the $p > 1$ case but replacing Ω with Ω_{out} . Note that while Ω_{out} is not a closed subset of Ω , we nevertheless see that D , D^ε are closed with respect to the subspace topology on $\Omega_{\text{out}} \times X$. Since we also have that h is continuous on $\Omega_{\text{out}} \times X$, the hypotheses of Proposition 4.1 are satisfied and as in the $p > 1$ case we obtain measurable selections $\hat{\pi}_X^*$, $\hat{\pi}_{\varepsilon, X}^*$ such that

$$\text{for all } \omega \in \Omega_{\text{out}}, \quad h^*(\omega) = h(\omega, \hat{\pi}_X^*) \quad \text{and} \quad h_\varepsilon^*(\omega) = h(\omega, \hat{\pi}_{\varepsilon, X}^*).$$

With this we recover (4.9) as follows. Extend $\hat{\pi}_X^*$ to also be defined on Y via an arbitrary measurable selection of the (potentially) set-valued map $\omega \mapsto f^{-1}(\omega)$. Regardless of our choice, $h^* \equiv 0$ on Y , so the Ω integrals in (4.9) are independent of the extension. Similarly, since we took the convention $\hat{\mathbf{0}} = \mathbf{0}$ in the definition of $F_{\hat{\pi}_X}$ (Theorem 4.3), the right-hand side is also independent of the extension. Thus we obtain (4.9) as in the $p > 1$ case.

As in the $p > 1$ case it now suffices to show

$$\text{for } \rho\text{-a.e. } \omega, \quad \lim_{\varepsilon \rightarrow 0} \delta_\varepsilon(\omega) = h^*(\omega)$$

Recall that by hypothesis $\rho(Y_{\text{out}}) = 0$, so in fact it suffices to just verify the limit by casework on Ω_{out} and $Y_{\text{in}} := Y \setminus Y_{\text{out}}$. Hence, let $\omega \in \Omega_{\text{out}}$ be arbitrarily chosen. As in the $p > 1$ case we obtain (4.10), that is,

$$\underbrace{\frac{|g^\varepsilon - \varepsilon \xi(\hat{\pi}_{\varepsilon, X}^*)|^p - |g^\varepsilon|^p}{\varepsilon}}_{\text{(I)}} \leq \delta_\varepsilon \leq \underbrace{\frac{|g - \varepsilon \xi(\hat{\pi}_X^*)|^p - |g|^p}{\varepsilon}}_{\text{(II)}}.$$

Since ξ is bounded (H.1), taking ε sufficiently small yields $\omega \notin Y_\varepsilon$. Thus we may Taylor expand (I) and (II) as in the $p > 1$ case to obtain, respectively,

$$\text{(I)} = h_\varepsilon^*(\omega) + o(1) \quad \text{and} \quad \text{(II)} = h^*(\omega) + o(1).$$

Note that unlike in the $p > 1$ case the $\varepsilon^{p-1} |\xi|^p$ error terms do not appear, as these estimates were relevant only when $\omega \in Y_\varepsilon$ or $\omega \in Y$. In any case, $(\omega, x) \mapsto h(\omega, x)$

is continuous on $\Omega_{\text{out}} \times Y$ and $\varepsilon \mapsto f_\varepsilon$ is continuous everywhere, which implies

$$h^*(\omega) \leq \liminf_{\varepsilon \rightarrow 0} h_\varepsilon^*(\omega)$$

Since $\omega \in \Omega_{\text{out}}$ was arbitrary we thus have

$$\text{for all } \omega \in \Omega_{\text{out}}, \quad \lim_{\varepsilon \rightarrow 0} \delta_\varepsilon(\omega) = h^*(\omega)$$

which completes the Ω_{out} case.

For Y_{in} , observe that we may write $Y_{\text{in}} = \{\omega \in Y \mid \liminf_{\varepsilon \rightarrow 0} 1_{Y_\varepsilon}(\omega) = 1\}$. So, fixing an arbitrary $\omega \in Y_{\text{in}}$, we see there exists $\varepsilon_0 > 0$ such that for all $0 < \varepsilon \leq \varepsilon_0$ we have $\omega \in Y_\varepsilon$. Recalling that we defined $\delta_\varepsilon(\omega) = \frac{1}{\varepsilon} [\inf_{x \in X} |\omega - f_\varepsilon(x_\varepsilon)|^p - \inf_{x \in X} |\omega - f(x)|^p]$, it follows that for all $0 < \varepsilon \leq \varepsilon_0$, $\delta_\varepsilon(\omega) = 0$. In particular, since $\omega \in Y_{\text{in}}$ was arbitrarily chosen we get

$$\text{for all } \omega \in Y_{\text{in}}, \quad \lim_{\varepsilon \rightarrow 0} \delta_\varepsilon(\omega) = 0,$$

thus completing the Y_{in} case. Therefore, combining the above results we have the desired limit:

$$\lim_{\varepsilon \rightarrow 0} \delta_\varepsilon(\omega) = h^*(\omega) \text{ for } \rho\text{-a.e. } \omega.$$

This completes the $p = 1$ case, and so the theorem. ■

Remark 4.9. To highlight why the $p = 1$ case is special in Theorem 4.8, fix some X , Ω and let $v_0 \in \Omega^\circ$, $\rho = \delta_{v_0}$, and $f \equiv v_0$. Note that regardless of the choice of selection $\hat{\pi}_X(\omega)$ we have $F_{\hat{\pi}_X} \equiv \mathbf{0}_{\mathbb{R}^n}$. Fix $\hat{v} \in \mathbb{S}^{n-1}$ and let $\xi(x) \equiv \hat{v}$. Then $\mathcal{G}_1(f_\varepsilon) = |\varepsilon \hat{v}| = \varepsilon$ and $\mathcal{G}_p(f) = 0$, so

$$\lim_{\varepsilon \rightarrow 0} \frac{\mathcal{G}_1(f_\varepsilon) - \mathcal{G}_1(f)}{\varepsilon} = 1 \neq 0 = \int_X \langle -F_{\hat{\pi}_X}(x), \xi(x) \rangle d\mu_{\hat{\pi}_X}(x).$$

In this particular example, we can at least get an integral representation of the first variation by defining the modified function $\tilde{h}(\omega, x)$ to be $h(\omega, x)$ on $\{\omega \neq f(x)\}$ and $|\xi(x)|$ on $\{\omega = f(x)\}$, whence $\lim_{\varepsilon \rightarrow 0} \frac{\mathcal{G}_1(f_\varepsilon) - \mathcal{G}_1(f)}{\varepsilon} = \int_\Omega \tilde{h}^* d\rho$.

However, this does not always work. Fixing a particular $\varepsilon > 0$ and comparing the functions in (4.10) at an $\omega \in Y_{\text{out}}$, we see $f(\hat{\pi}_X^*) = \omega$ and so we may write δ_ε as

$$(4.12) \quad \frac{1}{\varepsilon} |f_\varepsilon(\hat{\pi}_{\varepsilon, X}^*) - \omega| = \frac{1}{\varepsilon} |f_\varepsilon(\hat{\pi}_{\varepsilon, X}^*) - f(\hat{\pi}_X^*)| = |\xi(\hat{\pi}_{\varepsilon, X}^*) + \frac{1}{\varepsilon} (f(\hat{\pi}_{\varepsilon, X}^*) - f(\hat{\pi}_X^*))|,$$

while (II) reduces to $|\xi(\hat{\pi}_X^*)|$ by virtue of $g = 0$. The result is that the inequalities in (4.10) can become strict, with the gap in some sense controlled by the “angle” ξ makes relative to Y at ω .

As an elementary example, let $X = [-1, 1]$ and consider $f(x) = \frac{1}{\sqrt{2}}(x, x)$ and $\xi(x) = \hat{v} \in \mathbb{S}^1$. Then $Y_{\text{out}} = Y$, so we may pick $\omega = (0, 0)$, whence $\hat{\pi}_X^*(\omega) = 0$. If $\hat{v} = \frac{1}{\sqrt{2}}(-1, 1)$ then $\hat{\pi}_{\varepsilon, X}^* = 0 = \hat{\pi}_X^*$, so (4.12) reduces to just $|\xi(0)|$, the exact form of (II). So in this case the upper bound in (4.10) is tight. On the other hand, if we choose $\hat{v} = \frac{1}{\sqrt{2}}(1, 1)$ then for small ε we get $\hat{\pi}_{\varepsilon, X}^*(\omega) = -\varepsilon$ whence (4.12) gives $\delta_\varepsilon(\omega) = 0 < 1 = |\xi(0)| = \text{(II)}$. So in this case the modification \tilde{h} is not sufficient to recover the limit in Theorem 4.8.

It is also instructive to repeat similar analysis for $f(x) = (x, -|x|)$ and $\xi(x) = (0, 1)$. From these examples it seems likely that in the $p = 1$ case, on Y_{out} the relevant quantity for \tilde{h} is not $|\xi(\hat{\pi}_X^*)|$ but rather something like $\inf_{v \in \text{PCone}(T_\omega Y)} \langle v, \xi(\hat{\pi}_X^*) \rangle$. However, as the original $f(x) \equiv v_0$ shows, this too can fail at “boundary” points of Y .

Theorem 4.8 can be written in terms of an integral over $Y = f(X)$:

Corollary 4.10. *Take the hypotheses of Theorem 4.8 and let $\hat{\pi}_Y^* = f(\hat{\pi}_X^*)$, $\nu_{\hat{\pi}_Y^*} = f_{\#}(\mu_{\hat{\pi}_X^*})$, and*

$$\tilde{Y} = \{y \in Y \mid f^{-1}(y) \text{ is non-unique}\}.$$

Suppose $\nu_{\hat{\pi}_Y^}(\tilde{Y}) = 0$ and let $\xi_Y(y) = \xi(f^{-1}(y))$. Then*

$$(4.13) \quad \lim_{\varepsilon \rightarrow 0} \frac{\mathcal{G}_p(f_\varepsilon) - \mathcal{G}_p(f)}{\varepsilon} = \int_Y \langle -F_{\hat{\pi}_Y^*}(y), \xi_Y(y) \rangle d\nu_{\hat{\pi}_Y^*}(y).$$

In particular, if $\rho(\mathcal{A}_f) = 0$ then F_Y , ν_ρ are independent of both the choice of $\xi \in C(X; \mathbb{R}^n)$ and the choice of $\hat{\pi}_Y \in \hat{\Pi}_Y$, so we may simply write

$$(4.14) \quad \lim_{\varepsilon \rightarrow 0} \frac{\mathcal{G}_p(f_\varepsilon) - \mathcal{G}_p(f)}{\varepsilon} = \int_Y \langle -F_Y(y), \xi_Y(y) \rangle d\nu_\rho(y).$$

Proof. Let $\tilde{X} = f^{-1}(\tilde{Y})$ and note $\mu_{\hat{\pi}_X^*}(\tilde{X}) = 0$. So

$$\int_X \langle -F_{\hat{\pi}_X^*}(x), \xi(x) \rangle d\mu_{\hat{\pi}_X^*}(x) = \int_{X \setminus \tilde{X}} \langle -F_{\hat{\pi}_X^*}(x), \xi(x) \rangle d\mu_{\hat{\pi}_X^*}(x).$$

By definition, for all $x \in X \setminus \tilde{X}$ we have $(\hat{\pi}_X^*)^{-1}(x) = (\hat{\pi}_Y^*)^{-1}(f(x))$ whence expanding $F_{\hat{\pi}_X^*}$, applying the change-of-variables $y = f(x)$, and using $\nu_{\hat{\pi}_Y^*}(Y) = \nu_{\hat{\pi}_Y^*}(Y \setminus \tilde{Y})$ gives the result. \blacksquare

Remark 4.11. Verifying the $\nu_{\hat{\pi}_Y^*}(\tilde{Y}) = 0$ hypothesis does not always require precise knowledge of $\nu_{\hat{\pi}_Y^*}$. For example, suppose $f(X)$ is a C^1 -manifold with all self-intersections transverse. Then for each $y \in \tilde{Y}$ Proposition 4.5 gives $(\hat{\pi}_Y^*)^{-1}(y) = \{y\}$, whence if ρ has no atoms we are guaranteed $\nu_{\hat{\pi}_Y^*}(\tilde{Y}) = 0$.

Before continuing, it is worth discussing an important distinction between Theorem 4.8 and Corollary 4.10. In a nutshell, Corollary 4.10 is a weaker form of Theorem 4.8 that is easier to work with visually (and hence numerically as well): Provided $\rho(Y_{\text{in}}) = 0$, one may compute the first variation by simply computing the fibers $\hat{\pi}_Y^{-1}(y)$ and, if necessary, assigning points in \mathcal{A}_f to the y where $|\xi_Y|$ is the largest. In this way, Corollary 4.10 also discretizes nicely; see Section 5.2.

The tradeoff is that Corollary 4.10 is insufficient to analyze an important class of perturbations, namely those for which the parametrization of Y is key. In loose terms, these are the perturbations that change the topology of Y (or at least appear to locally) on a non-null set. Simple examples arise when $\rho(\tilde{Y}) > 0$; e.g. $X = [-1, 1]$, ρ uniform on $[-1, 1]^2$, $f(x) = (1 - |x|, 0)$, and $\xi(x) = (0, t)$. Pictorially, $\varepsilon\xi$ has the effect of “splitting” a line segment into a narrow wedge shape, which cannot be encoded via a $\nu_{\hat{\pi}_Y^*}$ -a.e. well-defined ξ_Y , hence we must use Theorem 4.8.

For the case $\nu_{\hat{\pi}_Y^*}(\tilde{Y}) \neq 0$ but $\rho(\tilde{Y}) = 0$, an illustrative example is $X = [-1, 1]$, $\rho = \frac{1}{2}\delta_{(0,1)} + \frac{1}{2}\text{Unif}_{[-1,1] \times \{0\}}$, and f is a parametrization of $[-1, 1] \times \{0\}$ that is identically $(0, 0)$ on $[-1/2, 1/2]$ and linear elsewhere. Here, Theorem 4.8 allows perturbations like $\xi(x) = \chi_{[-1/2, 1/2]}(x) (0, 1 - 2|x|)$ (which adds a vertical spike at $(0, 0)$) and correctly predicts that f_ε gives an $O(\varepsilon)$ improvement. However, as before this cannot be encoded via a $\nu_{\hat{\pi}_Y^*}$ -a.e. well-defined ξ_Y .

4.4. Local Improvements and First-Order Conditions. Theorem 4.8 shows that if there exist $\xi, \hat{\pi}_X$ yielding $\mu_{\hat{\pi}_X}(\{F_{\hat{\pi}_X} \neq 0\}) > 0$ then it should be possible to improve $\mathcal{G}_p(f)$ by “following” $F_{\hat{\pi}_X}(x)$, as long as the modification still stays in the same Sobolev class $W^{k,q}(X; \Omega)$. This regularity condition requires some care because as seen in Counterexamples 4.6 and 4.7, $F_{\hat{\pi}_X}$ often lacks regularity, so we typically cannot guarantee $f + \varepsilon F_{\hat{\pi}_X} \in W^{k,q}(X; \Omega)$. Nevertheless, our second main theorem of this section, Theorem 4.14 below shows that we can at least find a smooth local approximant to F_X around a density point of $\{F_{\hat{\pi}_X} \neq 0\}$. The argument is essentially measure-theoretic and relies in the last step on a simple fact about Radon measures (Corollary 4.13). Though Lemma 4.12 and Corollary 4.13 are surely well-known, we are not aware of a reference, and so for completeness have included two short proofs we learned of from Pablo Shmerkin.

Lemma 4.12. *Let μ be a Radon measure on \mathbb{R}^d . Define*

$$P = \left\{ x \in \mathbb{R}^d \mid \liminf_{r \rightarrow 0} \frac{\mu(B_r(x))}{r^d} = 0 \right\}.$$

Then $\mu(P) = 0$.

Proof. If $\mu(\{x\}) > 0$ then immediately $x \notin P$, hence we may exclude these points. We first treat the case where μ has bounded support. Let $\varepsilon > 0$ and define

$$P_\varepsilon = \left\{ x \mid \mu(\{x\}) = 0 \text{ and } \liminf_{r \rightarrow 0} \frac{\mu(B_r(x))}{r^d} < \varepsilon \right\}$$

and

$$\mathcal{B}_\varepsilon = \left\{ B_r(x) \mid x \in P_\varepsilon, r \leq 1, \text{ and } \frac{\mu(B_r(x))}{r^d} < \varepsilon \right\}.$$

Note $P \subseteq P_\varepsilon$ and that for all $x \in P_\varepsilon$ we get $\inf \{r \mid B_r(x) \in \mathcal{B}_\varepsilon\} = 0$. By Vitali’s covering theorem for Radon measures (see, e.g., [53, Thm 2.8]) there exists a pairwise-disjoint, at-most-countable set $\{B_{r_i}(x_i)\} \subseteq \mathcal{B}_\varepsilon$ with $\mu(P_\varepsilon \setminus \bigcup_i B_{r_i}(x_i)) = 0$. So

$$\mu(P) \leq \mu(P_\varepsilon) \leq \sum_i \mu(B_i) \leq \varepsilon \sum_i r_i^d \leq \varepsilon \frac{\mathcal{L}(\text{supp}(\mu))}{\mathcal{L}(B_1(0))},$$

and taking $\varepsilon \rightarrow 0$ yields the desired result.

Now suppose μ has unbounded support. For each $j \in \mathbb{N}$ define μ_j to be the restriction of μ to $B_j(0)$. Then each $P_j := \{x \mid \liminf_{r \rightarrow 0} \mu_j(B_r(x))/r^d = 0\}$ is μ_j -null and so μ -null. Writing $P = \bigcup_j P_j$ then yields the result. \blacksquare

Corollary 4.13. *Let μ be a Radon measure on \mathbb{R}^d . Then for all $\lambda \in (0, 1)$, for μ -a.e. x ,*

$$(4.15) \quad \limsup_{r \rightarrow 0} \frac{\mu(B_{\lambda r}(x))}{\mu(B_r(x))} \geq \lambda^{d+1} > 0.$$

Proof. By Lemma 4.12, for μ -a.e. x there exists $c_x > 0$ and $R_x > 0$ such that for all $0 < r \leq R_x$, $\mu(B_r(x)) \geq c_x r^d$. Fix some such x and for all $j \in \mathbb{N}$ sufficiently large define $a_j = \mu(B_{\lambda^j}(x))$; note $a_j \geq c_x \lambda^{dj}$. Suppose, to obtain a contradiction, that

$$\limsup_{j \rightarrow \infty} \frac{a_{j+1}}{a_j} < \lambda^{d+1}.$$

Then there exists j_0 such that for all $j \geq j_0$ one has $a_{j+1} < \lambda^{d+1}a_j$, whence

$$a_j < a_{j_0} \lambda^{(d+1)(j-j_0)} = [a_{j_0} \lambda^{-(d+1)j_0} \cdot \lambda^j] \lambda^{dj}.$$

Taking j sufficiently large one gets $a_{j_0} \lambda^{-(d+1)j_0} \cdot \lambda^j < c_x$ whence $a_j < c_x \lambda^{dj}$, a contradiction. \blacksquare

With this we can prove our local modification result:

Theorem 4.14 (Local Improvement). *Take the hypotheses of Theorem 4.8 and suppose that*

$$(4.16) \quad \text{for some } \hat{\pi}_X \in \hat{\Pi}_X \text{ we have } \mu_{\hat{\pi}_X}(\{F_{\hat{\pi}_X} \neq 0\}) > 0.$$

Then for all $\varepsilon > 0$ there exists $\xi_\varepsilon \in C^\infty(X; \mathbb{R}^n)$, depending on $F_{\hat{\pi}_X}$, such that

$$\mathcal{G}_p(f + \xi_\varepsilon) < \mathcal{G}_p(f) \quad \text{and} \quad \mathcal{C}(f + \xi_\varepsilon) < \mathcal{C}(f) + \varepsilon.$$

Furthermore, if $\mu_{\hat{\pi}_X}(f^{-1}(\partial\Omega)) = 0$, then ξ_ε can be chosen so that $f + \xi_\varepsilon$ takes values only in Ω , whence f is not a local minimum of \mathcal{G}_p in $W^{k,q}(X; \Omega)$.

This result says that the barycenter field, under the condition (4.16), allows local modifications that reduce \mathcal{G}_p with only small additional budget. It also implies that the function $J(\ell)$ is strictly decreasing at those ℓ where there exists an ℓ -optimizer f_ℓ having nontrivial barycenter field in the sense of (4.16).

Proof of Theorem 4.14. Let $\varepsilon > 0$ be given. Let $V = \{v_j\}_{j=1}^\infty \subseteq \mathbb{R}^n \setminus \{0\}$ be dense and fix $c \in (0, 1)$. For all j define

$$X_j = \{x \in X \mid |F_{\hat{\pi}_X}(x) - v_j| < c|v_j|\}$$

Observe $\{F_{\hat{\pi}_X} \neq 0\} = \bigcup_j X_j$, and that because $F_{\hat{\pi}_X}$ is Borel-measurable, each X_j is measurable. Since $\{X_j\}$ is countable and $\mu_{\hat{\pi}_X}(\{F_{\hat{\pi}_X} \neq 0\}) > 0$, for at least one j_0 we have $\mu_{\hat{\pi}_X}(X_{j_0}) > 0$. Now because $\mu_{\hat{\pi}_X}$ is Radon, the density theorem (see, e.g., [53, Cor. 2.14(1)]) and Corollary 4.13 imply $\mu_{\hat{\pi}_X}$ -a.e. $x \in X_{j_0}$ is a density point of $\mu_{\hat{\pi}_X}$ for which (4.15) holds. Fix one and call it x_{j_0} .

Let η be a bump function on $B_1(0; \mathbb{R}^n)$ and define

$$\xi_\delta(x) = v_{j_0} \eta((x - x_{j_0})/\delta),$$

which is compactly supported in the ball $B_\delta(x_{j_0})$. Applying Theorem 4.8, since $\hat{\pi}_X$ might not be optimal for ξ_δ we get the inequality

$$(*) = \lim_{a \rightarrow 0} \frac{\mathcal{G}_p(f + a\xi_\delta) - \mathcal{G}_p(f)}{a} \leq - \int_{B_\delta(x_{j_0})} \langle F_{\hat{\pi}_X}, \xi_\delta \rangle d\mu_{\hat{\pi}_X}(x).$$

Let $A_0 = B_\delta(x_{j_0}) \cap X_{j_0}$ and $A_1 = B_\delta(x_{j_0}) \setminus A_0$. Then we can rewrite the above as

$$(*) \leq - \int_{A_0} \langle F_{\hat{\pi}_X}, \xi_\delta \rangle d\mu_{\hat{\pi}_X}(x) - \int_{A_1} \langle F_{\hat{\pi}_X}, \xi_\delta \rangle d\mu_{\hat{\pi}_X}(x).$$

For the A_0 integral: By the definition of X_{j_0} , for all $x \in A_0$,

$$-\langle F_{\hat{\pi}_X}(x), v_{j_0} \rangle < -\frac{1}{2} \left(|F_{\hat{\pi}_X}(x)|^2 + (1 - c^2)|v_{j_0}|^2 \right).$$

We ignore the $|F_{\hat{\pi}_X}(x)|^2$ term and define

$$\beta_0 = \frac{1 - c^2}{2} |v_{j_0}|^2 \quad (\text{note } \beta_0 > 0).$$

For the A_1 integral, the global bound $|F_{\hat{\pi}_X}| \leq \text{diam}(\Omega)$ gives

$$-\langle F_{\hat{\pi}_X}, v_{j_0} \rangle \leq \text{diam}(\Omega)|v_{j_0}| =: \beta_1 \quad (\text{note } \beta_1 > 0).$$

Thus we have

$$(4.17) \quad (*) < -\beta_0 \int_{A_0} \eta\left(\frac{x-x_{j_0}}{\delta}\right) d\mu_{\hat{\pi}_X} + \beta_1 \int_{A_1} \eta\left(\frac{x-x_{j_0}}{\delta}\right) d\mu_{\hat{\pi}_X}.$$

Now fix some $\lambda \in (0, 1)$. On the one hand,

$$\begin{aligned} \int_{A_0} \eta\left(\frac{x-x_{j_0}}{\delta}\right) d\mu_{\hat{\pi}_X} &\geq \mu_{\hat{\pi}_X}(A_0 \cap B_{\lambda\delta}(x_{j_0})) \inf_{A_0 \cap B_{\lambda\delta}(x_{j_0})} \eta\left(\frac{x-x_{j_0}}{\delta}\right) \\ &\geq \mu_{\hat{\pi}_X}(A_0 \cap B_{\lambda\delta}(x_{j_0})) \exp(-1/(1-\lambda^2)), \end{aligned}$$

while on the other hand $\int_{A_1} \eta\left(\frac{x-x_{j_0}}{\delta}\right) d\mu_{\hat{\pi}_X} \leq C\mu_{\hat{\pi}_X}(A_1)$ with C depending on η only. For concision, we now suppress writing the center x_{j_0} of the balls $B_\delta(x_{j_0})$, $B_{\lambda\delta}(x_{j_0})$. Letting $\beta'_0 = \beta_0 e^{-1/(1-\lambda^2)} > 0$, factoring $\mu_{\hat{\pi}_X}(A_0)$ out of the right side of (4.17) thus gives

$$\lim_{a \rightarrow 0} \frac{\mathcal{G}_p(f + a\xi_\delta) - \mathcal{G}_p(f)}{a} \leq \mu_{\hat{\pi}_X}(A_0) \left[-\beta'_0 \frac{\mu_{\hat{\pi}_X}(A_0 \cap B_{\lambda\delta})}{\mu_{\hat{\pi}_X}(A_0)} + C\beta_1 \frac{\mu_{\hat{\pi}_X}(A_1)}{\mu_{\hat{\pi}_X}(A_0)} \right].$$

Since x_{j_0} is a $\mu_{\hat{\pi}_X}$ -density point of X_{j_0} , the second term vanishes as $\delta \rightarrow 0$. For the first term, recalling $A_0 = B_\delta \cap X_{j_0}$ we may rewrite the fraction as

$$\frac{\mu_{\hat{\pi}_X}(X_{j_0} \cap B_{\lambda\delta})}{\mu_{\hat{\pi}_X}(X_{j_0} \cap B_\delta)} = \frac{\mu_{\hat{\pi}_X}(X_{j_0} \cap B_{\lambda\delta})}{\mu_{\hat{\pi}_X}(B_{\lambda\delta})} \cdot \frac{\mu_{\hat{\pi}_X}(B_{\lambda\delta})}{\mu_{\hat{\pi}_X}(B_\delta)} \cdot \frac{\mu_{\hat{\pi}_X}(B_\delta)}{\mu_{\hat{\pi}_X}(X_{j_0} \cap B_\delta)}.$$

Since x_{j_0} is a $\mu_{\hat{\pi}_X}$ -density point of X_{j_0} for which (4.15) holds, we thus see that

$$\limsup_{\delta \rightarrow 0} \frac{\mu_{\hat{\pi}_X}(A_0 \cap B_{\lambda\delta})}{\mu_{\hat{\pi}_X}(A_0)} \geq 1 \cdot \lambda^{n+1} \cdot 1 > 0.$$

Hence there exists a choice of $\delta > 0$ such that

$$\lim_{a \rightarrow 0} \frac{\mathcal{G}_p(f + a\xi_\delta) - \mathcal{G}_p(f)}{a} \leq -\beta'_0 \mu_{\hat{\pi}_X}(A_0) \lambda^{n+1} + C\beta_1 \mu_{\hat{\pi}_X}(A_1) < 0.$$

In particular, for $a > 0$ sufficiently small, taking $\xi_\varepsilon = a\xi_\delta$ yields $\mathcal{G}_p(f + \xi_\varepsilon) < \mathcal{G}_p(f)$ as well as $\mathcal{C}(a\xi_\delta) < \varepsilon$.

Finally, if $\mu_{\hat{\pi}_X}(f^{-1}(\partial\Omega)) = 0$ then we may assume x_{j_0} is chosen so that $f(x_{j_0}) \in \Omega^\circ$. Taking δ sufficiently small then yields $d(f(B_\delta(x_{j_0})), \partial\Omega) > 0$ and taking $a < d(f(B_\delta(x_{j_0})), \partial\Omega)/|v_{j_0}|$ guarantees $f + a\xi_\delta$ takes values only in Ω . \blacksquare

5. THE DISCRETE PROBLEM & SIMULATIONS

In this section we discuss some theoretical justifications for two discretization schemes for the problem.

5.1. Discretizing ρ . A natural idea is to discretize ρ by representing it with an empirical measure ρ_N . We then obtain a consistency result for the ρ_N formulation for (HC) directly from Lemma 2.3 and Theorem 2.12.

Corollary 5.1 (Consistency of (HC)). *Take (H.1), (H.2), (H.3.a), and (H.3.b). Suppose that ρ_N converges weak-* to ρ . Fix $\ell \geq \ell_{\min}$ and for all N let f_N be a ℓ -optimizer for (HC) with respect to the objective $\mathcal{G}_p(\square; \rho_N)$. Then every subsequence of $\{f_N\}$ has a weakly-convergent (and thus, by Corollary 2.5, uniformly-convergent)*

subsequence whose limit is an ℓ -optimizer for (HC) with respect to the objective $\mathcal{G}_p(\square; \rho)$.

In particular, taking the ρ_N to be empirical measures for ρ yields the almost-sure equalities

$$\lim_{N \rightarrow \infty} \mathcal{G}_p(f_N; \rho_N) \stackrel{\text{a.s.}}{=} \lim_{N \rightarrow \infty} \mathcal{G}_p(f_N; \rho) \stackrel{\text{a.s.}}{=} J(\ell).$$

In Section 6 we will shift focus toward the (SP) formulation owing to its computational benefits. Hence we now prove a consistency result for (SP).

Corollary 5.2 (Consistency of (SP)). *Take the same hypotheses as Corollary 5.1, only this time fixing $\lambda > 0$ and defining the f_N to be optimizers of (SP) with respect to the objective $\mathcal{G}_p^\lambda(\square; \rho_N)$. Then every subsequence of $\{f_N\}$ has a weakly-convergent (and thus, by Corollary 2.5, uniformly-convergent) subsequence whose limit is a solution to (SP) with $\mathcal{G}_p^\lambda(\square; \rho)$.*

Proof. First we show $\sup_N \mathcal{C}(f_N) < \infty$. To that end let ω_0, ω_1 such that $d(\omega_0, \omega_1) = \text{diam}(\Omega)$ and let $f_{\max} = \omega_0$, $\rho_{\max} = \delta_{\omega_1}$; observe that they achieve $\sup_{f, \rho} \mathcal{G}_p(f; \rho) = \text{diam}(\Omega)^p$. Then for all N , taking f_{\max} as a competitor yields

$$\lambda \mathcal{C}(f_N) \leq \mathcal{G}_p^\lambda(f_N; \rho_N) \leq \mathcal{G}_p^\lambda(f_{\max}; \rho_N) \leq \mathcal{G}_p^\lambda(f_{\max}; \rho_{\max}) = \text{diam}(\Omega)^p + \lambda \mathcal{C}(f_{\max}),$$

whence we see $\sup_N \mathcal{C}(f_N) < \infty$ as desired (note that it was necessary to pass through $\mathcal{G}_p^\lambda(f_{\max}; \rho_N)$ since priori we cannot compare $\mathcal{C}(f_N)$ and $\mathcal{C}(f_{\max})$).

In any case, after obtaining this uniform boundedness $\sup_N \mathcal{C}(f_N) < \infty$, the consistency result follows from Lemma 2.3 and Theorem 2.12. \blacksquare

5.2. Representing f by Samples. In this subsection we discuss some theoretical justifications for a particular discretization scheme we use to simulate (SP). To that end we define discretized analogues of $F_{\hat{\pi}_X}$ (Theorem 5.3) and Corollary 4.10. We focus on discretizations related to f and its perturbations by the barycenter field, but will not consider simultaneous discretization of ρ (though note ρ might happen to be discrete on its own anyways).

The idea is to sample $Y = f(X)$, perturb the samples by a discretized analogue of $F_{\hat{\pi}_X}$, smooth any discontinuities, reparametrize, and then repeat. We believe this scheme could be particularly useful in real-world situations where f is being modified in real-time; for example if we are continuously collecting new samples from ρ .

To help distinguish with the continuous case we will endeavor to denote all discretized objects with sans-serif letters.

Definition 5.3 (Discrete Barycenter Field). Let Y_N be a collection of N points in $f(X)$ and let $\hat{\pi}_{Y_N}$ be a measurable selection of the closest-point projection onto Y_N . Let $(\rho_{Y, \hat{\pi}_{Y_N}}, \nu_{\hat{\pi}_{Y_N}})$ denote the disintegration of ρ by $\hat{\pi}_{Y_N}$. Then we define the *discrete barycenter field* at $y_j \in Y_N$ to be

$$(5.1) \quad F_{\hat{\pi}_{Y_N}}(y_j) = p \int_{\hat{\pi}_{Y_N}^{-1}(y_j)} (\omega - y_j) |\omega - y_j|^{p-2} d\rho_{y_j, \hat{\pi}_{Y_N}}(\omega),$$

again taking the convention that $v|v|^{p-2} = 0$ when $v = 0$.

Note, $F_{\hat{\pi}_{Y_N}}(y_j)$ is (up to the constant p) just the $p-1$ barycenter of the Voronoi cell in coordinates with the base point y_j at the origin.

Remark 5.4. For each N let X_N be an N -sample empirical measure for some absolutely continuous $\mu \in \mathcal{P}(X)$ and let $Y_N = f(X_N)$. One may show that as $N \rightarrow \infty$, $\hat{\pi}_{Y_N} \rightarrow \hat{\pi}_Y^*$ a.s. on $\Omega \setminus \mathcal{A}_f$, whence with (H*) we get $\nu_{\hat{\pi}_{Y_N}} \rightarrow \nu_{\hat{\pi}_Y^*}$ weak-* a.s. While we have not investigated the matter in detail, we therefore suspect there could be a consistency result along the lines of $F_{\hat{\pi}_{Y_N}} \rightarrow F_{\hat{\pi}_Y^*}$, in the sense that for all $\xi_Y \in C(Y; \mathbb{R}^n)$ one should have something like

$$\lim_{N \rightarrow \infty} - \int_Y \langle F_{\hat{\pi}_{Y_N}}(y), \xi_Y(y) \rangle d\nu_{\hat{\pi}_{Y_N}}(y) \stackrel{\text{a.s.}}{=} - \int_Y \langle F_{\hat{\pi}_Y^*}(y), \xi_Y(y) \rangle d\nu_{\hat{\pi}_Y^*}(y).$$

The intuition would be that $F_{\hat{\pi}_{Y_N}}$ is averaging $F_{\hat{\pi}_Y^*}$ over $\hat{\pi}_{Y_N}^{-1}(y_N)$, up to error arising from treating y_N as the base point instead of $\hat{\pi}_Y^*(\omega)$, which should be small in light of $\hat{\pi}_{Y_N} \rightarrow \hat{\pi}_Y^*$.

In analogy with Theorem 4.8 (more precisely with Corollary 4.10) we have the following:

Proposition 5.5. *Take (H.2). Let $\xi_N : Y_N \rightarrow \mathbb{R}^n$ such that for all $\varepsilon > 0$ sufficiently small, $Y_{N,\varepsilon} = \{y + \varepsilon \xi_N(y) \mid y \in Y_N\} \subseteq \Omega$. Let $Y_{N,\text{out}} = \{y \in Y_N \mid \xi_N(y) \neq 0\}$ and suppose either $p > 1$, or that $p = 1$ and $\rho(Y_{N,\text{out}}) = 0$. Then*

$$\lim_{\varepsilon \rightarrow 0} \frac{\mathcal{G}_p(Y_{N,\varepsilon}) - \mathcal{G}_p(Y_N)}{\varepsilon} = - \sum_{Y_N} \langle F_{\hat{\pi}_{Y_N}}(y), \xi_N(y) \rangle \nu_{\hat{\pi}_{Y_N}}(y).$$

On the other hand, if $p = 1$ and $\rho(Y_{N,\text{out}}) > 0$ then the same result holds with the modification

$$\lim_{\varepsilon \rightarrow 0} \frac{\mathcal{G}_1(Y_{N,\varepsilon}) - \mathcal{G}_1(Y_N)}{\varepsilon} = - \sum_{Y_N} \left\langle F_{\hat{\pi}_{Y_N}}(y) - \chi_{Y_N}(y) \hat{\xi}_N(y), \xi_N(y) \right\rangle \nu_{\hat{\pi}_{Y_N}}(y).$$

where $\hat{\xi}_N(y)$ is the unit vector $\frac{1}{|\xi_N(y)|} \xi_N(y)$ (again, taking the convention $\hat{0} = 0$).

Proof. Define $\hat{\pi}_{Y_{N,\varepsilon}}$ to be a measurable selection of the closest point projection onto $Y_{N,\varepsilon}$. Note that since $Y_N, Y_{N,\varepsilon}$ are discrete, the $\hat{\pi}_{Y_{N,\varepsilon}}$ can be chosen such that for any fixed $\omega \in \Omega$, there exists ε_ω such that

$$\text{for all } 0 < \varepsilon \leq \varepsilon_\omega, \quad \hat{\pi}_{Y_{N,\varepsilon}}(\omega) = \hat{\pi}_{Y_N}(\omega) + \varepsilon \xi_N(\hat{\pi}_{Y_N}(\omega)).$$

Hence fix $\varepsilon > 0$ and let

$$\Omega_\varepsilon = \{\omega \mid \hat{\pi}_{Y_{N,\varepsilon}}(\omega) = \hat{\pi}_{Y_N}(\omega) + \varepsilon \xi_N(\hat{\pi}_{Y_N}(\omega))\}; \text{ note } \bigcup_{\varepsilon > 0} \Omega_\varepsilon = \Omega.$$

Since Ω is bounded (H.2) and $Y_{N,\varepsilon} \subseteq \Omega$, we thus get

$$\begin{aligned} \lim_{\varepsilon \rightarrow 0} \frac{\mathcal{G}_p(Y_{N,\varepsilon}) - \mathcal{G}_p(Y_N)}{\varepsilon} &= \lim_{\varepsilon \rightarrow 0} \int_\Omega \frac{d(\omega, Y_{N,\varepsilon})^p - d(\omega, Y_N)^p}{\varepsilon} d\rho \\ &= \lim_{\varepsilon \rightarrow 0} \left[\int_{\Omega_\varepsilon} \frac{|\omega - (\hat{\pi}_{Y_N} + \varepsilon \xi(\hat{\pi}_{Y_N}))|^p - |\omega - \hat{\pi}_{Y_N}|^p}{\varepsilon} d\rho + O(\rho(\Omega \setminus \Omega_\varepsilon)) \right], \end{aligned}$$

where we have suppressed writing the ω in $\hat{\pi}_{Y_N}(\omega)$ (notice we get the term $O(\rho(\Omega \setminus \Omega_\varepsilon))$ due to $\frac{d(\omega, Y_{N,\varepsilon})^p - d(\omega, Y_N)^p}{\varepsilon} \leq C$ independent of ε). Further decomposing the domain of integration of the Ω_ε integral into $\Omega_\varepsilon \setminus Y_N$ and Y_N , we see the Y_N integral reduces to $\sum_{Y_N} \varepsilon^{p-1} |\xi_N| \rho(y)$, which is nonzero iff $\rho(Y_{N,\text{out}}) > 0$. On the

other hand, Taylor expanding the integrand of the $\Omega_\varepsilon \setminus Y_N$ integral around $\varepsilon = 0$ yields, as in Theorem 4.8,

$$h(\omega, \hat{\pi}_{Y_N}) = \langle -p(\omega - \hat{\pi}_{Y_N})|\omega - \hat{\pi}_{Y_N}|^{p-2}, \xi_N(\hat{\pi}_{Y_N}) \rangle + O(\varepsilon).$$

Taking the convention $h(\omega, y) = 0$ when $\omega = y$ we may thus write

$$\lim_{\varepsilon \rightarrow 0} \frac{\mathcal{G}_p(Y_{N,\varepsilon}) - \mathcal{G}_p(Y_N)}{\varepsilon} = \int_{\Omega} h(\omega, \hat{\pi}_{Y_N}) + \lim_{\varepsilon \rightarrow 0} \varepsilon^{p-1} \chi_{Y_N}(\omega) |\xi_N(\hat{\pi}_{Y_N})| d\rho,$$

the second term vanishing if $p \neq 1$ or if $\rho(Y_{N,\text{out}}) = 0$. Finally, applying the disintegration theorem to the h integral obtains the desired result. \blacksquare

Now we discuss a discrete analogue of Theorem 4.14. To consider a discrete analogue of the cost $\mathcal{C}(f)$, start with an arbitrarily-chosen discrete set $Y_N = \{\omega_1, \dots, \omega_N\} \subseteq \Omega$ and define the collection of admissible parametrizations by

$$(5.2) \quad \Phi(Y_N) = \{f \in W^{k,q}(X; \Omega) \mid Y_N \subseteq f(X)\}.$$

A construction similar to Proposition 3.9 shows that there always exists a smooth $f : X \rightarrow \Omega$ for which $Y_N \subseteq Y$, whence $\Phi(Y_N)$ is nonempty. So we may define a discrete analogue of the cost $\mathcal{C}(f)$ by taking

$$(5.3) \quad \mathcal{C}(Y_N) = \inf_{f \in \Phi(Y_N)} \mathcal{C}(f).$$

Remark 5.6. We note that the definition of \mathcal{C} succinctly encodes that N is a proxy for the “complexity” of the approximation Y_N : If $Y_N \subseteq Y_{N+1}$ then $\Phi(Y_N) \supseteq \Phi(Y_{N+1})$, which implies $\mathcal{C}(Y_N) \leq \mathcal{C}(Y_{N+1})$.

We may state the analogue of Theorem 4.14 in these terms. Note that in contrast to Theorem 4.14, in this case the proof is almost trivial: Because Y_N is discrete, we do not have to treat the same regularity concerns for $F_{\hat{\pi}_{Y_N}}$ that we did for $F_{\hat{\pi}_X}$ in Theorem 4.14.

Corollary 5.7. *Let $Y_N = \{y_1, \dots, y_N\} \subseteq \Omega^\circ$ be given and suppose there exists a measurable selection of the closest-point projection onto Y_N such that*

$$\nu_{\hat{\pi}_{Y_N}}(\{F_{\hat{\pi}_{Y_N}} \neq 0\}) > 0.$$

Then if $p > 1$, or if $p = 1$ and $\rho(Y_{N,\text{out}}) = 0$, there exists ξ_N such for ε sufficiently small,

$$\mathcal{G}_p(Y_{N,\varepsilon}) < \mathcal{G}_p(Y_N) - C\varepsilon \quad \text{and} \quad \mathcal{C}(Y_{N,\varepsilon}) < \mathcal{C}(Y_N) + \varepsilon,$$

where C is a constant dependent on Y_N and ρ .

Proof. By construction of $F_{\hat{\pi}_{Y_N}}$, there exists an $\varepsilon_N > 0$ such that for all $y \in Y_N$ we have $y + \varepsilon_N F_{\hat{\pi}_{Y_N}}(y) \in \Omega$. Let $f_{\varepsilon_N} \in \Phi(Y_N)$ such that

$$\mathcal{C}(f_{\varepsilon_N}) - \frac{\varepsilon_N}{2} < \mathcal{C}(Y_N).$$

From now on write $f = f_{\varepsilon_N}$. Now for each $j = 1, \dots, N$, let $x_j \in f^{-1}(y_j)$ and pick $\delta_j > 0$ such that for all $i \neq j$, $f(B_{\delta_j}(x_j)) \cap f(B_{\delta_i}(x_i)) = \emptyset$. Finally, for some choice of coefficients $c_1, \dots, c_N > 0$ define $\xi : X \rightarrow \mathbb{R}^n$ by $\xi(x) = \sum_{j=1}^N c_j \eta_{\delta_j}(x - x_j) F_{\hat{\pi}_{Y_N}}(y_j)$, where η_{δ_j} denotes a smooth nonnegative function compactly supported in the δ_j -ball

such that $\eta_{\delta_j}(0) = 1$. Notice that although a priori δ_j depends on $f = f_{\varepsilon_N}$, we can make it depend only on Y_N for sufficiently small ε_N . Then taking each

$$c_j = \frac{1}{2N \|\eta_{\delta_j}\|_{W^{k,q}(X;\Omega)} |F_{\hat{\pi}_{Y_N}}(y_j)|}$$

yields $\mathcal{C}(\xi(x)) \leq \frac{1}{2}$.

Finally, let $\xi_N(y_j) = \xi(x_j)$ and as before let $Y_{N,\varepsilon_N} = \{y + \varepsilon_N \xi \mid y \in Y_N\}$. Note that since $f + \varepsilon_N \xi \in \Phi(Y_{N,\varepsilon_N})$,

$$\mathcal{C}(Y_{N,\varepsilon}) \leq \mathcal{C}(f) + \varepsilon_N \mathcal{C}(\xi) < \mathcal{C}(Y_N) + \varepsilon_N.$$

By Proposition 5.5, we see that for ε_N sufficiently small,

$$(5.4) \quad \mathcal{G}_p(Y_{N,\varepsilon_N}) - \mathcal{G}_p(Y_N) = -\varepsilon_N \sum_j \frac{|F_{\hat{\pi}_{Y_N}}(y_j)|}{N \|\eta_{\delta_j}\|_{W^{k,q}(X;\Omega)}} \nu_{\hat{\pi}_{Y_N}}(y) + O(\varepsilon_N^2)$$

where the summands on the right-hand side are independent of ε_N . This completes the proof. \blacksquare

Note that (5.4) immediately allows us to see a coarse upper bound on how small ε_N must be for the approximation to hold: Since $0 \leq \mathcal{G}_p(Y_{N,\varepsilon}) = \mathcal{G}_p(Y_N) - C\varepsilon_N + O(\varepsilon_N^2)$, we need at least

$$(5.5) \quad \varepsilon_N \leq \mathcal{G}_p(Y_N)/C.$$

5.3. Simulations Of (SP) In Two Dimensions With Uniform Target Measure. Corollary 5.7 provides theoretical motivation for a numerical scheme for performing gradient descent on $\mathcal{G}_p(Y_N) + \lambda \mathcal{C}(f)$ by taking discrete steps along $F_{\hat{\pi}_{Y_N}} + \lambda \nabla \mathcal{C}(f)$. Similar ideas have been pursued many times before: In the context of principal curves and surfaces, see e.g. [39, 42], and particularly [26]; in the context of spline fitting see the references for *unstructured* fitting listed in Section 1.7.6, particularly [78], which uses a penalty similar to ours for $k = 2$.

However, there is a sense in which these algorithms are all primarily designed for use in *real-world* contexts rather than in studying *theoretical* properties of (HC), (SP). In Section 5.3.1 we explain this distinction in greater detail, and particularly highlight the motivation for developing algorithms tailored toward the “theoretical” case. Then in Section 5.3.2 we introduce such a routine for the special case where $m = 1$, $n = 2$, ρ is uniform, and $\partial \text{supp}(\rho)$ is piecewise linear (note there is no restriction on p beyond $p \geq 1$). Example outputs are shown in Appendix A. We hypothesize that the algorithm could be adapted to other values of m, n ; however, loosening the restrictions on ρ would be more difficult.

5.3.1. (SP) in “Real-world” vs. “Theoretical” Cases. We propose to draw a distinction between numerical algorithms for (SP) in “real-world” vs. “theoretical” contexts. The difference is essentially one of data resolution and hence only applies when ρ has a non-atomic part; let us assume this in the below.

(Real-world case): In real-world cases we typically do not have access to ρ itself but rather a finite set of M (possibly-noisy) observations $\omega_1, \dots, \omega_M$. In this case, discretizing $Y = f(X)$ into N samples $Y_N = \{y_1, \dots, y_N\}$, we see that for each y_j the integral expression for $F_{\hat{\pi}_{Y_N}}(y_j)$ (5.1) reduces to a summation, making it simple to compute. Then, we may take a gradient step à la Corollary 5.7 and iterate (note the c_j ’s in Corollary 5.7 may be chosen heuristically; see Section 5.3.3).

In this scheme, we are free to choose N but not M . This begs the question: Given a fixed M , what is a “reasonable” choice of N ? Observe that if $N > M$ then the evolution behavior of Y_N will likely be highly distorted: On any given iteration at most M of the y_j would have $F_{\hat{\pi}_{Y_N}}(y_j) \neq 0$ (denote them Y_N^{lead}), while the remaining $N - M$ points have their behavior dictated purely by $\lambda \nabla \mathcal{C}(f)$ (denote them Y_N^{follow}). Note that in the steady state we expect the points of Y_N^{follow} to simply interpolate Y_N^{lead} according to some f achieving $\mathcal{C}(Y_N^{\text{lead}})$; thus the points of Y_N^{follow} encode no meaningful information, and might as well be omitted by choosing $N \leq M$ from the start. Stated plainly, in the real-world case, our data sampling resolution M is an upper bound on the maximum “meaningful” resolution of the approximant Y_N .

(Theoretical case): Now suppose, by contrast, that we are working in a context where we have direct access to the ground-truth measure ρ (since we assumed ρ has nontrivial non-atomic part, this typically occurs only in theoretical contexts). We may obtain a Monte-Carlo scheme for $F_{\hat{\pi}_{Y_N}}$ by simply drawing M samples from ρ at each iteration and proceeding as in the real-world case. Importantly, we are now free (modulo computational constraints) to take as many samples as we want from ρ , i.e. to make M arbitrarily large. This offers some important benefits.

1. Since there is no constraint on M , we also no longer have a constraint on what constitutes a “reasonable” N . In particular, it becomes possible to take $N \rightarrow \infty$, which (see Theorem 5.6) opens the door to studying an approximate asymptotic relationship between \mathcal{G}_p and \mathcal{C} .
2. By taking M to be large, we can also improve the precision of our approximation of $F_{\hat{\pi}_{Y_N}}$. This is noteworthy because the scheme can exhibit instabilities with respect to $F_{\hat{\pi}_{Y_N}}$. Loosely speaking, the problem is that $F_{\hat{\pi}_{Y_N}}$ is dependent on the $\hat{\pi}_{Y_N}^{-1}(y_j)$, which themselves depend on the *global* structure of Y_N (note, e.g. that updating the position of one of the y_j typically modifies *all* of the cells sharing a face with $\hat{\pi}_{Y_N}^{-1}(y_j)$). Thus, a distortion in $F_{\hat{\pi}_{Y_N}}$ at one iteration typically results in a distortion to Y_N at the next iteration, thereby distorting the subsequent $F_{\hat{\pi}_{Y_N}}$, and so on. (In our experiments this was partially mitigated by the $\lambda \nabla \mathcal{C}(f)$ term but nonetheless caused some problems).

In practice, however, a naïve implementation of this Monte-Carlo scheme can require intractable values of M to achieve these effects. We illustrate this in the special case $m = 1$, $n = 2$. For each j , define

$$\sigma_j = \text{Var}_{\rho_{y_j, \hat{\pi}_{Y_N}}} [(\omega - y_j)|\omega - y_j|^{p-2}].$$

Let $N = 200$ and suppose we want to guarantee with $\geq 99\%$ confidence that we approximate each $F_{\hat{\pi}_{Y_N}}(y_j)$ within, say, $\frac{\sigma_j}{100}$ of the true value. At first glance this degree of precision might appear overly demanding, but again recall that since each step of the simulation depends on the previous steps, small initial errors in $F_{\hat{\pi}_{Y_N}}$ may propagate to significant end-state differences.

In any case, denote the number of sample points $\omega_j \in \hat{\pi}_{Y_N}^{-1}(y_j)$ by M_j ; it suffices to choose the M_j such that the probability of being within $\frac{\sigma_j}{100}$ of $F_{\hat{\pi}_{Y_N}}$ is $\geq \sqrt[p]{.99} \approx .9999$. Via a standard Z -score argument we find that choosing $M_j \geq \lceil (100 \cdot 3.89)^2 \rceil = 151274$ suffices. Applying this to each j , we see that we’d need at *minimum* $M \approx M_j \times N \approx 3 \times 10^7$ samples at each iteration to get the desired precision.

Actually, even this is not enough, as a priori there is no guarantee the sample points will be uniformly distributed across the $\hat{\pi}_{\mathbf{V}_N}^{-1}(y_j)$. For example, if all the $\rho_{y_j, \hat{\pi}_{\mathbf{V}_N}}$ have identical total mass, then one may compute that in order to get $\geq 99\%$ probability that randomly assigning samples to each $\hat{\pi}_{\mathbf{V}_N}^{-1}(y_j)$ yields each $M_j \geq 3 \times 10^7$, the number of points M to draw is lower bounded by 2.92×10^{13} , which is prohibitively large.

For some choices of ρ this could be avoided by employing *low-discrepancy sequences*. It is essentially trivial to do so for simple $\text{supp}(\rho)$ (e.g., the unit square), but if $\partial \text{supp}(\rho)$ is sufficiently complex, this too could become computationally burdensome. In any case, there remains a “hard” step of assigning each of the M sample points to the corresponding closest y_j . Naïvely this can be done in $O(MN)$ time; however, this was prohibitively slow on our hardware.

A faster approach can be obtained by preprocessing the Voronoi cells into an efficient *point location* datastructure (see e.g. [2, Ch. 6]), which reduces the complexity to $O(M \log(N) + N)$. However, as it turns out, when $m = 1$, $n = 2$, and ρ is uniform, the preprocessing required to compute these point location datastructures (typically some form of triangulation procedure) is sufficient for running a fast algorithm that computes $F_{\hat{\pi}_{\mathbf{V}_N}}$ via approximating an *analytic* formula, thus obviating the need for a Monte Carlo procedure. We discuss this algorithm now.

5.3.2. A Deterministic Algorithm For Theoretical Applications. We now demonstrate that in at least one special case, for all $p \geq 1$ one may obtain a fast algorithm for computing $F_{\hat{\pi}_{\mathbf{V}_N}}$. Note that some of the precise implementation details and runtime analysis are beyond the scope of this paper, and hence we postpone them for a later work.

The particular requirements for our algorithm are

- $m = 1$,
- $n = 2$, and
- ρ is uniform with $\partial \text{supp}(\rho)$ piecewise linear (PL).

With these hypotheses we are able to represent $F_{\hat{\pi}_{\mathbf{V}_N}}$ analytically rather than by approximation via Monte Carlo methods. As far as we are aware this has not been done before. Performance is discussed briefly in Section 5.3.3; for now, we focus on the high-level consequences. Essentially, by removing this source of randomness, our method appears to offer better stability for properties of theoretical interest such as symmetry, self-similarity, and so on, as can be seen comparing the curves in Fig. 9 against the curve obtained via stochastic gradient descent in [18, Fig. 1]. We believe this stability is highly desirable when using the algorithm for purposes such as formulating conjectures, e.g. “if ρ is uniform, then as $p \rightarrow \infty$, to what extent does the regularity of a prototypical ‘good solution’ tend towards that of $\partial\Omega$?”

We choose to represent f by a cubic spline, which we parametrize by its knots. We initialize with some seed function f_0 (either chosen randomly or set by the user) and then iterate as follows. In the first step of the j^{th} iteration, we sample $N_j = \left\lceil \frac{\text{length}(f_j)}{\delta} \right\rceil$ points from f_j uniformly with respect to arc length, where δ is a parameter controlling the maximum distance between two adjacent points. Call the sampled points \mathbf{Y}_{N_j} . To compute \mathbf{Y}_{N_j} efficiently, we give a numerically stable method to calculate the roots of the “squared speed” quartic, which we can substitute into the routine of [37]. That routine then calculates the arc length of a cubic parametric curve in two dimensions by reduction to an elliptic integral, which was previously

solved in [10]. Using this we can efficiently compute an approximate arc length parametrization of f_j using Newton's method since the speed of the curve is easily computed. Thus Y_{N_j} is given by evaluating evenly-spaced points of $[0, \text{length}(f_j)]$.

Once we have Y_{N_j} , we compute the Voronoi cells $\hat{\pi}_{Y_N}^{-1}(y_j)$ using a standard algorithm. Then for each cell, we compute $F_{\hat{\pi}_{N_j}}$ by decomposing the cell into triangles and computing the contribution of each triangle individually. If $\text{supp}(\rho)$ is convex, then $\text{supp}(\rho) \cap \hat{\pi}_{Y_N}^{-1}(y_j)$ is a convex polygon and we obtain a triangulation by enumerating the vertices $\{v_1, \dots, v_M\}$ and iterating through the triangles $\Delta v_1 v_i v_{i+1}$ where $i = 2, \dots, M-1$. Otherwise, we run a Weiler-Atherton routine [80] to compute $\text{supp}(\rho) \cap \hat{\pi}_{Y_N}^{-1}(y_j)$ and apply a standard triangulation algorithm to the result.

Since ρ is uniform, any two of the resulting triangles intersect on at most a ρ -null set, whence we avoid double-counting in (5.1). Again since ρ is uniform, each triangle integral has a “nice” expression for general p in terms of the Gaussian hypergeometric function, which can be evaluated efficiently. Here, “nice” is in scare quotes because while the expressions are numerically efficient to evaluate, writing them down by hand for general p involves some slightly-messy casework. Hence, we simply note that in the $p = 2$ case, the contribution of triangle Δuvw can be computed instead via

$$2 \cdot \left(\frac{1}{3}(\mathbf{u} + \mathbf{v} + \mathbf{w}) - y_j \right) \rho(\Delta uvw),$$

where $\rho(\Delta uvw)$ can be computed e.g. via Heron's formula. Summing over all triangles then yields $F_{\hat{\pi}_{N_j}}$ precisely. Note that in practice we found that performance sometimes improved significantly when we reweighted $F_{\hat{\pi}_{N_j}}$ by $1/(\rho(\hat{\pi}_{Y_N}^{-1}(y_j)))^\kappa$, where $\kappa \in [0, 1]$ is a parameter chosen by the user.

Next, we approximate the gradient $\nabla \mathcal{C}$ of the Sobolev constraint with respect to the points Y_{N_j} as follows. First note that since f is a piecewise cubic polynomial, it will generally lack regularity higher than third differentiability, which is insufficient for computing $\mathcal{C}(f)$ for general k . Hence we first compute a new, sufficiently high-order spline \tilde{f} interpolating the arclen-evenly-spaced samples of f , and represent it via B-Splines. Then, we approximate the Sobolev norm of \tilde{f} with the vector q -norm of the derivatives of all orders evaluated at each of the interpolated points (by the regularity properties of the splines, this scheme is consistent).

We then take the gradient of this expression with respect to the locations of the points Y_{N_j} , resulting in an approximation $G_{Y_{N_j}}$. This can be done efficiently because the derivatives at the sample points depend linearly on the points being interpolated and moreover the linear relationship has the form of the inverse of a $(k+1)$ -width banded matrix, which can be computed very quickly. Finally, given a learning rate c we make the perturbation

$$Y_{N_{j+1}} = Y_N + c(F_{\hat{\pi}_{N_j}} - \lambda G_{Y_{N_j}}).$$

These perturbed points then become the knots of the next curve, and the algorithm terminates after reaching a prescribed number of iterations.

Initially, f does not cover Ω well and so the barycenter field has very large magnitude. To counteract this, we choose c to be small near the beginning of the simulation and increase it as a function of the iteration index i . We find that when we do this the arc length of the curve grows at a steady rate. We show the resulting curves at several points in time in Fig. 9. The curves themselves are in blue, the Voronoi cells are drawn with red edges and cell barycenters are shown as green

dots. Note that regions with dark-red shading represent the convergence of many Voronoi cell boundaries while white regions represent regions where few Voronoi cell boundaries converge. Hence (with the exception of the white regions corresponding to the endpoints) dark-red and bright-white regions tend to reflect base points on the curve where curvature is high.

In any case, we see that as time progresses, the curve begins to evenly fill the square in a fractal-like manner.

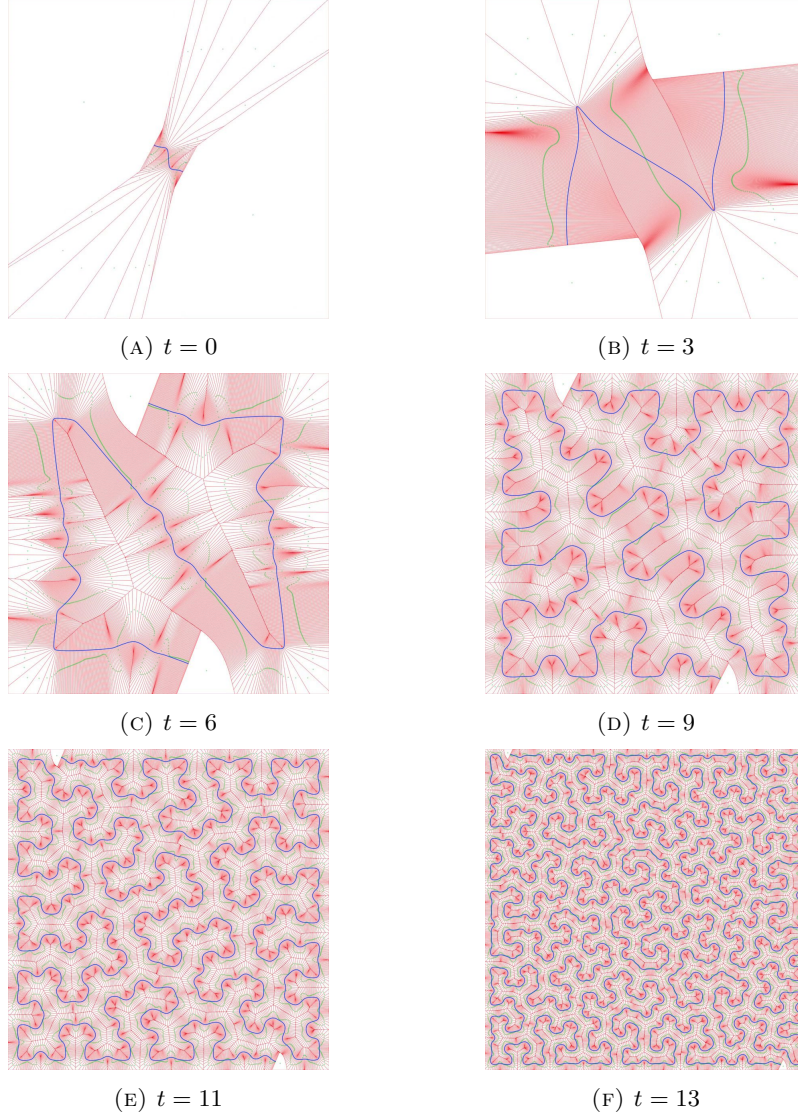


FIGURE 9. Evolving a curve according to $F_{\hat{\pi}_{Y_N}}$.

We also experimented in cases where λ decays as $\frac{1}{c} - 1$, this also yielded good curves, especially when the seed f_0 was very messy, e.g. interpolating random points. See Fig. 10 for an example.

5.3.3. *Discussion.* The algorithm is quite fast in practice when $\text{supp}(\rho)$ is convex, typically approaching a steady state after 10-20 seconds on a Mid-2015 MacBook Pro. For simple nonconvex domains like the one in Appendix A.2, performance was similar. However, we did see noticeable slowdowns when $\text{supp}(\rho)$ is highly nonconvex, e.g. the branching shape in Fig. 10.

One drawback of the approach above is that it involves a long list of somewhat-obscure parameters to tune (e.g. the κ in the $F_{\hat{\pi}_{N_j}}$ reweighting step), though in practice when $\text{supp}(\rho)$ was only mildly-nonconvex we saw decent behavior over a wide range of parameter values. Implementations that include a parameter search can remove some of this hand-tuning; for example, the choices of $c(i)$ and $\lambda(i)$ can be done away with by employing a line search. In our experiments, this yielded greatly-improved stability, though at a cost to runtime.

An alternative approach is to try and derive theoretical heuristics that yield decent (though perhaps not optimal) behavior. As a case study, let us consider the learning rate c that we use to scale $F_{\hat{\pi}_Y}$ for each update. What can the theory tell us about how to choose a “good” value of c ?

Some guidance comes from examining the c_j in the proof of Corollary 5.7. Note that the η_{δ_j} in the definition were chosen for two reasons. First, the η_{δ_j} ensured that the effects of the perturbations at each y_j were isolated from one another. In practice, we can guarantee this instead by choosing our resampling resolution such that at each iteration we have enough points to ensure $\inf_{j \neq j'} d(y_j, y_{j'}) \ll \inf_j \text{diam}(\hat{\pi}_{Y_N}^{-1}(y_j))$, whence the effects of each ξ at each y_j remain isolated. Second, the controlled smoothness of the η_{δ_j} ’s gives us an elementary way to ensure $C(Y_{N,\varepsilon}) < C(Y_N) + \varepsilon_N$. But since large changes in the cost are penalized already by the Sobolev gradient approximation λG (and there is little harm in *undershooting* the proper c_j), we may choose to ignore the $\|\eta_{\delta_j}\|_{W^{k,q}(X;\Omega)}$ and take $c_j \propto \frac{1}{N|F_{\hat{\pi}_{Y_N}}(y_j)|}$. Applying the coarse bound on ε_N (5.5) then gives

$$\varepsilon_N c_j \leq \frac{g_p(Y_N)}{CN|F_{\hat{\pi}_{Y_N}}(y_j)|} = \frac{\sum_i \int_{\hat{\pi}_{Y_N}^{-1}(y_i)} |\omega - y_i|^p d\rho}{|F_{\hat{\pi}_{Y_N}}(y_j)| \sum_i |F_{\hat{\pi}_{Y_N}}(y_i)|},$$

whence taking the coarse approximation

$$\int_{\hat{\pi}_{Y_N}^{-1}(y_i)} |\omega - y_i|^\alpha d\rho \approx C \max_{\omega \in \hat{\pi}_{Y_N}^{-1}(y_i)} |\omega - y_i|^{\alpha+1} \approx C' (\text{diam}(\hat{\pi}_{Y_N}^{-1}(y_i)))^{\alpha+1}$$

and supposing the $\text{diam}(\hat{\pi}_{Y_N}^{-1}(y_i))$ are relatively uniform in i (not unreasonable on average since ρ is uniform), we obtain the *very* coarse heuristic of selecting $\varepsilon_N c_j = O(\text{diam}(\hat{\pi}_{Y_N}^{-1}(y_j))^{1-p})$. However, in practice we do not compute $\text{diam}(\hat{\pi}_{Y_N}^{-1}(y_j))$, and we do not have *a priori* estimates on how quickly the $\text{diam}(\hat{\pi}_{Y_N}^{-1}(y_i))$ decay. Obtaining such estimates could be a useful direction for future work.

In any case, denoting the iteration index by i and the total iterations by N_{tot} , empirically we have observed good performance choosing $\varepsilon_N c_j \propto (i/N_{\text{tot}})^p$, but as of yet we do not have good theoretical justification.

6. TOWARD APPLICATIONS TO GENERATIVE LEARNING

Note that in the below we consider the soft penalty problem (SP) rather than the hard constraint (HC). However, as discussed in Section 1.2, (SP) gives solutions to (HC) while being easier to simulate.

As mentioned in Section 1.6.1, one possible application of (SP) is in studying generative modeling problems. In this section, we will expand on those remarks. We begin by giving a brief overview of generative machine learning problems (Section 6.1) and then discuss how our framework can be applied to (unconditional) generative modeling (Section 6.2). In particular, we show that (SP) is essentially a regularized, non-stochastic analogue of a certain class of generative machine learning problems, and propose mechanisms beyond the standard “avoidance of overfitting” by which the regularization can offer training improvements. In light of this connection, we propose that it could be of interest to further investigate the theoretical properties of (SP), as well as those of the associated numerical methods (e.g. Section 5.3.2), with the hope that insights from the (SP) context could help inform work on generative learning problems.

To that end, in Section 6.3 we offer some proof-of-concept experiments demonstrating that adding $\lambda\mathcal{C}$ to \mathcal{G}_p for a simple feedforward neural network yields training improvements in two generative tasks: learning the uniform measure on a disk (Section 6.3.2) and learning to generate images of handwritten digits (Section 6.3.3). Finally, in Section 6.4 we give a simple MNIST experiment demonstrating that the regularization benefits we propose appear in real data even when the data has been in some sense “maximally overfitted.”

More work would be required to understand whether the phenomena we observe persist in more complicated settings.

6.1. Brief Overview of Generative Learning Problems. In generative modeling, it is typical to treat our training data as being samples from some abstract distribution ρ and to view the generative model itself as an estimating distribution σ_θ parametrized by θ . The goal is to find θ such that σ_θ is close to ρ in some statistical sense [1, 28, 24, 62]. In many cases ρ is embedded in \mathbb{R}^n with large n , however in most applications it is reasonable to assume ρ is concentrated on a set of local dimension $m \ll n$ [20, 22, 71, 75, 34, 12, 11, 63, 4].

A further distinction can be drawn between *unconditional* and *conditional* generative learning problems. In *unconditional* problems, the goal is essentially to approximate a random sampling scheme for ρ by randomly sampling σ_θ . To facilitate this, σ_θ is typically constructed as the pushforward of a fixed, high-regularity distribution μ (e.g. a Gaussian) under a learned map f_θ , whence sampling σ_θ is essentially trivial (see e.g. [28, 66, 38]). Note that in this case, the user cannot specify a particular *part* of ρ they want to sample from. For example, if training a model to generate images of common pets, a user cannot specify whether they want to see a cat or a dog.

By contrast, a *conditional* model takes an input prompt from a user (e.g. “a Labrador retriever”) and tries to sample from the conditional distribution $\rho|_Q$, where Q is the set of outputs that can be described by the user query [72, 70, 60]. Although conditional modeling is generally more difficult, an unconditional model can sometimes be extended to support conditioning after the fact (see, e.g. works on guided diffusion [41, 19, 15, 65], where an unconditional diffusion model is extended to support conditioning). Thus, we will leave conditional generation to future work and restrict ourselves to examining unconditional generation.

A prototypical example of an unconditional generation problem is generating images from a distribution. Supposing the images have resolution 512×512 it is typical to embed them into $\Omega \subseteq \mathbb{R}^n$ for $n = 512 \times 512 \times 3 = 786432$ where each

dimension encodes one of the RGB components of the color of one pixel. We imagine that there is some real-world stochastic process that randomly produces images in Ω ; the measure ρ then describes how likely a given set of images is to contain the next one produced. The model itself is a neural network f_θ with parameters θ ; f_θ is used to transform a distribution μ on \mathbb{R}^m (usually Gaussian) to the distribution σ_θ on \mathbb{R}^n via

$$\sigma_\theta = (f_\theta)_\# \mu.$$

In practice, the precise relationship between θ and the shape of f may be nontrivial. In any case, the network f_θ is often taken to be either smooth or piecewise linear so we may assume σ_θ has local dimension m a.e. (c.f. Proposition 3.8). Since perturbing a natural-looking image in a random direction is overwhelmingly likely to degrade its appearance [69], it is typical to assume ρ is concentrated on a very thin set in Ω . Thus we may take m to be relatively small—for example $m = 128$ —and still hope for σ_θ to approximate ρ well.

6.1.1. *A Case Study: WGAN.* As proposed in [1], when ρ is concentrated on a thin set, one good choice for the notion of statistical “closeness” of σ_θ and ρ is the Monge-Kantorovich 1-distance. Note that $p = 1$ is chosen essentially just because $\mathbb{W}_1(\rho, \sigma_\theta)$ can be represented computationally-tractably via the dual formula

$$(6.1) \quad \mathbb{W}_1(\rho, \sigma_\theta) = \sup \left\{ \int \varphi \, d(\rho - \sigma_\theta) \mid \varphi \text{ is 1-Lipschitz} \right\}.$$

See e.g. [77, Thm. 1.14] for a rigorous proof of (6.1). In any case, the authors of [1] use (6.1) to propose the so-called *Wasserstein GAN* (WGAN), which can offer notable improvements to training stability over classical GAN designs.

To summarize, WGAN alternately trains two separate networks, parametrized by w and θ , respectively: a *critic* or *discriminator* D_w and a *generator* f_θ . The critic plays the role of φ in (6.1) and thus for fixed θ tries to learn to estimate $\mathbb{W}_1(\rho, \sigma_\theta)$. Then, the generator uses the trained critic to estimate how best to adjust σ_θ to decrease $\mathbb{W}_1(\rho, \sigma_\theta)$. Explicitly, for fixed θ we train D_w by iteratively sampling M -point batches $\omega^{(i)} \sim \rho$ and $x^{(i)} \sim \mu$ and updating D_w via a small step along

$$\nabla_w \left[\frac{1}{M} \sum_{i=1}^M [D_w(\omega^{(i)}) - D_w(f_\theta(x^{(i)}))] \right] \approx \nabla_w \int D_w \, d(\rho - \sigma_\theta),$$

using some regularization scheme to try and ensure D_w remains 1-Lipschitz. After training the critic for some number of iterations N_{critic} , we then take another M -point batch $x^{(i)} \sim \mu$ and update the generator f_θ via a small step along

$$(6.2) \quad \nabla_\theta \left[\frac{1}{M} \sum_{i=1}^M D_w(f_\theta(x^{(i)})) \right] \approx \nabla_\theta \int D_w \circ f_\theta \, d\mu = -\nabla_\theta \int D_w \, d(\rho - \sigma_\theta).$$

This process is then repeated until convergence.

In the original work [1], D_w was regularized via the (as they described it) “clearly terrible” method of *weight clipping*. In [30] it was demonstrated that a better method is to instead augment the objective (6.1) with a *gradient penalty* term

$$(6.3) \quad \frac{\lambda}{M} \sum_{i=1}^M [|\nabla_{u_\theta^{(i)}} D_w(u_\theta^{(i)})| - 1]^2,$$

where $u_\theta^{(i)} = s_i \omega^{(i)} + (1 - s_i) f_\theta(x^{(i)})$ for $s_i \sim \text{Unif}[0, 1]$. The justification was that given an optimal coupling π_θ^* for $\mathbb{W}_1(\rho, \sigma_\theta)$, one can show [30, Prop. 1] that for π_θ^* -a.e. pair $\omega, \omega' \in \Omega^2$, if an optimal critic D_w^* is differentiable at $\omega_t = t\omega + (1 - t)\omega'$,

then $|\nabla D_w^*(\omega_t)| = 1$. However, in [67] it was demonstrated that this scheme has some noteworthy problems, a key one being that the product measure $\rho \otimes \sigma_\theta$ often gives positive mass to null sets of π_θ^* , and hence it is not guaranteed that sampling $\omega^{(i)} \sim \rho$, $f_\theta(x^{(i)}) \sim \sigma_\theta$ will yield a point in $\text{supp}(\pi_\theta^*)$. Therefore, the authors of [67] propose replacing the $|\nabla D_w| - 1$ term in (6.3) with just the positive part $(|\nabla D_w| - 1)_+$, thus enforcing only the 1-Lipschitz condition. An interpretation of this revised formulation (called WGAN-GP) in terms of a congested transport problem was introduced in [59].

In any case, given the relationship between \mathcal{G}_p and $\mathbb{W}_p^p(\rho, \cdot)$ we established in Proposition 2.7, the inclusion of these penalization terms makes WGAN-GP evocative of (SP), the difference being that the penalty in (SP) enforces regularization on the *generator* rather than on the critic. We discuss this comparison now.

6.2. WGAN and The Constrained Monge-Kantorovich Fitting Problem.

By Proposition 2.7, we see that when $p = 1$, (SP) and WGAN essentially treat the same objective, but there are two main distinctions between the formulations.

First, (SP) depends solely on the geometry of the image set $Y = f_\theta(X)$ —in particular it is agnostic with regards to the distribution μ on X —while WGAN explicitly seeks to minimize $\mathbb{W}_p^p(\rho, \sigma_\theta)$. Thus, as we proposed in Section 1.6.1, we may loosely view (SP) as the first step in a “factorization” of WGAN into two parts:

- 1) Learning the *shape* of $\text{supp}(\sigma_\theta^*)$, where σ_θ^* is an optimal approximating measure, and then
- 2) Learning a reparametrization map φ so that σ_θ^* can be expressed as the pushforward of a particular μ .

Intuitively, we expect step 1 might be the “hard” step (though we have not investigated this carefully) as it involves learning an m -to- n map (typically $m \ll n$), while step 2 involves learning only an m -to- m map. However, we note that step 2 can still be nontrivial if the optimal φ badly lacks regularity.

The second main difference is that (SP) enforces regularization on f (which plays the role of the WGAN generator) rather than on the critic. To our knowledge, the closest analogous idea in the literature is the recent work of [76], in which a “left-invertibility” penalty was used to regularize the WGAN generator. The authors of that work found that such a regularization scheme resulted in improved creativity of the model, without sacrificing statistical optimality. (This is loosely analogous to our discussion of generalization performance in the toy problem in Section 6.4).

By analogy with our “factored” WGAN problem, we now propose some qualitative explanations for why such behavior might be expected.

6.2.1. Classical Benefits of Regularization. Classically, the training benefits of regularization terms like $\lambda\mathcal{C}$ terms are typically understood in terms of “avoiding overfitting.” In our language we may understand this as follows: Since we are in a “real-world” context (Section 5.3.1) we do not actually have access to ρ , but rather a finite number of (possibly noisy) training samples, which we denote by the empirical measure ρ_M . By Corollary 5.2, when M is large, an optimizer f_M of $\mathcal{G}_p^\lambda(\square; \rho_M)$ approximates an optimizer of $\mathcal{G}_p^\lambda(\square; \rho)$ with high probability.

However, in practice, the threshold for what constitutes a “sufficiently large” M depends on λ . Essentially this is because for any fixed M the constraint is not *effective* for ρ_M (see Proposition 3.8), and so if λ is very small, f_M will more or less

interpolate the atoms of ρ_M . Typically this yields poor generalization performance because f_M has “fit” random variations in ρ_M that are not present in ρ . On the other hand, we expect that for a proper choice of λ (i.e. not too small) the λC term will force f_M to “average out” the noise in ρ_M , thus helping to ensure f_M is a good approximant of *both* ρ and ρ_M , especially perhaps when the differentiability order k in the Sobolev constraint is chosen based on the regularity of ρ .

6.2.2. Proposed Additional Benefits of Regularization. In light of the two-step “factorization” of WGAN we proposed earlier, we hypothesize that the inclusion of the regularization term λC actually offers an additional benefit: Encouraging solutions Y for step 1 such that the optimal reparametrization φ in step 2 has a small (local) Lipschitz constant at most points (thus potentially improving training stability). In particular we propose that λC encourages the following properties in Y :

- 1) Avoidance of self-intersections,
- 2) Few points outside $\text{supp}(\rho)$, and
- 3) Better preservation of locality, in the sense that the Lipschitz constant of f_θ is relatively small.

To illustrate the point in cases 1 and 2, suppose μ, ρ are uniform and f_θ has constant speed, so that σ_θ is uniform on Y . Then near self-intersections, the local density of σ_θ is approximately double that of ρ , and so a reparametrization φ would need to compensate by moving faster near these points so as to lower the density of σ_θ . Similarly, near a point outside $\text{supp}(\rho)$, φ should become discontinuous as it approaches optimality so as to ensure the density of σ_θ vanishes. For case 3, suppose μ is uniform, ρ is a bimodal Gaussian, and f_θ is constant speed. If Y contains many oscillations between the two peaks, then φ will have to be highly oscillatory to compensate; on the other hand, if Y “fills” the region near the first peak first and only then moves to the second, φ can be taken to be smoother.

To give a tangible example of these effects, we initialize the algorithm in Section 5.3.2 on a highly nonconvex domain with an initial condition given by interpolating 200 randomly-chosen points, with learning rate $\eta(i) = (i/2000)^2$ and decaying regularization parameter $\lambda(i) = 0.01(1 - c(i))/c(i)$ (Fig. 10). After just 20 iterations the curve has a substantially simplified topology. By 110 iterations the curve has no more self-intersections, and by 800 iterations it has learned the basic shape of the domain, with only one arc outside $\text{supp}(\rho)$, though this arc later disappears at around iteration 1120. By iteration 1850, the behavior of the curve has stabilized, and there are no self-intersections or external arcs, with relatively even coverage of ρ . In this case, good performance can be obtained by taking φ approximately uniform.

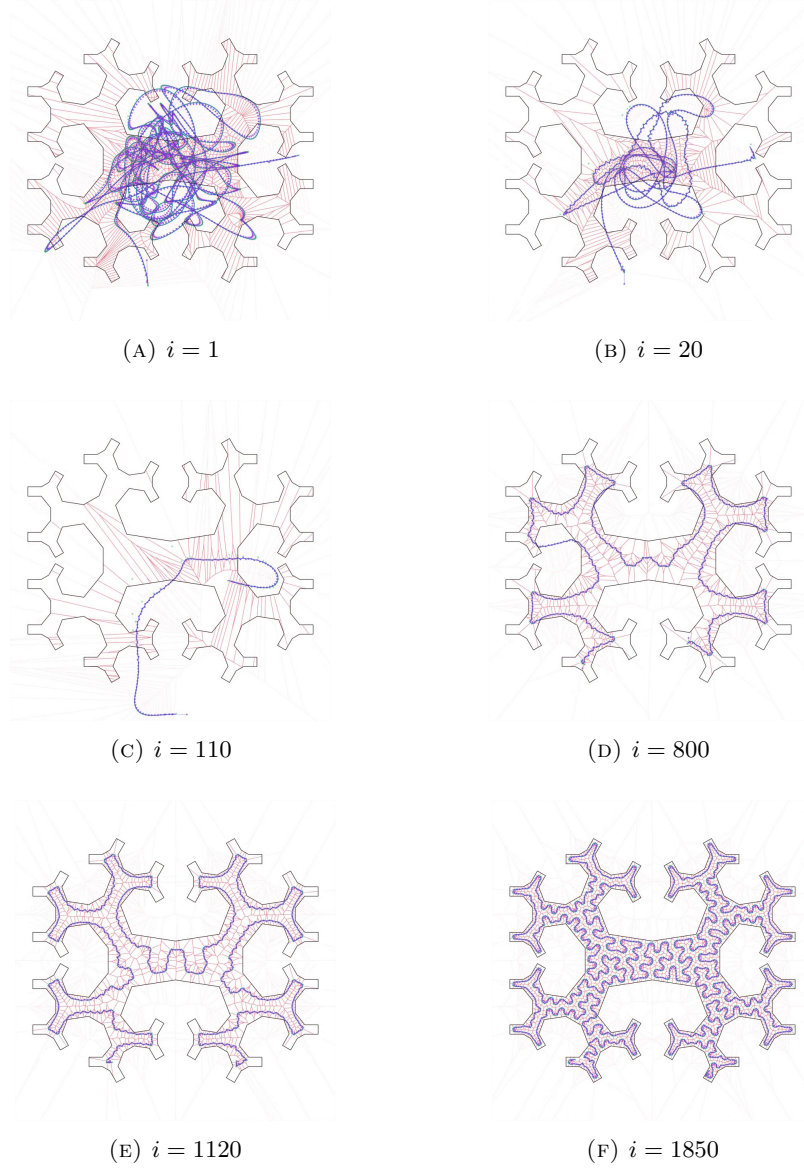


FIGURE 10. Regularized curves.

By contrast, the unregularized curve (Fig. 11) initialized with the same parameters but $\lambda(i) \equiv 0$ improves the objective much more rapidly (though in practice we found the gap can be substantially narrowed by decreasing the coefficient on $\lambda(i)$, at the cost of introducing two or three persistent arcs outside of $\text{supp}(\rho)$). However, the resulting shape suffers from many self-intersections and arcs escaping $\text{supp}(\rho)$, as well as a higher point density near the center than near the edges. Additionally, we see the formation of a very dense spiral shape on the right edge. Thus this shape would require a very complicated reparametrization φ to yield a good approximation σ_θ .

If the reparametrization were taken to be a neural network, the network would typically require very extreme weights to effectively remove density from the arcs outside of $\text{supp}(\rho)$. This would be a poor fit for learning with gradient descent as very large weights tend to lead to slow convergence and unstable training.

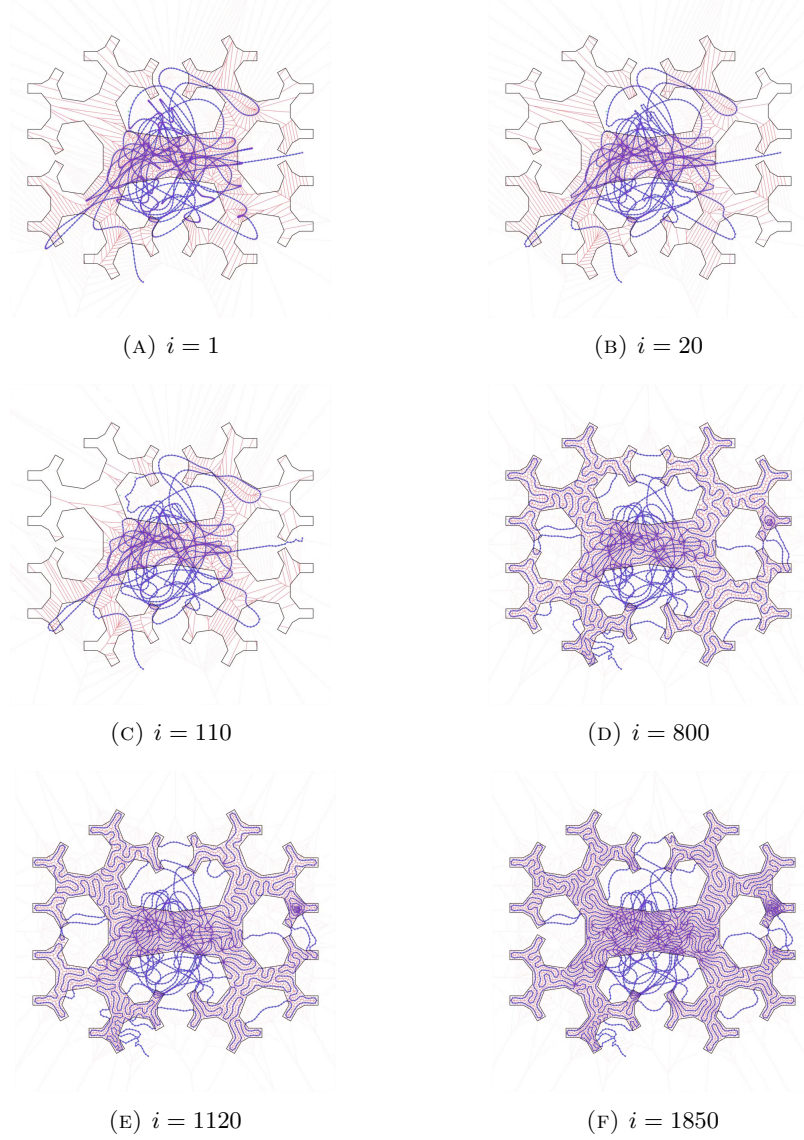


FIGURE 11. Unregularized curves.

We propose that a similar mechanism could operate in general generative learning tasks, even in the case where the problem is not “factored” into the two steps we described earlier.

To that end in Section 6.3 below we offer two proof-of-concept experiments demonstrating the utility of a $k = 1$ penalty in training neural nets to produce

the uniform measure on a disk in \mathbb{R}^2 , as well as in generating images of handwritten digits. Then, to highlight the distinction between the “reparametrization” benefits we described in this subsection and the “overfitting avoidance” benefits we described in Section 6.2.1, we perform an MNIST experiment in Section 6.4 which demonstrates that even when λ is too small to prevent overfitting, the regularizing effects of \mathcal{C} encourage σ_θ to “interpolate” ρ_M more intelligently, thus possibly producing a σ_θ that better approximates ρ than an unregularized solution might.

6.3. Training Neural Networks with a $k = 1$ Penalty. In this subsection we exhibit two simple proof-of-concept experiments demonstrating that adding a $\lambda\mathcal{C}$ term to \mathcal{G}_p can yield training improvements in some generative learning tasks. Note that as it is generally computationally intensive to compute higher-order derivatives for neural networks, we will focus our attention particularly on the case $k = 1$. The setup is the same in both cases (up to a choice of parameters), hence we begin by describing it in generality.

6.3.1. Setup. We consider the “real-world” case of Section 5.3.1 where we do not know ρ and instead receive M samples $D = \{\omega_1, \dots, \omega_M\}$ from ρ . In each of the experiments below we consider $m = 1$ and model $f : \mathbb{R}^d \rightarrow \mathbb{R}^n$ using an L layer fully connected neural network $h_L : \mathbb{R}^d \rightarrow \mathbb{R}^n$ of hidden dimension d with

$$h_0(x) = A_0x, \quad h_l(x) = \sigma(A_l h_{l-1}(x) + b_l)$$

where $A_0 \in \mathbb{R}^{n \times d}$, $A_l \in \mathbb{R}^{d \times d}$, $b_l \in \mathbb{R}^d$ for all l , and σ notates the GeLU nonlinearity [36]. It is well-known that such networks perform poorly when modeling functions with behavior at varying scales in Ω [74, 57], so we adopt a modification of the positional encoding $\gamma : \mathbb{R}^d \rightarrow \mathbb{R}^d$ of [57],

$$\gamma(x) = \left(\frac{\sin(2^1 \pi x)}{\sqrt{2^1}}, \frac{\cos(2^1 \pi x)}{\sqrt{2^1}}, \dots, \frac{\sin(2^{d/2} \pi x)}{\sqrt{2^{d/2}}}, \frac{\cos(2^{d/2} \pi x)}{\sqrt{2^{d/2}}} \right).$$

Compared to [57], we damp each coordinate by the square root of its frequency, otherwise we found the initial arc length would tend to explode as d increased, leading to poor numerical stability at initialization. Finally, we have $f = h_L \circ \gamma$.

We approximate the (SP) objective $\mathcal{G}_p^\lambda = \mathcal{G}_p + \lambda\mathcal{C}$ via an empirical loss \mathcal{L} defined as follows. First, to approximate \mathcal{G}_p , for each evaluation we sample a set of N points $X_N = \{x_0, \dots, x_N\} \sim \mu$ and define

$$\mathcal{L}_{\text{obj}} = \frac{1}{M} \sum_{i=1}^M \min_{x \in X_N} \|\omega_i - f(x)\|.$$

Note that because this is a $p = 1$ objective, properly speaking, in order to interpret the gradient of \mathcal{L}_{obj} in terms of the barycenter field (Proposition 5.5), we need to know $\{\omega_i\} \cap f(X_N) = \emptyset$. Typically this will not be an issue: Since $\{\omega_i\}$ is countable, as long as f is nonconstant and μ is absolutely continuous, $f^{-1}(\{\omega_i\})$ should be μ -null, whence $\{\omega_i\} \cap f(X_N) = \emptyset$ μ -a.s.

For the \mathcal{C} part, since we will be primarily interested in large-budget solutions we ignore the 0th-order term and use the approximation

$$\mathcal{L}_{\text{cost}} = \frac{1}{N} \sum_{i=1}^N \|f'(x_i)\|.$$

Note that $\mathcal{L}_{\text{cost}}$ is implicitly a $q = 1$ penalty, whereas in our earlier theory work we considered only the case $1 < q < \infty$. In practice we do not expect this to yield different qualitative behavior than the $q = 1 + \varepsilon \approx 1$ case; hence we chose $q = 1$ simply as a matter of computational convenience.

In any case, the final loss is then $\mathcal{L} = \mathcal{L}_{\text{obj}} + \lambda \mathcal{L}_{\text{cost}}$ for some regularization parameter $\lambda > 0$, just as in (SP).

6.3.2. Experiment 1: Fitting Toy Data. Here we consider the case $m = 1$, $n = 2$ and take ρ to be the uniform measure on a set of 50 points randomly sampled from the unit circle in \mathbb{R}^2 . We perform 300,000 iterations of gradient descent to optimize f , choosing $d = 10^3$ and $N = 10^4$. We show results for $\lambda = 10^{-4}$ as well as $\lambda = 0$ in Fig. 12. These results highlight the regularizing effect of the constraint. In Fig. 12a we see that the curve passes through all 50 points almost perfectly, but interpolates them in a messy fashion. In contrast, the curve in Fig. 12b interpolates almost linearly between successive points in a manner reminiscent of a traveling salesperson path, but there remain three points quite far from the curve.

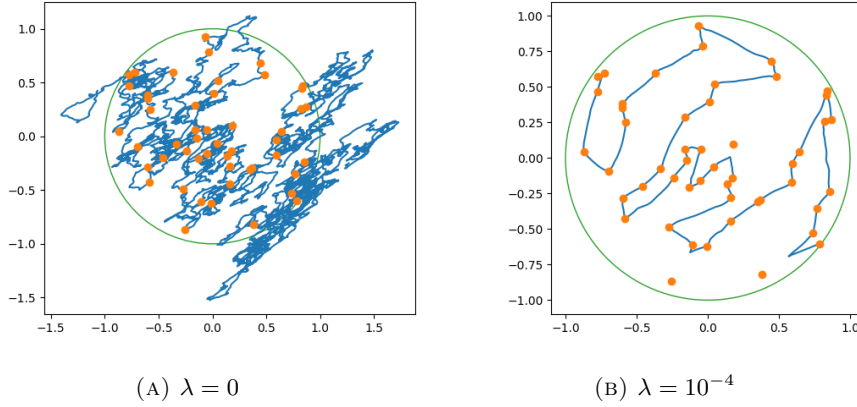


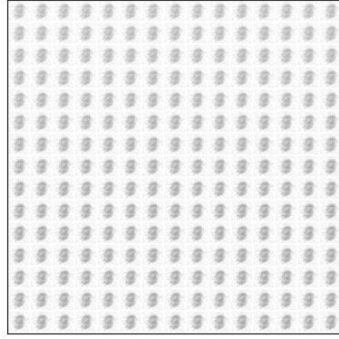
FIGURE 12. Visualization of f for different values of λ .

This failure to fit all of the points is due to the Lagrangification of the constraint. As $\lambda \rightarrow 0$ we would expect this effect to vanish while maintaining the desired regularizing effect. Of course, as $\lambda \rightarrow 0$, our optimization problem becomes increasingly ill-conditioned, which prevents gradient descent from quickly finding effective minimizers.

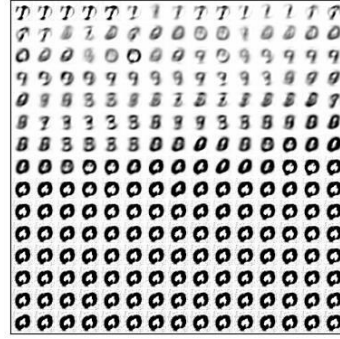
6.3.3. Fitting MNIST. Here we take $X = [0, 1]$ with μ the uniform measure on X and D given by MNIST.

For our experiments, we chose a small value of $\lambda = 10^{-4}$. We optimized the weights (A_l, b_l) to minimize \mathcal{L} in expectation using stochastic gradient descent, performing 1000 epochs over the dataset. We also chose $d = 10^3$ and $N = 10^4$.

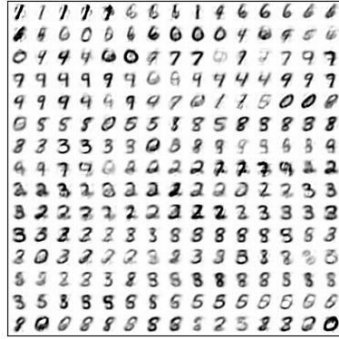
We plot the evolution of f over the course of training in Fig. 13, where we can see that the visual quality of the digits produced improves as training progresses.



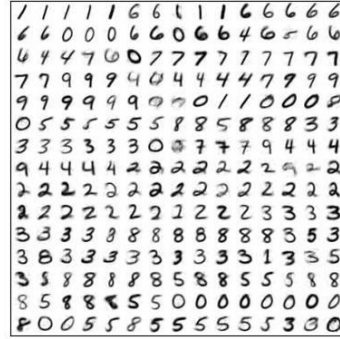
(A) 1 epoch



(B) 30 epochs



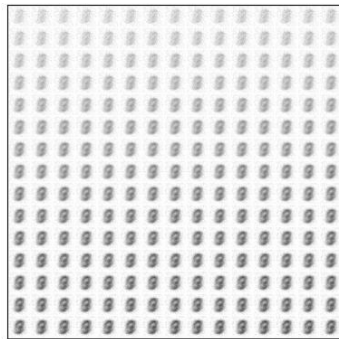
(C) 100 epochs



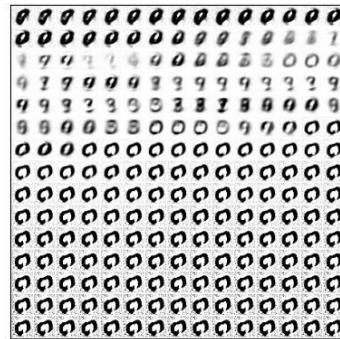
(D) 1000 epochs

FIGURE 13. Visualization of f sampled at 15^2 uniformly-spaced points (for convenience) from 0 to 1 at several points during the training process.

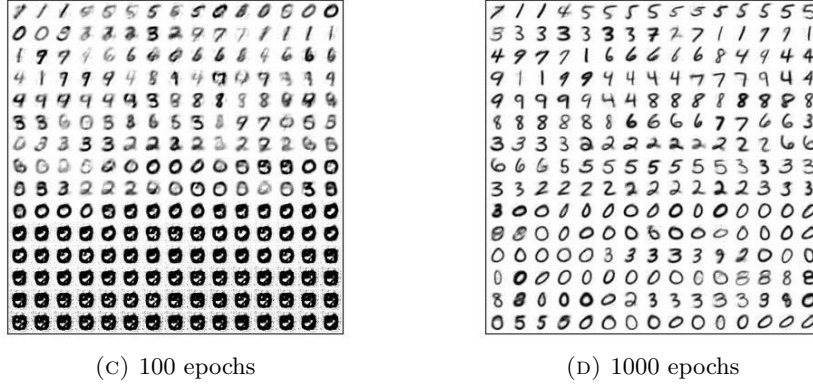
To demonstrate the importance of the constraint, we perform a similar run setting $\lambda = 0$. The results are shown in Fig. 14.



(A) 1 epoch



(B) 30 epochs

FIGURE 14. Visualization of f as in Fig. 13 but with $\lambda = 0$.

Here we can see that after 100 epochs, the result without regularization in Fig. 14c is far worse than the regularized result in Fig. 13c. In this case in Fig. 14c, a large portion of X is “wasted” because large intervals of the domain map to nearly the same image, which leads to poor coverage of the rest of MNIST.

Although the arclength penalty does not directly penalize this behavior (since regions of X where f is approximately constant do not contribute to the arclength), it is clearly beneficial in this situation. Note that after sufficient iterations, even the unregularized network begins to make full use of X , as seen in Fig. 14d. We hypothesize the following explanation for the behavior in these two cases.

Recall from our earlier discussion of \mathcal{L}_{obj} that we may interpret the gradient of \mathcal{L}_{obj} (with respect to the locations of the sample points $f(x)$) in terms of the barycenter field. So, at each iteration, our weight updates should be modifying f in a way that approximates following the barycenter field.

Suppose there is a region X_{static} where f is approximately constant. Unless the $\{\omega_i\}$ are highly concentrated around $f(X_{\text{static}})$, this typically implies the barycenter will approximately vanish everywhere except a few points near the boundary of $f(X_{\text{static}})$ (since only these outer points will get data samples projecting to them).

Consider such an “outer” point $x \in X_{\text{static}}$. In the update step, x will be pulled towards more useful regions of Ω by the barycenter field. Without the arclength penalty, the curve will simply lengthen to accommodate this, leaving X_{static} largely intact. In contrast, the arclength penalty causes the shifted point x to “pull” some of X_{static} with it. Thus, the regularization will promote effective usage of the entirety of X much more quickly than in the unregularized case.

6.3.4. Comparison with weight decay. One popular form of regularization for neural networks is L_2 regularization of the network’s weights which is sometimes called “weight decay” in the context of gradient descent [44, 84, 27]. Under gradient descent with weight decay, we multiply the weights of the network by $1 - \lambda_{\text{wd}}$ after each gradient step, where $\lambda_{\text{wd}} > 0$ is typically quite small. A notable connection between our constraint and weight decay was explored in [84]; there the authors propose that weight decay may behave similarly to a penalty on the Frobenius norm of the network’s Jacobian, which has a similar form to our constraint when $k = 1$ and $q = 2$. We show results when running under weight decay in Fig. 15. We chose $\lambda_{\text{wd}} = 10^{-4}$ so that the amount of regularization would be similar to that in

Section 6.3.3. Comparing Fig. 13c and Fig. 15c we see that our constraint produces better results than weight decay after 100 epochs although after 1000 epochs the gap has narrowed considerably.

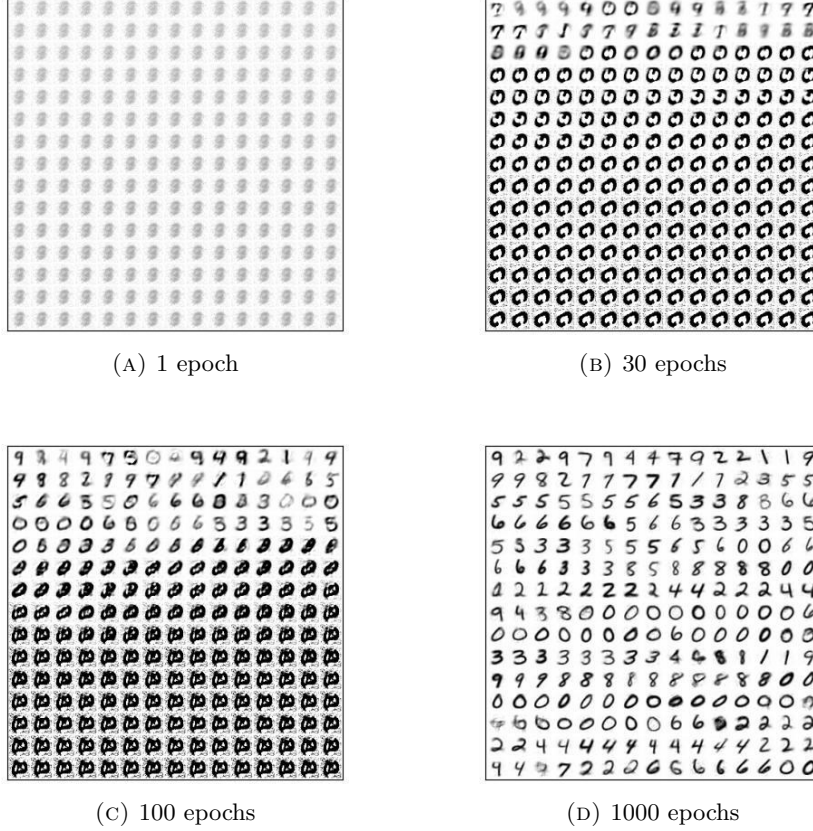


FIGURE 15. Visualization of f as in Fig. 13 but using weight decay with $\lambda_{\text{wd}} = 10^{-4}$.

Unlike our constraint, the effect of weight decay varies with the architecture and parametrization of the neural network being optimized. This may be seen as a weakness or a strength depending on the details of the task being performed. In this particular setting, weight decay does not appear to offer much advantage over not using regularization at all.

6.4. Demonstrating the Interpolation Benefits of a $k = 1$ Penalty. Recall that in Section 6.2 we hypothesized that, in addition to avoidance of overfitting, the penalty term $\lambda \mathcal{C}$ could improve training efficiency by encouraging regularity in the optimal reparametrization map φ . To illustrate this point, we initialized our “theoretical” algorithm from Section 5.3.2 with and without regularization, yielding the outputs in Fig. 10 and Fig. 11.

In this final subsection, we perform an analogous “real-world” experiment using MNIST data. So as to emphasize the distinction with the “avoidance of overfitting” effects described in Section 6.2.1, we will compare two curves that both *fully*

interpolate the data but differ in their \mathcal{C} values. Typically such interpolation can occur only when $\lambda = 0$ in (SP); to avoid some technical hand-wringing around this case we instead formalize our experiments via an “adjoint” formulation of (HC):

Problem 3 (“Adjoint” Problem (AdjHC)). Minimize $\mathcal{C}(f)$ over $\{g_p(f) \leq \zeta\}$.

While (AdjHC) is similar to (HC) in the sense that we have a hard constraint instead of a soft penalty, note that (AdjHC) recovers the property that all optimizers must be maximally-efficient, and is thus equivalent to (SP) and not (HC) (see Section 1.7.4).

Now, let $m = 1$, $k = 1$, and $q = 1$ (as in Section 6.3 we do not expect $q = 1$ to cause problems), and suppose our target is a discrete measure $\rho_M = \sum_{j=1}^M \delta_{\omega_j}$. We now show that in this case the $\zeta = 0$ (AdjHC) essentially recovers the Euclidean traveling salesperson problem (TSP), whence we may approximate solutions to (AdjHC) using TSP solvers.

To that end, note that if f is a $\zeta = 0$ optimizer of (AdjHC) then f must visit every point in $S = \text{supp}(\rho_M)$. Due to our choice of $k = 1$ and negligibility of the 0^{th} -order term for large ℓ (a reasonable assumption for large M), the optimal way to travel between two points of S is via a straight line. Accordingly, we are interested in choosing an ordering on S such that visiting the points of S in that order, connected by straight lines, gives the shortest overall arc length. This is precisely the Euclidean TSP.

Although the Euclidean TSP is known to be NP-hard, mature numerical solvers exist which produce solutions of very high quality. We use the LKH solver [35], an optimized implementation of the Lin-Kernighan heuristic, to produce an approximate tour of the MNIST training set. By drawing random samples uniformly from the domain set $[0, 1]$, we may visually compare random samples from this optimized tour against those from a random tour:

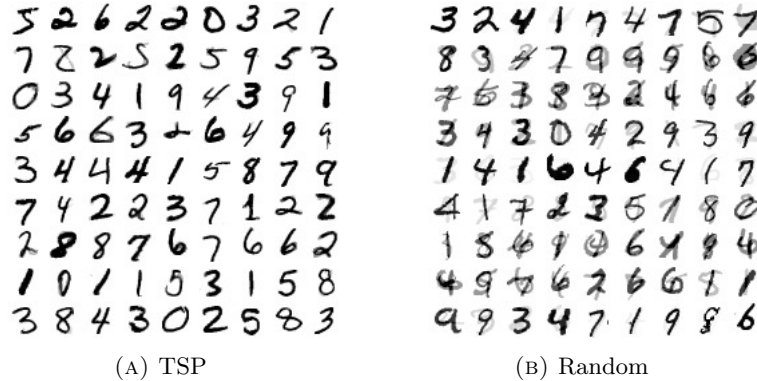


FIGURE 16. Samples from tours of MNIST with Fig. 16a a tour optimized by LKH and Fig. 16b a random tour.

Perhaps unsurprisingly, the interpolated images from the optimized tour in Fig. 16a appear more similar to real MNIST digits than the ones from the random tour in Fig. 16b do. Since the domain samples were chosen uniformly at random from $[0, 1]$, we see that in this case taking φ to be identity yields good performance in the second step of our “factorization” in Section 6.2.

In particular, note that this improvement is not due to “prevention of overfitting,” as both tours fully interpolate the data. This suggests that even when λ is too small to prevent overfitting, the inclusion of a regularization term may still yield training improvements via the mechanisms in Section 6.2.2.

While it is certainly possible to reparametrize the random curve to produce reasonable-looking images (by placing point masses at the original data points, for example) this model does not effectively generalize the examples seen. In contrast, the TSP path is able to produce novel images that are visually consistent with those of MNIST.

7. CONCLUSION

In this paper, we analyzed a certain variational problem regarding approximating high-dimensional measure ρ via a lower-dimensional measure ν whose complexity is bounded. We showed that in fact it is sufficient to treat the *support* of ν (parametrized by some f) as the fundamental variable of optimization, yielding the problem (HC), as well as the nearly-equivalent and nicer-to-simulate problem (SP). Importantly, the fact that we optimize over f instead of ν in these problems allowed us to use simpler, geometric techniques in our analysis.

We used this perspective to propose a two-step “factorization” of a WGAN problem in which there is regularization on the generator. In the first step, we obtain an f that is optimal in the sense of (HC)/(SP), and then in the second step, f is reparametrized to properly push-forward a given measure μ . Since the essential qualitative behavior of the solution is determined primarily in the first step, we proposed that theoretical study of (HC)/(SP) could provide insights into the qualitative behavior of WGAN, and other similar problems.

To that end, we examined basic properties of (HC) over a general class of regularity parameters for f . We placed a particular focus on understanding the “gradient” of the objective functional $\mathcal{G}_p(f)$; we called this gradient the *barycenter field*. Under mild hypotheses, we showed (in both the continuous and discrete cases) that the barycenter field has a simple geometric interpretation that is amenable to visualization. Then, in the discretized case, we proposed an efficient, deterministic numerical scheme that used the barycenter field to simulate (SP) for a special family of targets ρ , provided f is a curve.

The resulting simulations had intuitive qualitative behavior that offered a simple explanatory narrative for how the regularization on f in the first step of the “factored” WGAN problem results in a much more well-behaved reparametrization in the second step. Importantly, we hypothesized such regularization could yield benefits in both training and generalization performance, even when no explicit factorization of WGAN is performed. In this vein, we gave simple, proof-of-concept experiments demonstrating both effects manifesting in an “unfactored” model when generating MNIST data in the presence/absence of our regularization.

In future work it would be interesting to quantitatively examine the extent to which similar effects persist in more nontrivial datasets.

REFERENCES

1. Martin Arjovsky, Soumith Chintala, and Léon Bottou, *Wasserstein generative adversarial networks*, International conference on machine learning, PMLR, 2017, pp. 214–223.
2. Mark Berg, Otfried Cheong, Marc Kreveld, and Mark Overmars, *Computational Geometry*, Springer, Berlin, Germany, 2008.

3. Dimitri P. Bertsekas, Steven E. Shreve, and Elsevier All Access Books, *Stochastic optimal control: the discrete time case*, vol. 139, Academic Press, New York, 1978 (English).
4. Pratik Prabhanjan Brahma, Dapeng Wu, and Yiyuan She, *Why deep learning works: A manifold disentanglement perspective*, IEEE transactions on neural networks and learning systems **27** (2015), no. 10, 1997–2008.
5. Haim Brezis, *Functional Analysis, Sobolev Spaces and Partial Differential Equations*, Springer New York, New York, NY, 2011 (en).
6. Giuseppe Buttazzo, Edoardo Mainini, and Eugene Stepanov, *Stationary configurations for the average distance functional and related problems*, Control and Cybernetics **38** (2009), no. 4A, 1107–1130 (eng).
7. Giuseppe Buttazzo and Eugene Stepanov, *Optimal transportation networks as free Dirichlet regions for the Monge-Kantorovich problem*, Annali della Scuola Normale Superiore di Pisa - Classe di Scienze **2** (2003), no. 4, 631–678.
8. Giuseppe Buttazzo, Edouard Oudet, and Eugene Stepanov, *Optimal Transportation Problems with Free Dirichlet Regions*, Variational Methods for Discontinuous Structures (Basel) (Gianni dal Maso and Franco Tomarelli, eds.), Progress in Nonlinear Differential Equations and Their Applications, Birkhäuser, 2002, pp. 41–65.
9. Iván Caamaño, Jesús Á. Jaramillo, Ángeles Prieto, and Alberto Ruiz de Alarcón, *Sobolev spaces of vector-valued functions*, RACSAM **115** (2021), no. 1, 1–14.
10. BC Carlson, *A table of elliptic integrals: Two quadratic factors*, mathematics of computation **59** (1992), no. 199, 165–180.
11. Gunnar Carlsson, *Topology and data*, Bulletin of the American Mathematical Society **46** (2009), no. 2, 255–308.
12. Lawrence Cayton, *Algorithms for manifold learning*, Tech. report, University of California at San Diego, 2005.
13. Nicolas Chauffert, Philippe Ciuciu, Jonas Kahn, and Pierre Weiss, *A Projection Method on Measures Sets*, Constructive Approximation **45** (2017), no. 1, 83–111.
14. Hyeon In Choi, Sung Woo Choi, and Hwan Pyo Moon, *Mathematical theory of medial axis transform*, Pacific Journal of Mathematics **181** (1997), no. 1, 57–88.
15. Katherine Crowson, *CLIP Guided Diffusion HQ 512x512 Uncond*, <https://colab.research.google.com/drive/1QBsaDAZv8np29FPbvjffbE1eytoJcsgA>, 2021, [Accessed 29-07-2024].
16. Juan A. Cuesta and Carlos Matrán, *Uniform consistency of r-means*, Statist. Probab. Lett. **7** (1988), no. 1, 65–71.
17. Juan A. Cuesta and Carlos Matran, *Asymptotic Behavior of p-Predictions for Vector Valued Random Variables*, Proceedings of the American Mathematical Society **100** (1987), no. 4, 716 (en).
18. Sylvain Delattre and Aurélie Fischer, *On principal curves with a length constraint*, Annales de l'Institut Henri Poincaré, Probabilités et Statistiques **56** (2020), no. 3, 2108–2140.
19. Prafulla Dhariwal and Alexander Nichol, *Diffusion models beat gans on image synthesis*, Advances in neural information processing systems **34** (2021), 8780–8794.
20. David L Donoho and Carrie Grimes, *Hessian eigenmaps: Locally linear embedding techniques for high-dimensional data*, Proceedings of the National Academy of Sciences **100** (2003), no. 10, 5591–5596.
21. Nikita Evseev, *Vector-valued Sobolev spaces based on Banach function spaces*, Nonlinear Analysis **211** (2021), 112479 (en).
22. Charles Fefferman, Sanjoy Mitter, and Hariharan Narayanan, *Testing the manifold hypothesis*, Journal of the American Mathematical Society **29** (2016), no. 4, 983–1049.
23. J. A. Fessler, *Nonparametric fixed-interval smoothing with vector splines*, IEEE Trans. Signal Process. **39** (1991), no. 4, 852–859.
24. Ronald Aylmer Fisher, *Theory of statistical estimation*, Mathematical proceedings of the Cambridge philosophical society, vol. 22, Cambridge University Press, 1925, pp. 700–725.
25. Wilfrid Gangbo and Robert J. McCann, *The geometry of optimal transportation*, Acta Mathematica **177** (1996), no. 2, 113–161.
26. Samuel Gerber, Tolga Tasdizen, and Ross Whitaker, *Dimensionality reduction and principal surfaces via Kernel Map Manifolds*, 2009 IEEE 12th International Conference on Computer Vision (Kyoto), IEEE, September 2009, pp. 529–536 (en).
27. Giorgio Gnecco, Marcello Sanguineti, et al., *The weight-decay technique in learning from data: An optimization point of view*, Computational Management Science **6** (2009), no. 1, 53–79.

28. Ian Goodfellow, Jean Pouget-Abadie, Mehdi Mirza, Bing Xu, David Warde-Farley, Sherjil Ozair, Aaron Courville, and Yoshua Bengio, *Generative adversarial networks*, Communications of the ACM **63** (2020), no. 11, 139–144.
29. P. J. Green and Bernard W. Silverman, *Nonparametric Regression and Generalized Linear Models: A roughness penalty approach*, Chapman and Hall/CRC, New York, April 1993.
30. Ishaan Gulrajani, Faruk Ahmed, Martin Arjovsky, Vincent Dumoulin, and Aaron Courville, *Improved training of wasserstein GANs*, Proceedings of the 31st International Conference on Neural Information Processing Systems (Red Hook, NY, USA), NIPS’17, Curran Associates Inc., December 2017, pp. 5769–5779.
31. Piotr Hajłasz, *On an old theorem of Erdős about ambiguous locus*, Colloq. Math. **168** (2022), 249–256.
32. Trevor Hastie, *Principal curves and surfaces*, Ph.D. thesis, Stanford University, 1984.
33. Trevor Hastie and Werner Stuetzle, *Principal Curves*, Journal of the American Statistical Association **84** (1989), no. 406, 502–516, Publisher: [American Statistical Association, Taylor & Francis, Ltd.].
34. Matthias Hein and Jean-Yves Audibert, *Intrinsic dimensionality estimation of submanifolds in \mathbb{R}^d* , Proceedings of the 22nd international conference on Machine learning, 2005, pp. 289–296.
35. Keld Helsgaun, *An effective implementation of the lin-kernighan traveling salesman heuristic*, European journal of operational research **126** (2000), no. 1, 106–130.
36. Dan Hendrycks and Kevin Gimpel, *Gaussian error linear units (gelus)*, arXiv preprint arXiv:1606.08415 (2016).
37. Hartmut Henkel, *Calculating the cubic bézier arc length by elliptic integrals*, 2014.
38. Jonathan Ho, Ajay Jain, and Pieter Abbeel, *Denoising diffusion probabilistic models*, Advances in neural information processing systems **33** (2020), 6840–6851.
39. B. Kegl, A. Krzyzak, T. Linder, and K. Zeger, *Learning and design of principal curves*, IEEE Transactions on Pattern Analysis and Machine Intelligence **22** (2000), no. 3, 281–297 (en).
40. Kavita Khanna and Navin Rajpal, *Survey of Curve and Surface Reconstruction Algorithms from a Set of Unorganized Points*, Proceedings of the Third International Conference on Soft Computing for Problem Solving, Springer, Delhi, NY, USA, March 2014, pp. 451–458.
41. Gwanghyun Kim, Taesung Kwon, and Jong Chul Ye, *Diffusionclip: Text-guided diffusion models for robust image manipulation*, Proceedings of the IEEE/CVF conference on computer vision and pattern recognition, 2022, pp. 2426–2435.
42. Slav Kirov and Dejan Slepčev, *Multiple Penalized Principal Curves: Analysis and Computation*, Journal of Mathematical Imaging and Vision **59** (2017), no. 2, 234–256 (en).
43. Marcel Kreuter, *Sobolev Spaces of Vector-Valued Functions*, Master’s thesis, University of Ulm, 2015.
44. Anders Krogh and John A. Hertz, *A simple weight decay can improve generalization*, Proceedings of the 5th International Conference on Neural Information Processing Systems (San Francisco, CA, USA), NIPS’91, Morgan Kaufmann Publishers Inc., 1991, p. 950–957.
45. Lin Lan, Ye Ji, Meng-Yun Wang, and Chun-Gang Zhu, *Full-LSPIA: A Least-Squares Progressive-Iterative Approximation Method with Optimization of Weights and Knots for NURBS Curves and Surfaces*, Comput.-Aided Des. **169** (2024), 103673.
46. Pascal Laube, Matthias O. Franz, and Georg Umlauf, *Deep learning parametrization for b-spline curve approximation*, 2018 International Conference on 3D Vision (3DV), 2018, pp. 691–699.
47. Léo Lebrat, Frédéric De Gournay, Jonas Kahn, and Pierre Weiss, *Optimal Transport Approximation of 2-Dimensional Measures*, SIAM Journal on Imaging Sciences **12** (2019), no. 2, 762–787 (en).
48. A. Lemenant, *A presentation of the average distance minimizing problem*, Journal of Mathematical Sciences **181** (2012), no. 6, 820–836.
49. Xin Yang Lu and Dejan Slepčev, *Average-distance problem with curvature penalization for data parameterization: Regularity of minimizers*, ESAIM: Control, Optimisation and Calculus of Variations **27** (2021), 8.
50. Xin Yang Lu and Dejan Slepčev, *Properties of Minimizers of Average-Distance Problem via Discrete Approximation of Measures*, SIAM Journal on Mathematical Analysis **45** (2013), no. 5, 3114–3131, Publisher: Society for Industrial and Applied Mathematics.

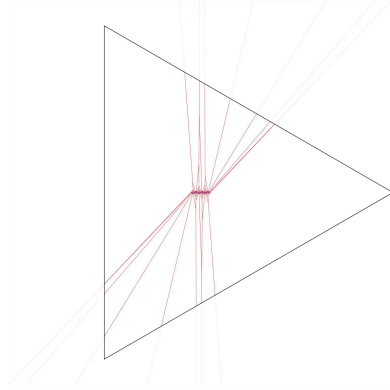
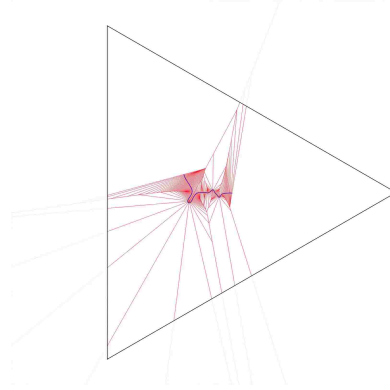
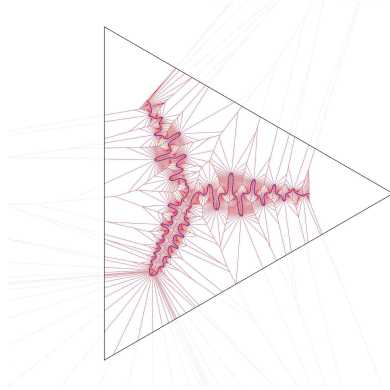
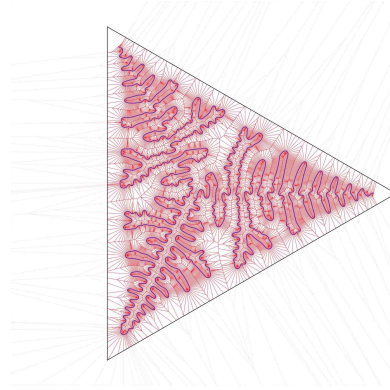
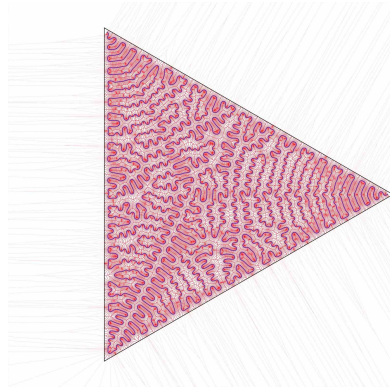
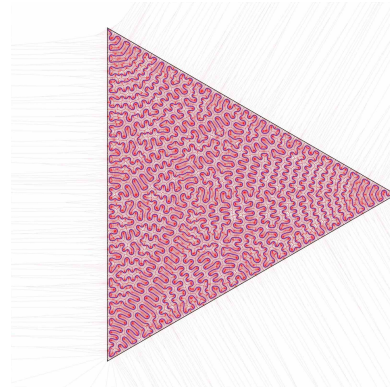
51. ———, *Average-distance problem for parameterized curves*, ESAIM: Control, Optimisation and Calculus of Variations **22** (2016), no. 2, 404–416 (en), Number: 2 Publisher: EDP Sciences.
52. Weiyin Ma and Peiren He, *B-spline surface local updating with unorganized points*, Comput.-Aided Des. **30** (1998), no. 11, 853–862.
53. Pertti Mattila, *Geometry of Sets and Measures in Euclidean Spaces: Fractals and Rectifiability*, Cambridge Studies in Advanced Mathematics, Cambridge University Press, Cambridge, 1995.
54. Pertti Mattila, Manuel Morán, and José-Manuel Rey, *Dimension of a measure*, Studia Math. **142** (2000), 219–233.
55. Robert J. McCann and Brendan Pass, *Optimal Transportation Between Unequal Dimensions*, Arch. Ration. Mech. Anal. **238** (2020), no. 3, 1475–1520.
56. Marina Meilă and Hanyu Zhang, *Manifold Learning: What, How, and Why*, Annu. Rev. Stat. Appl. (2024), no. Volume 11, 2024, 393–417.
57. Ben Mildenhall, Pratul P Srinivasan, Matthew Tancik, Jonathan T Barron, Ravi Ramamoorthi, and Ren Ng, *Nerf: Representing scenes as neural radiance fields for view synthesis*, Communications of the ACM **65** (2021), no. 1, 99–106.
58. John J. Miller and Edward J. Wegman, *Vector function estimation using splines*, J. Stat. Plan. Inference **17** (1987), 173–180.
59. Tristan Milne and Adrian I. Nachman, *Wasserstein GANs with Gradient Penalty Compute Congested Transport*, Conference on Learning Theory, PMLR, June 2022, pp. 103–129.
60. Mehdi Mirza and Simon Osindero, *Conditional generative adversarial nets*, arXiv preprint arXiv:1411.1784 (2014).
61. Tatsuya Miura, *A characterization of cut locus for C^1 hypersurfaces*, Nonlinear Differential Equations and Applications NoDEA **23** (2016), no. 6, 60 (en).
62. In Jae Myung, *Tutorial on maximum likelihood estimation*, Journal of mathematical Psychology **47** (2003), no. 1, 90–100.
63. Ryumei Nakada and Masaaki Imaizumi, *Adaptive approximation and generalization of deep neural network with intrinsic dimensionality*, Journal of Machine Learning Research **21** (2020), no. 174, 1–38.
64. Luca Nenna and Brendan Pass, *Variational problems involving unequal dimensional optimal transport*, Journal de Mathématiques Pures et Appliquées **139** (2020), 83–108.
65. Alexander Quinn Nichol, Prafulla Dhariwal, Aditya Ramesh, Pranav Shyam, Pamela Mishkin, Bob McGrew, Ilya Sutskever, and Mark Chen, *Glide: Towards photorealistic image generation and editing with text-guided diffusion models*, International Conference on Machine Learning, PMLR, 2022, pp. 16784–16804.
66. George Papamakarios, Eric Nalisnick, Danilo Jimenez Rezende, Shakir Mohamed, and Balaji Lakshminarayanan, *Normalizing flows for probabilistic modeling and inference*, Journal of Machine Learning Research **22** (2021), no. 57, 1–64.
67. Henning Petzka, Asja Fischer, and Denis Lukovnikov, *On the regularization of wasserstein GANs*, International Conference on Learning Representations, 2018.
68. Gabriel Peyré and Marco Cuturi, *Computational Optimal Transport: With Applications to Data Science*, MAL **11** (2019), no. 5-6, 355–607.
69. Phil Pope, Chen Zhu, Ahmed Abdelkader, Micah Goldblum, and Tom Goldstein, *The intrinsic dimension of images and its impact on learning*, International Conference on Learning Representations, 2021.
70. Aditya Ramesh, Mikhail Pavlov, Gabriel Goh, Scott Gray, Chelsea Voss, Alec Radford, Mark Chen, and Ilya Sutskever, *Zero-shot text-to-image generation*, International conference on machine learning, Pmlr, 2021, pp. 8821–8831.
71. Sam T. Roweis and Lawrence K. Saul, *Nonlinear Dimensionality Reduction by Locally Linear Embedding*, Science **290** (2000), no. 5500, 2323–2326.
72. Chitwan Saharia, William Chan, Saurabh Saxena, Lala Li, Jay Whang, Emily L Denton, Kamyar Ghasemipour, Raphael Gontijo Lopes, Burcu Karagol Ayan, Tim Salimans, et al., *Photorealistic text-to-image diffusion models with deep language understanding*, Advances in neural information processing systems **35** (2022), 36479–36494.
73. Filippo Santambrogio, *Optimal Transport for Applied Mathematicians*, Springer International Publishing, Cham, Switzerland, 2015.

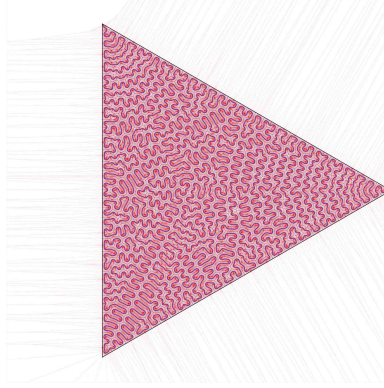
74. Matthew Tancik, Pratul P. Srinivasan, Ben Mildenhall, Sara Fridovich-Keil, Nithin Raghavan, Utkarsh Singhal, Ravi Ramamoorthi, Jonathan T. Barron, and Ren Ng, *Fourier features let networks learn high frequency functions in low dimensional domains*, Proceedings of the 34th International Conference on Neural Information Processing Systems (Red Hook, NY, USA), NIPS '20, Curran Associates Inc., 2020.
75. Joshua B Tenenbaum, Vin de Silva, and John C Langford, *A global geometric framework for nonlinear dimensionality reduction*, science **290** (2000), no. 5500, 2319–2323.
76. Elen Vardanyan, Sona Hunanyan, Tigran Galstyan, Arshak Minasyan, and Arnak S. Dalalyan, *Statistically Optimal Generative Modeling with Maximum Deviation from the Empirical Distribution*, International Conference on Machine Learning, PMLR, July 2024, pp. 49203–49225.
77. Cédric Villani, *Topics in optimal transportation*, Graduate Studies in Mathematics, no. v. 58, American Mathematical Society, Providence, R.I., 2003.
78. Wenping Wang, Helmut Pottmann, and Yang Liu, *Fitting B-spline curves to point clouds by curvature-based squared distance minimization*, ACM Trans. Graph. **25** (2006), no. 2, 214–238.
79. Yuedong Wang, *Smoothing Splines: Methods and Applications*, Taylor & Francis, Andover, England, UK, June 2011.
80. Kevin Weiler and Peter Atherton, *Hidden surface removal using polygon area sorting*, SIGGRAPH Comput. Graph. **11** (1977), no. 2, 214–222.
81. Zhouwang Yang, Jiansong Deng, and Falai Chen, *Fitting unorganized point clouds with active implicit B-spline curves*, Visual Comput. **21** (2005), no. 8, 831–839.
82. Thomas W. Yee, *Vector Generalized Linear and Additive Models*, Springer, New York, NY, USA, 2015.
83. Cheng Chun You, Seng Poh Lim, Seng Chee Lim, Joi San Tan, Chen Kang Lee, and Yen Min Jasmina Khaw, *A survey on surface reconstruction techniques for structured and unstructured data*, 2020 IEEE Conference on Open Systems (ICOS), 2020, pp. 37–42.
84. Guodong Zhang, Chaoqi Wang, Bowen Xu, and Roger Grosse, *Three mechanisms of weight decay regularization*, International Conference on Learning Representations, 2019.
85. Xiuyang Zhao, Caiming Zhang, Bo Yang, and Pingping Li, *Adaptive knot placement using a GMM-based continuous optimization algorithm in B-spline curve approximation*, Comput.-Aided Des. **43** (2011), no. 6, 598–604.
86. Zaiping Zhu, Andres Iglesias, Lihua You, and Jian Jun Zhang, *A Review of 3D Point Clouds Parameterization Methods*, Computational Science – ICCS 2022, Springer, Cham, Switzerland, June 2022, pp. 690–703.

APPENDIX A. GALLERY OF NUMERICAL EXPERIMENTS

A.1. Triangular Domain. The numerics below were obtained with the following choices of parameters:

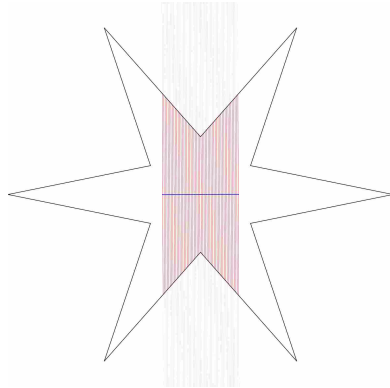
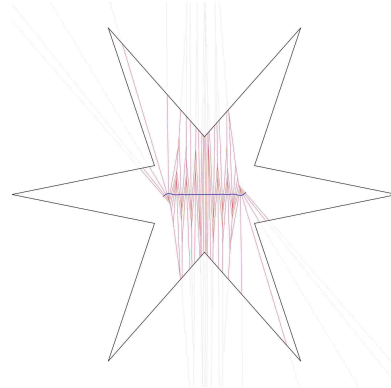
- Domain: Triangle with vertices $\{(1, 2\pi k/3) \mid k = 0, 1, 2\}$,
- Objective functional exponent: $p = 2$,
- Sobolev parameters: $k = 2, q = 2$
- Initial condition: 500 equally-spaced samples of $(t, \frac{1}{200} \sin(200t))$ on $[-1/20, 1/20]$
- Spline resampling resolution: $\frac{3}{1000}$
- Learning rate: $c(i) = (i/500)^2$
- Regularization penalty: $\lambda(i) = \frac{1}{100}(1 - c(i))$
- Area rescaling: $F_{\hat{\pi}_{Y_N}}(y_j) \mapsto F_{\hat{\pi}_{Y_N}}(y_j)/\rho(\hat{\pi}_{Y_N}^{-1}(y_j))^{17/20}$
- Smoothing window width: 1 point each side for the y_j , 3 points each side for $F_{\hat{\pi}_{N_j}}$, 3 points each side for $\nabla \mathcal{C}$.

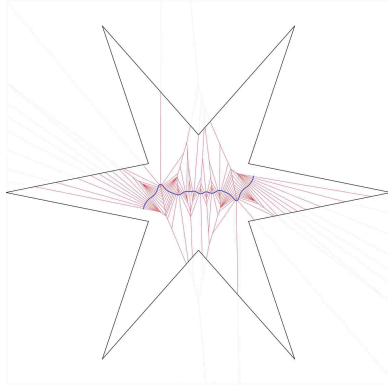
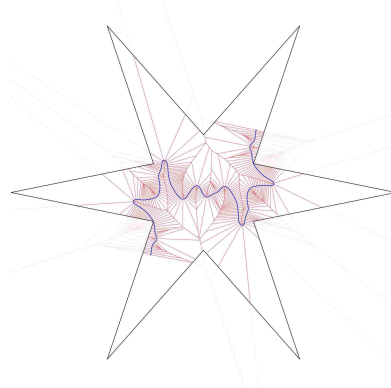
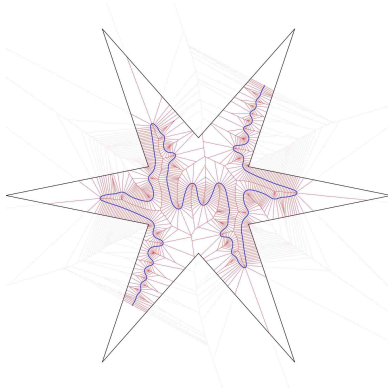
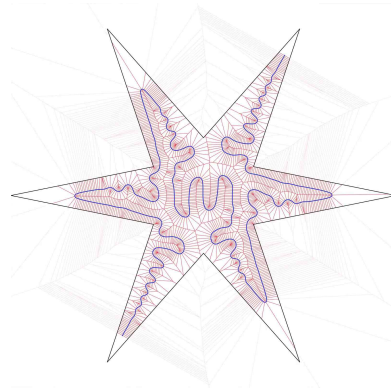
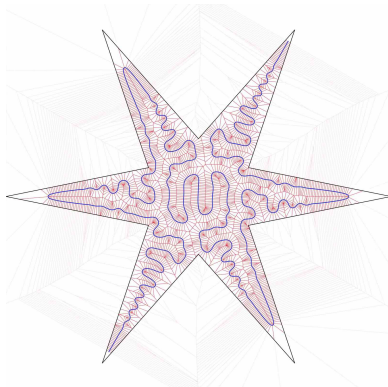
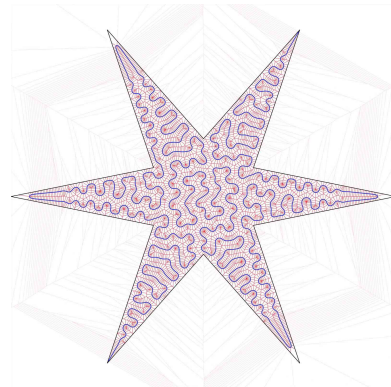
(A) $i = 1$ (B) $i = 50$ (C) $i = 100$ (D) $i = 150$ (E) $i = 200$ (F) $i = 250$

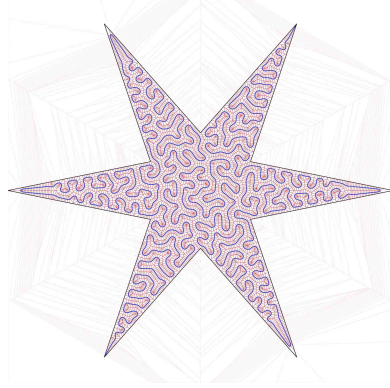
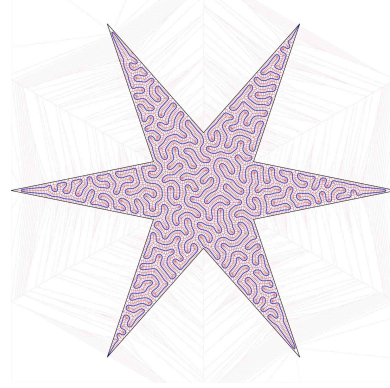
(G) $i = 300$

A.2. Hexagonal Star Domain. The numerics below were obtained with the following choices of parameters:

- Domain: Hexagonal star with vertices $\{(\frac{3}{10} + \frac{7}{10}((i+1) \bmod 2), \frac{2\pi k}{12}) \mid k = 0, \dots, 11\}$,
- Objective functional exponent: $p = 2$,
- Sobolev parameters: $k = 2, q = 2$
- Initial condition: 500 equally-spaced samples of $(t, t/250)$ on $[-1/5, 1/5]$
- Spline resampling resolution: $\frac{1}{125}$
- Learning rate: $c(i) = \frac{9}{10}(i/1000)^2$
- Regularization penalty: $\lambda(i) = \frac{1}{10000}(1 - c(i))$
- Area rescaling: $F_{\hat{\pi}_{Y_N}}(y_j) \mapsto F_{\hat{\pi}_{Y_N}}(y_j)/\rho(\hat{\pi}_{Y_N}^{-1}(y_j))^{17/20}$
- Smoothing window width: 1 point each side for the y_j , 1 point each side for $F_{\hat{\pi}_{Y_j}}$, 1 point each side for $\nabla \mathcal{C}$.

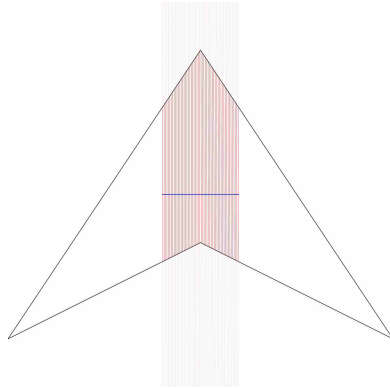
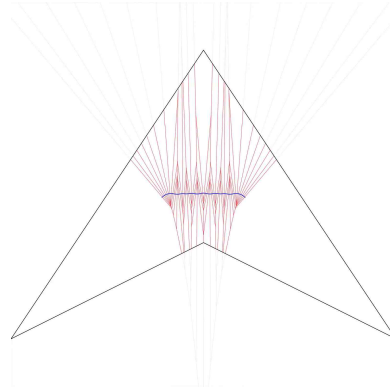
(A) $i = 1$ (B) $i = 50$

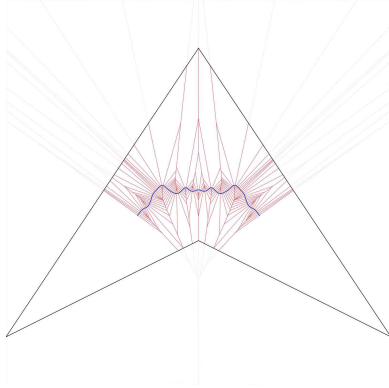
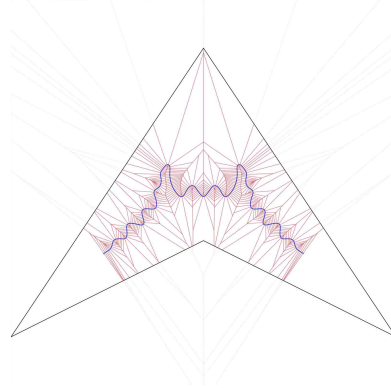
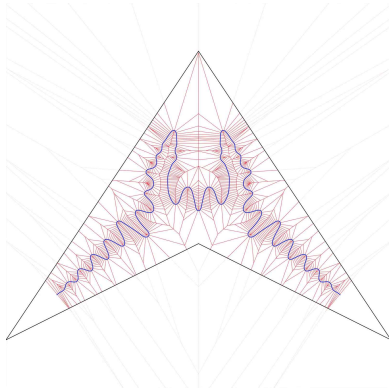
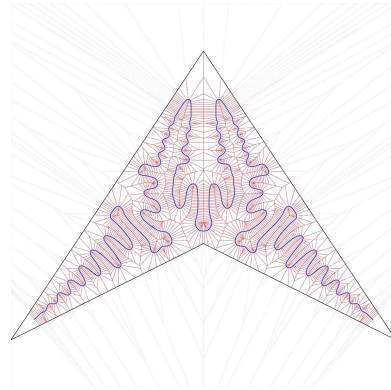
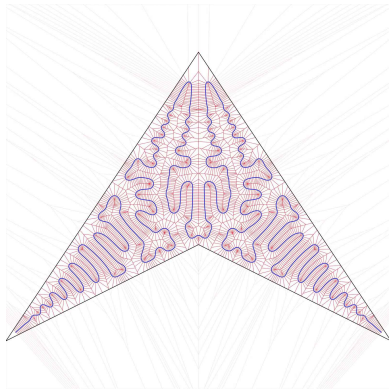
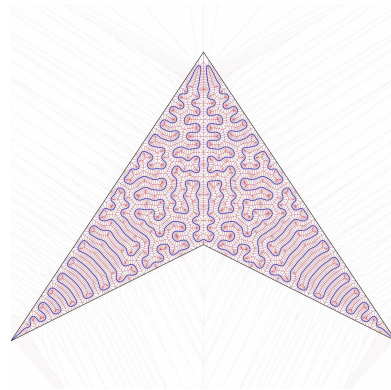
(c) $i = 100$ (d) $i = 150$ (e) $i = 200$ (f) $i = 250$ (g) $i = 300$ (h) $i = 500$

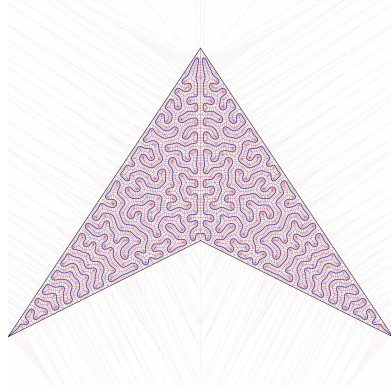
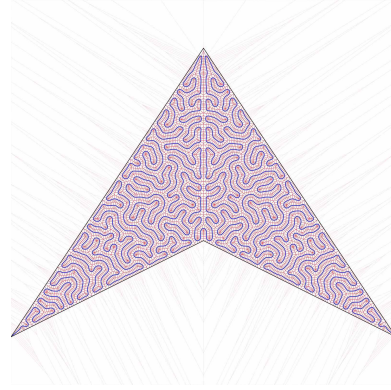
(I) $i = 750$ (J) $i = 1000$

A.3. Chevron Domain. The numerics below were obtained with the following choices of parameters:

- Domain: Chevron shape with vertices $\{(-1, -\frac{3}{4}), (0, \frac{3}{4}), (1, -\frac{3}{4}), (0, -\frac{1}{4})\}$
- Objective functional exponent: $p = 2$,
- Sobolev parameters: $k = 2, q = 2$
- Initial condition: 500 equally-spaced samples of $(t, t/250)$ on $[-1/5, 1/5]$
- Spline resampling resolution: $\frac{1}{125}$
- Learning rate: $c(i) = \frac{9}{10}(i/1000)^2$
- Regularization penalty: $\lambda(i) = \frac{1}{10000}(1 - c(i))$
- Area rescaling: $F_{\hat{\pi}_{Y_N}}(y_j) \mapsto F_{\hat{\pi}_{Y_N}}(y_j)/\rho(\hat{\pi}_{Y_N}^{-1}(y_j))^{17/20}$
- Smoothing window width: 1 point each side for the y_j , 1 point each side for $F_{\hat{\pi}_{Y_j}}$, 1 point each side for ∇C .

(A) $i = 1$ (B) $i = 50$

(c) $i = 100$ (d) $i = 150$ (e) $i = 200$ (f) $i = 250$ (g) $i = 300$ (h) $i = 500$

(i) $i = 750$ (j) $i = 1000$

FOREST KOBAYASHI, DEPARTMENT OF MATHEMATICS, UNIVERSITY OF BRITISH COLUMBIA, VANCOUVER, CANADA, EMAIL: FKOBAYASHI@MATH.UBC.CA

JONATHAN HAYASE, PAUL G. ALLEN SCHOOL OF COMPUTER SCIENCE & ENGINEERING, UNIVERSITY OF WASHINGTON, SEATTLE, USA, EMAIL: JHAYASE@CS.WASHINGTON.EDU

YOUNG-HEON KIM, DEPARTMENT OF MATHEMATICS, UNIVERSITY OF BRITISH COLUMBIA, VANCOUVER, CANADA, EMAIL: YHKIM@MATH.UBC.CA